Tremor Suppression in the Human Hand and Forearm

by Seyedeh Marzieh Hosseini

Thesis submitted in fulfilment of the requirements for the degree of

Doctor of Philosophy

under the supervision of Dr Adel Al-Jumaily

University of Technology Sydney
Faculty of Engineering and Information Technology

January 2019

In the name of GOD

The Most Compassionate

The Most Merciful

DEDICATED TO

My husband and my parents

CERTIFICATE OF ORIGINAL AUTHORSHIP

I, Seyedeh Marzieh Hosseini, certify that the work in this thesis has not previously been submitted for a degree nor has it been submitted as part of requirements for a degree except as fully acknowledged within the text.

I also certify that the thesis has been written by me. Any help that I have received in my research work and the preparation of the thesis itself has been acknowledged. In addition, I certify that all information sources and literature used are indicated in the thesis.

This research is supported by the Australian Government Research Training Program.

Signature of Student: *Seyedeh Marzieh Hosseini*

Production Note:
Signature removed prior to publication.

Date: 29/12/2018

ACKNOWLEDGEMENT

Foremost, I would like to express my sincere gratitude to my supervisor, Associate Professor Dr. Adel Al-Jumaily for the continuous support of my Ph.D study and research, for his patience, motivation, enthusiasm, and immense knowledge. His guidance helped me in all the time of research and writing of this thesis.

I would like to thank University of Technology Sydney (UTS) for providing me with the UTS International Research Scholarship (UTS IRS) during my PhD study. Special thanks also go to the Faculty of Engineering and Information Technology (FEIT) for providing the fund to travel to Tokyo in Japan to attend a conference.

I am sincerely grateful to Professor Simon Lewis and his team at Parkinson's disease Research Clinic at the Brain and Mind Centre, University of Sydney Royal Prince Alfred Hospital (RPAH), for their kind collaboration for data collection from patients with Parkinson's disease. I would also like to extend my genuine appreciations to Professor CT Lin and his team for their support and help during the data recording process in RPAH.

I would like to thank my lovely family: my parents Seyed Noureddin and Khadijeh, and my siblings, Tahereh, Maryam, and Mohammad Hossein for supporting me spiritually throughout my life.

Last but not the least I would also like to thank my dear husband, Hamed, for his continued and unfailing love, support and understanding which made the completion of this thesis possible.

ABSTRACT

Tremor is a neurological disorder characterized by involuntary oscillations and poses a functional problem to a large number of patients. The most preferred description for tremor is an involuntary movement that is an approximately rhythmic and roughly sinusoidal movement. It results from a neurological disorder which can affect many daily activities. People who are affected by Parkinson's diseases (PD) have tremor on their upper limb especially in the forearm and hand. Difficulties associated with tremor in patients with PD have motivated the researchers to work on developing various methods for tremor suppression. There is some medical and non-medical treatment for tremor reduction. Despite the considerable experience in tremor management, current treatment based on drugs or surgery does not achieve an effective reduction in 25 % of patients.

For such case, many researchers concentrated on finding non-medical treatments for tremor diminution. Active force control (AFC) or active vibration control (AVC) is one of the most famous non-medical methods for tremor suppression and control. Active vibration control is an alternate way to control and attenuate the vibration. In this method a counter force which is equal to the original vibration force but in the opposite direction is applied to the vibrating structure to supress the vibration. Finally, the vibration of structures will be stopped as two opposite forces cancel each other. The AFC method for tremor attenuation in the human forearm and hand is considered in this thesis. An AFC system is proposed which has a piezoelectric actuator and a classic proportional-derivative (PD) controller. Tremor behavior is investigated in three different models. The first model is a four degrees-of-freedom (4-DOF) biodynamic model of the human hand, which is the combination of mass-spring-damper system. The second model is a one degree-of-freedom (1-DOF) musculoskeletal model of the elbow joint with two links and one joint which includes two muscles, biceps, and triceps as the flexor and the extensor of the elbow joint. The third model is a three degrees-of-freedom (3-DOF) musculoskeletal model including wrist flexion-extension (FE), radial-ulnar deviation (RUD), and pronation supination (PS). The musculoskeletal model contains four muscles; extensor carpi radialis longus, extensor carpi

ulnaris, flexor carpi ulnaris and flexor carpi radialis. First, simulation of the tremor generation in the model is performed and then the performance of the AFC system for suppressing tremor is investigated in all three models. A single piezoelectric actuator is embedded in the AFC system for controlling the behavior of the PD controller. MATLAB Simulink is used to analyze the model. Results show that the proposed AFC-based system with a piezoelectric actuator and a PD controller is very effective in suppressing the tremor for the three models.

Using piezoelectric material as a smart material for AVC has been of interest to many researchers. Human forearm is modelled as a continuous beam which has a layer of piezoelectric actuator on its top surface and tremor is controlled actively. Also using piezoelectric material as an actuator and sensor in the closed loop control system has a very significant effect on tremor suppression. A closed loop active control system is developed and the human forearm is modeled as a beam which has two layers of piezoelectric on its top and bottom surface as an actuator and sensor respectively. Tremor behaviour of the model is studied in this control system to identify the effect of piezoelectric material on tremor suppression. Hamilton principle is used to obtain the equation of motion of both beam model. Thus, by employing the Galerkin procedure, the governing equation of motion which is a second order ordinary differential equation in time is derived. An external force as a tremor disturbance is applied to the beam by a sinusoidal force to analyse the beam behaviour. The response of the system to the force stimulation gives the analytical relations for natural frequency and amplitude of the vibration. Using the obtained analytical relations, the effects of different factors and piezoelectric properties on the vibration of this beam are examined. The results indicate that the piezoelectric layer as an actuator provides an effective tool for active control of vibration. Also using a piezoelectric layer as a sensor and actuator on the closed loop control system has a significant effect on tremor suppression.

Tremor characteristics help researchers to find the best treatment for its suppression. The frequency and amplitude of tremor have different level in patients. Some patients experience a severe kind of tremor compared to others who have weak tremor. As a result, tremor classification for PD subjects provides beneficial information for the researchers.

Human hand tremor is recorded using electromyography (EMG) from 14 patients who are affected by Parkinson's disease. Different signal-processing including filtering and data segmentation, feature extraction, feature reduction and classification are applied to the raw EMG signal to get accurate and useful information from recorded signals. Extreme learning machine (ELM) was used to classify data into three different classifications; severe, moderate and weak. The results illustrate that the proposed system which consists of the PCA, ELM and the majority vote is successful to recognising the tremor severity in three different classes; weak, moderate and severe.

Abbreviations

AFC	Active Force Control
ANN	Artificial Neural Network
AR	Autoregressive
AVC	Active Vibration Control
BaSTO	Barium Strontium Titanate
CR	Crossing Rate
DBS	Deep Brain Stimulation
DOF	Degree of Freedom
ECG	Electrocardiography
ECRL	Extensor Carpi Radialis Longus
ECU	Extensor carpi ulnaris
EEG	Electroencephalography
ELM	Extreme Learning Machine
EMG	Electromyography
EMG-PR	EMG-based Pattern Recognition
EMG-non-PR	EMG-based non-Pattern Recognition
EOG	Electrooculography
ET	Essential Tremor
EWT	Empirical Wavelet Transform
EWPT	Empirical Wavelet Packet Transform
FCR	Flexor Carpi Radialis
FCU	Flexor Carpi Ulnaris
FD	Frequency Domain
FE	Flexion-Extension
FES	Functional Electrical Stimulation
FGM	Functionally Graded Material

FNN	Feed-Forward Neural Networks
FP	Feature Projection
FS	Feature Selection
HAL	Hybrid Assistive Limb
HMM	Hidden Markov Model
HTD	Hjorth Time Domain
I controller	Integral controller
IEMG	Integrated EMG
IMU	Inertial Measurement Unit
KKT	Karush-Khun-Tucker
KNN	K-Nearest Neighbour
LDA	Linear Discriminant Analysis
LFP	Local Field Potentials
LH	(Biceps) Long Head
LtH	(Triceps) Lateral Head
MAV	Mean Absolute Value
MDF	Median Frequency
MES	Myoelectric Signal
MLP	Multiple Layer Perceptron
MNF	Mean Frequency
MNP	Mean Power
MU	Motor Unit
OFNDA	Orthogonal Fuzzy Neighbourhood Discriminant Analysis
P controller	Proportional controller
PCA	Principle Component Analysis
PD	Parkinson's Disease
PD controller	Proportional–Derivative controller
PI controller	Proportional –Integral controller

PID controller	Proportional–Integral–Derivative controller
PKF	Peak Frequency
PLZT	Lead Lanthanum Zirconate Titanate
PNN	Probabilistic Neural Network
PS	Pronation-Supination
PSD	Power Spectral Density
PT	Physical Therapy
PVDF	Polyvinylidene Fluoride
PW	Pulse Width
PZT	Lead Zirconate Titanate
RBN	Radial Basis Function Network
RUD	Radial-Ulnar Deviation
SCI	Spinal Cord Injury
sEMG	Surface Electromyography
SLFNs	Single-Hidden-Layer Feed-Forward Networks
SOM	Self-Organizing Map
SRDA	Spectral Regression Discriminant Analysis
SSC	Slope Sign Changes
SVD	Singular Value Decomposition
SVM	Support Vector Machine
TD	Time Domain
TFD	Time-Frequency Domain
TMS	Transcranial Magnetic Stimulation
WBV	Whole Body Vibration
WL	Waveform Length
WOTAS	Wearable Orthosis for Tremor Assessment and Suppression
ZC	Zero Crossings
2D	Two-Dimensional

Nomenclature

A	Area of cross-section
A_s	Area of the piezoelectric sensor
$A(s)$	Transfer function of the actuator
a	Muscle activation without fatigue
a_r	Normalized muscle recruitment curve
a_m	Muscle activation with fatigue
a_p	Feature vector
b	Dimensionless frequency of the beam
bi	Threshold for the ith hidden neuron
c	User-specified parameter
c_i	Damping coefficients
D	Displacement vector
D_T	Delay time for electromyography control system
d_{31}	Piezoelectric constant that relates the mechanical tension to electrical displacement
E	Modulus of elasticity of the beam /Elasticity coefficient matrix
ei	Eigenvectors
$e(t)$	Error in PD controller
e_{31}	Piezoelectric constant
F_a	Actuator force
F_{Di}	Dissipative force
F_e	Disturbance force
F'_e	Estimated disturbance force

F_i	Muscle force
F_{ki}	Restoring force
F_{max}	Muscle maximum isometric force
F_{Oi}	Excitation force
f	Stimulation frequency
f_l	Normalized factor
f_n	Frequency of EMG signal
f_v	Force -Velocity Factor
$f\,(x,t)$	External force on the beam
G	Shear modulus
G_a	Feedback control gain
G_s	Amplifier gain
G_T	Control gain
g	Gravitational constant
g(x)	Activation function of the hidden node
H	Hidden layer output matrix
H^*	Moore–Penrose generalized inverse of the matrix **G**
$H(x)$	Heaviside function
h	Coupling coefficients matrix
h_a	Piezoelectric actuator thickness
h_b	Beam thickness
h_p	Piezoelectric thickness
h_s	Piezoelectric sensor thickness
I	Second moment of inertia
I'	Vibratory inertia
$J(x)$	Polar moment of inertia
K	Shear correction factor

K_d	Derivative gain
K_i	Integral gain
K_p	Proportional gain
k_i	Linear stiffness
k_s	Spring stiffness
l	Length
l_a	Piezoelectric actuator length
l_b	Beam length
l_s	Piezoelectric sensor length
$\overline{l}$	Normalized muscle length
M	Bending moment
M'	Estimated Mass
m_a	Mass of the piezoelectric actuator
m_b	Mass of the Euler- Bernoulli beam model
m_i	Mass in 4-DOF palm model
m_s	Mass of the piezoelectric sensor
$m(x)$	Mass of the Timoshenko beam model
Nj	Number of samples in class j
P	Order of the AR model
P_l	Linear transformation for features
P_n	Frequency power spectrum
PW_d	Threshold pulse width
PW_s	Saturation pulse width
p	Muscle fatigue factor
p_{min}	Minimum fitness
$p(t)$	Applied voltage to the piezoelectric actuator
Q	Electrical field vector

Q_c	Covariance matrix
Q_n	Non-linear piecewise continuous function
$Q(t)$	Closed circuit charge
q	Actual position in AFC system
$\ddot{q}$	Measured acceleration of the AFC system
$q(f)$	Frequency characteristic factor
q(t)	Time-dependent function
r_i	Moment arm
S_{11}	Elastic constant of piezoelectric material
T	Kinetic energy
TF	Transfer function of piezoelectric actuator
T_g	Gravitational Moment
T_{inc}	Increment of the window
T_P	Internal passive moment
T_t	Muscle generated Moment through active electrical stimulation
Twl	Length of the window
t	Time
t_i	white noise error term
U	Potential energy
U_a	Potential energy piezoelectric actuator
U_b	Potential energy of the beam
U_s	Potential energy of the piezoelectric sensor
U_{spring}	Potential energy of the spring
V	Shear force
V_a	Applied external voltage to piezoelectric actuator
V_s	Applied external voltage to piezoelectric sensor

v_a	Volume of the piezoelectric actuator
v_b	Volume of the beam
$v_{\max}$	Maximum contraction (shortening) velocity
v_s	Volume of the piezoelectric sensor
$\overline{v}$	Normalized muscle velocity
W	Work
w_b	Beam width
w_a	Piezoelectric actuator width
w_s	Piezoelectric sensor width
$w_i = [w_{i1}, w_{i2}, \ldots, w_{im}]^T$	Vector of the weight for the i*th* hidden and input neurons
w_n	Weighted window function
w_p	Piezoelectric width
X= (x1,…, xN)	Feature set matrix with *t*-dimensional space
x_i^j	The *i*th sample of class *j*
$x_j = [x_{j1}, x_{j2}, \ldots, x_{jm}]^T$	Input for SLFN
Y	Vertical deflection in Euler-Bernoulli beam
Y(x)	Fundamental vibration mode shape for Euler-Bernouli beam
y	Lateral displacement in Euler-Bernoulli beam
$y_j = [y_{j1}, y_{j2}, \ldots, y_{jn}]^T$	Target for SLFN
z	Electrical Pulse width
Z(x)	Fundamental vibration mode shape in Timoshenko beam
$\beta_j = [\beta_1, \ldots, \beta_n]$	Output weight linking the hidden layer and the j*th* output node
$\beta_{jL} = [\beta_{j1}, \beta_{j2}, \ldots, \beta_{jL}]^T$	Weight vector of j*th* hidden and output neuron
β_s	Shaping factor

β_{33}	Impermittivity coefficients
γ_{xy}	Shear strain for Timoshenko beam
ε	Strain vector
$\zeta_i^T = [\zeta_{i,1}, \zeta_{i,2}, \ldots, \zeta_{i,n}]^T$	Output vector error
θ	Joint angle
$\ddot{\theta}$	Angular acceleration
λ	Frequency factor on fatigue
λ_i	Eigenvalue associated with the eigenvector e*i*
μ_j	Mean of the class j
ξ_{33}	Dielectric constant
ρ	Density
ρ_a	Density of piezoelectric actuator
ρ_b	Density of beam
ρ_s	Density of piezoelectric sensor
σ	Stress vector
τ	Processing time of pattern-recognition system
τ_{ac}	Activation time constant
τ_{da}	De-activation time constant
τ_{fat}	Fatigue time constant
τ_{rec}	Recovery time constant
τ_{xy}	Shear stress for Timoshenko
τ'_d	Estimated disturbance torque
$\emptyset$	Angle of rotation of the cross section due to bending
$\varphi(x)$	Fundamental vibration mode shapes

ψ	Bending slope of the beam
ω	Natural frequency
$\in_z$	Electric intensity in the z-direction
χ	Lateral displacement in Timoshenko beam

Table of Contents

List of Figures

LIST OF TABLES

CHAPTER 1: INTRODUCTION

Hand tremor suppression is one of the important research areas which is of interest to many researchers. This thesis discusses human hand and forearm tremor suppression especially in Parkinson's disease (PD). As an introduction, this chapter presents the background of this doctoral research. The next two sections discuss objectives of the research and thesis contributions. The organisation of the thesis is given afterwards. The last section provides some publications produced during this doctoral study.

1.1 BACKGROUND

Today, there are some diseases that are related to the human nervous system. One of these disorders is Parkinson's disease (PD). In PD the nerve cells which are in the special region of the brain that produces dopamine are damaged. Dopamine is a chemical which is essential for the smooth control of muscles and movement. As a result, PD patients have some symptoms such as tremor or shaking in the arm or hand, muscle rigidity or stiffness, stooped posture, slowing of movement, problems in balance and control movement. PD is progressive and its symptoms over time become worse and finally cause disabilities in the patients.

Tremor as one of the PD symptoms is a kind of annoying shaking in the human body especially in the forearm and hand. The most famous characteristics for tremor disability are involuntary, approximately rhythmic, and roughly sinusoid. There are many difficulties associated with tremor in PD patients' daily life such as eating, drinking, writing, walking and other activities which are related to the movement.

Medical and surgical treatments such as drugs therapy, surgery, deep brain stimulation (DBS) and thalamic stimulator are used to suppress hand and forearm tremor. However, medical treatments such as drug therapy decrease the progress of tremor, but most drugs have their intrinsic drawbacks on the human body. Also, surgery is not of interest to many patients as it is associated with a risk of operation on brain. In this regard, several researchers are motivated to investigate and control the human tremor using non-medical and non-surgical treatments.

Today, active vibration control (AVC) which is called active force control (AFC) too, is one of the areas of interest for movement control. This thesis aims to investigate and to define and develop an adequate AFC system to control and supress human tremor.

AFC is an intermittent way to control and supress the vibration of structures. In this method a counter force is applied to the vibrating structure to reduce the vibration. This applied force is equal to the original vibration force but in the opposite direction as it is out of phase. Therefore, the vibration of structures will be stopped as two opposite forces cancel each other.

Tremor characteristics including tremor amplitude and frequency, have valuable information for researchers to find the best treatment for its suppression. These characteristics have different values in patients. Some patients experience a severe kind of tremor compared to others who have weak tremor. Tremor classification using electromyography (EMG) for PD subjects provides beneficial information for the researchers.

1.2 OBJECTIVES

Considering problems associated with human hand and forearm tremor, the main purpose of this research is to develop a control system especially an AFC system to the control and suppress the tremor.

The main aim of this research is supported by specific research objectives, which are given in the following section.

i. The first objective of this research is developing a model for human hand and forearm to analyse the tremor behaviour in the model.
ii. The second objective of this research is deriving mathematical equations of the hand and forearm model to find an analytical solution and investigating MATLAB Simulink result for tremor control in the model.

iii. The third objective of this research is determining an effective control system for tremor control in the human hand and forearm. Using active vibration control system to suppress the tremor is of great benefit in this area.

iv. The fourth objective of this research is using smart materials as anti-vibration materials to suppress the tremor in the developed model of human hand and forearm.

v. The forth objective of this research is determining tremor characteristics to classify patients into different classes. To develop any kind of tremor reduction system, defining the most important features of tremor is noteworthy.

1.3 CONTRIBUTION OF DOCTORAL THESIS

i. In this research human hand and forearm were modelled in discrete and continuous format to analyse the effect of control system on the tremor reduction. In the first section of chapter 3, human hand was modelled as a 4-DOF mass-spring- damper model, in the second and third section of chapter 3, tremor in elbow and wrist joint were investigated in 1-DOF and 3-DOF musculoskeletal models respectively. An AFC system was developed to supress the tremor in all three models as part of an active force control system. In the AFC loop, a PD controller controls the piezoelectric actuator for tremor damping. MATLAB Simulink was used to investigate the effect of AFC on the tremor control. Results showed that for 4-DOF mass- spring- damper model during simulation time, the peak-to-peak amplitude of the hand tremor decreases from 7×10^{-3} m to 3×10^{-9} m. For 1-DOF musculoskeletal model of elbow joint, tremor peak-to-peak amplitude declines considerably from 12 degrees to 12×10^{-3} degrees. For the 3-DOF wrist joint model, tremor peak-to-peak amplitude was reduced from about 10 degrees to about 2×10^{-2} degrees in FE, from about 12 degrees to about 13×10^{-3} degrees in RUD and from about 5 degrees to about 2.7×10^{-2} degrees in PS using AFC system. Comparison between the tremor of all three models with and without AFC system showed that using AFC has a great significance on tremor suppression. This part of the research was covered in objectives i to iii.

ii. In the first part of chapter 4, the forearm was modelled as a continuous beam to analyse the effect of smart materials on tremor suppression in the human forearm. Beam model complies with Timoshenko beam theory which considers the effect of both rotary inertia and shear deformation. Beam model has a layer of piezoelectric material on its top surface as an actuator and an external force is applied to the beam by a sinusoidal force to investigate the beam behaviour. Piezoelectric materials are a smart material that can control the vibration of structures. The equation of motion of the beam with respect to the effect of a piezoelectric actuator was obtained using Hamilton principle. Finally, Galerkin procedure was used to derive the governing equation of motion which is a second order ordinary differential equation in time. The response of the system as an analytical solution was found to give the analytical relations for natural frequency and amplitude of the vibration. Using the analytical response, the effects of material properties such as density and modulus of elasticity of the piezoelectric layer and the piezoelectric coefficient on the vibration of this beam were investigated. The system response decreased almost three times faster when the beam is covered with a piezoelectric layer. The results indicate that the piezoelectric layer as an actuator is an effective tool for vibration control in the beam model. In the second section of chapter 4, human forearm was modelled as an Euler-Bernoulli beam that has two layers of piezoelectric material as a sensor and actuator on its top and bottom surface respectively. The aim of this part is to analyse the effect of active vibration control on human forearm tremor in the closed loop control system to suppress the human forearm tremor. A harmonic force was applied to the model to simulate the forearm tremor in the model. The equation of motion of the beam and second order ordinary differential equation of motion was attained using Hamilton principle and Galerkin procedure. Finally, the effect of closed loop control system as an AFC system was investigated on the model. For four different control gains of 0, 600, 1200 and1800, when the control gain was increased the vibration of the beam was decreased. Results showed that the proposed loop including piezoelectric sensor and actuator has a very significant effect on tremor suppression. This part of the research is covered in objectives i, ii and iv.

iii. In chapter 5 of this thesis tremor was recorded from PD patients at hospital to identify its characteristics. Researches have shown that tremor amplitude and frequency are different in PD patient groups. Some patients experience a severe kind of tremor in their hands but others have less problem as their tremor is weak. The main aim of this chapter is tremor classification for a group of Parkinson's patients. Electromyography was used to record data from 14 PD patients. Four EMG electrodes were attached to the subjects' forearm to record muscle activity. Patients were asked to move their hand and forearm to do some special tasks and EMG was recorded in different trials. After data recording, classification process which includes filtering, feature extraction and feature reduction was applied to the dataset. Finally, Extreme Learning Machine (ELM) was used to classify data into three different classifications; severe, moderate and weak tremor. The obtained results showed that the developed system which includes the PCA, ELM and the majority vote is able to recognize the tremor severity with the classification accuracy of 89.73% for picking up a cup activity using four EMG channels. This part of the research is covered in objectives v.

1.4 Thesis Organization

This thesis contains six chapters and references. The organization of chapters is as follows:

- Chapter 1: Introduction
- Chapter 2: Review of Related Work

- Chapter 3: Active Force Control Method for Tremor Suppression in Human Hand and Forearm
- Chapter 4: Analytical Solution for Vibration of Human Forearm Beam Model
- Chapter 5: Tremor Classification for Human Hand in Parkinson’s Disease
- Chapter 6: Conclusion

1.5 List of Publication Based on This Research

The publication outcomes during the doctoral study are as follows:

Journal papers:

- S. M. Hosseini and A. Al-Jumaily, "Analytical solution for forced vibration of piezoelectrically actuated Timoshenko beam," Journal of Intelligent Material Systems and Structures, vol. 30, pp. 1276-1284, 2019.
- S. Hosseini, A. Al-Jumaily**,** "Active vibration control in human forearm model using paired piezoelectric sensor and actuator" (Under preparation).
- S. Hosseini, A. Al-Jumaily**,** A. Ahmed, "Human hand tremor classification for Parkinson’s patients using machine learning (Under preparation).

Conference papers:

- S. Hosseini, A. Al-Jumaily, and H. Kalhori, "Tremor suppression in wrist joint using active force control method," in *9th Australasian Congress on Applied Mechanics (ACAM9)*, 2017, p. 349.
- S. Hosseini and A. Al-Jumaily, "Active force control system for tremor suppression in elbow joint," in *Robotics and Intelligent Sensors (IRIS), 2016 IEEE International Symposium on*, 2016, pp. 140-145.
- S. Hosseini, A. Al-Jumaily, and S. A. Abboud, "Active force control system for hand tremor suppression by different actuators," in *Electronic Devices, Systems*

and Applications (ICEDSA), 2016 5th International Conference on, 2016, pp. 1-4.

CHAPTER 2: REVIEW OF RELATED WORKS

2.1 INTRODUCTION

This chapter reviews some aspects of human body tremor. It also presents general information about the human hand and forearm tremor, as well as some information about tremor suppression method. This review does not aim at listing what has already been published, however it aims at providing general details and concepts about the definitions and related issues of the human hand and forearm tremor.

2.2 INTRODUCTION TO TREMOR

Tremor is defined as an involuntary oscillation of a part of the body. The most accepted definition of tremor is as follows: "an involuntary, approximately rhythmic, and roughly sinusoidal movement"[1, 2] . Tremor is one of the most general movement disorders that is a significant source of functional disability. It is resulting from a neurological disorder which can affect many of the daily living tasks. Some physical activities such as walking, writing, eating and drinking become difficult in the presence of tremor [3-6]. In this case, studying an effective way to supress the tremor is essential for affected people. Although all healthy people exhibit a certain degree of tremor that is called physiological tremor, there are several pathological tremors that affect 15 % of people with ages ranging between 50 and 69 years [7]. Moreover, among people suffering from upper limb tremors, 65 % of them report severe disability to perform their activities of daily living [8]. In addition to that, the mechanisms which are the main reason for tremor to happen in the human body are yet not understood, which often leads to some problems in tremor treatment [9].

2.3 Classification of Tremor

One of the most accepted classification for tremor is related to the hand position. The positions include rest or during action or within a certain posture. Tremors can be subclassified into the following categories:

- Rest
- Postural
- Kinetic
- Task-specific

2.3.1 A resting tremor

This kind of tremor is typically observed in Parkinson's disease. Tremor occurs when the affected body parts are not active and are completely supported against gravity, requiring no voluntary contraction [10]. Resting tremor which is a rhythmic tremor is seen when the limb is in a resting position. This tremor often occurs in the hands and forearms and with less frequency in other parts of the body. The resting tremor might decline with intentional movement and also disappear when the limbs are in extreme rest such as sleeping time. This tremor might be seen in other parts of the body such as leg, eyelids, jaw and lips [11].

2.3.2 The postural tremor

This tremor occurs when the subject attempts to maintain a special posture and muscles voluntarily contract. Postural tremor can be seen in the outstretched arms and become worse when the limb is actively moved, for example, during drinking from a cup. However, no tremor is observed when the limb is fully relaxed [10].

2.3.3 The kinetic tremor

This kind of tremor that occasionally is called action or intention tremor happens during purposeful movement of the body part affected with tremor. For example, this occurs during the test when the patient is asked to put the index finger on the nose and is called the finger-to-nose test. Generally, the kinetic tremor is seen in the patients with cerebellar disorder [10] .

2.3.4 The task-specific tremor

This tremor appears when the patient begins to perform some activities such as standing, handwriting and speaking that are goal-oriented activities. This group consists of primary vocal tremor, writing tremor and orthostatic tremor. Task-specific tremor can be defined as a form of kinetic tremor that appears during specific tasks [10].

2.4 Tremor Detection

Discovering tremor characteristic is essential for doing research in this area and also for developing any techniques for tremor reduction. Recording information about tremor amplitude and phase by effective detection techniques such as kinematics or muscle recordings is of great importance. To categorize tremor characteristic different methods of tremor measurement have been established in the past. Most methods are based on recording from mechanical devices such as potentiometers [12], velocity and displacement transducers [13, 14], accelerometers [15] while others use surface electromyography (sEMG) [16].

In the following sections, some of the tremor detection methods are described.

2.4.1 Potentiometer

One of the methods for tremor recording is using potentiometers. Ackmann et al. applied this method for recording tremor data with designing a system from two sites over long time periods [12]. The method was developed to record Parkinson’s tremor over extended time periods. The major objective, which was to obtain recording data from a patient in an environment which was close to daily living conditions was one of the great objectives of this method. Figure **2-1** shows the designed potentiometer which measured angular displacement of flexion-extension tremor at the wrist or metacarpal-phalangeal joints.

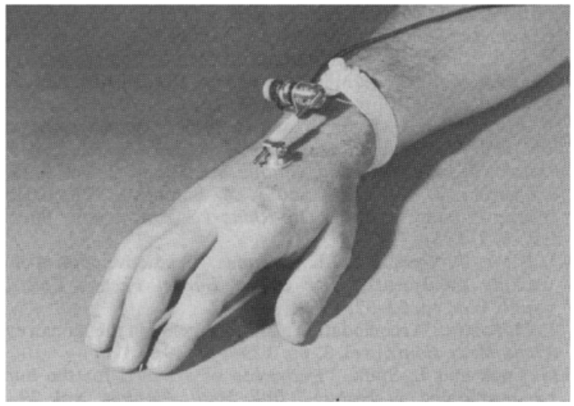

Figure 2-1. Potentiometers for tremor recording in flexion-extension at the wrist or metacarpal-phalangeal joints [12].

2.4.2 Velocity transducers

Using displacement or velocity is not a common way for tremor recording, although there are technologies that allow using accurate transducers for displacement or velocity recording. Norman et al. studied a way to use velocity transducers to identify tremor characteristics and different kinds of tremor. They used high precision techniques to record the tremor in the form of highly accurate signals of movement. There is a history of using velocity or displacement transducers for tremor recording but they have not been a preferred way for tremor detection. [12, 17-19]. The acceleration transducers are more commonly used for tremor data collecting as acceleration is a more relevant variable for tremor than is velocity or displacement.

2.4.3 Accelerometer

Use of an accelerometer is another way for tremor recording. The effect of changes in mechanical limb properties on the peak frequency of different tremor forms was analyzed by Hömberg et al. Wrist tremor was recorded by an accelerometer in the research which was done by Hömberg et al. The accelerometer was fixed to the dorsum of the hand and also surface EMG was recorded from the wrist extensors simultaneously while the heavier weights were added to the hand. The hand tremor peak frequency was gradually decreased when the load was increased as was expected from the properties of a passive spring-mass-system [15].

2.4.4 Electromyogram signals (EMG)

Electromyography (EMG) is a technique for measuring and recording muscle activity as electrical signals. EMG is achieved using an instrument called the electromyograph, to produce a record called an electromyogram. When the muscle cells are activated electrically or neurologically a signal is generated by muscle cells and an electromyograph distinguishes these signals. The recorded signals are studied to detect the characteristics of signals and analyze the biomechanics of human or animal movement [20, 21].

Todays EMG is used as an effective clinical and biomedical applications to diagnose neuromuscular diseases and motor control disorders. Recording data using EMG techniques is more effective on superficial muscles compared to deeper muscles as it is unable to bypass the action potentials of superficial muscles and detect deeper muscles.The EMG sensor is placed on the skin and the best location for that is the belly muscle [20].

A pair of electrodes or a set of multiple electrodes are needed for tremor recording with the EMG method. Using at least two electrodes is essential as EMG recordings show the voltage difference between two separate electrodes [20]. Bacher recorded long-term tremor quantification under daily-life conditions by surface EMG [22]. Also a long-term EMG-based procedure was done to separate Parkinsonian tremor from essential tremor [23].

2.5 Different Treatment Methods for Tremor Reduction

Several research works have been carried out to investigate and control the effect of human hand tremor. Tremor treatment methods are divided into two main parts: Medical and Surgical treatments and Non-pharmacological and Non-surgical treatments. These two main parts include different ways for tremor suppression in the affected people.

2.5.1 Medical and surgical treatments

There are some medical treatments for tremor reduction such as deep brain stimulation (DBS), a thalamic stimulator or using medicine. Although the medical treatment has a positive effect on tremor reduction and tremor progress, this kind of treatments have their disadvantages. In some cases, using drugs may cause irreparable drawbacks. Also, surgical therapy is a kind of high-risk treatment as the brain is involved in the surgery. All these problems cause the majority of patients who are affected by tremor to not use this kind of treatment. All these issues motivate researchers to find alternative approaches for tremor suppression in the human body [24].

2.5.2 Non-pharmacological and non-surgical treatments

There are some kinds of non-pharmacological and non-surgical treatments for tremor reduction such as Tremor-suppressing orthoses [25], Physical therapy [26, 27], Limb cooling [28, 29], Functional electrical stimulation [30-32], Vibration therapy [33, 34], Limb weights [35, 36], Bright light therapy [37] and Transcranial magnetic stimulation [38]. Table 2 shows brief information about non-pharmacological and non-surgical treatments.

Table 2-1. Information about non-pharmacological and non-surgical treatments for tremor reduction

Non-pharmacological and non-surgical treatments	Brief explanation
Tremor-suppressing orthosis	An orthosis is a device that is externally applied to a part of the human body to modify movement [25].
Physical therapy	Physical therapy or physiotherapy (PT)

	is a physical medicine that use mechanical force and movements for rehabilitation purpose. PT improves mobility and quality of life through examination, diagnosis, anticipation, and physical interposition [26].
Limb cooling	Limb cooling investigates a limb behavior using different temperatures on limbs [28].
Functional electrical stimulation	Functional electrical stimulation (FES) stimulates the nerves using electrical currents. This technique is effective for the patients who are affected by neurological disorders such as head injury, stroke, spinal cord injury (SCI), and other disorders [30].
Vibration therapy	Vibration therapy makes whole body vibration (WBV) to improve density of bones and strengthen them [33].
Limb weights	Limb weights helps to reduce tremor with applying a weight to the distal extremity is [35].
Bright light therapy	Light therapy or phototherapy apply some techniques to use light with special kind of wavelengths as a treatment for tremor suppression. Some kinds of these techniques are lasers, light-emitting diodes, fluorescent lamps,

	polychromatic polarized light , dichroic lamps or very bright, full-spectrum light [37].
Transcranial magnetic stimulation	Transcranial magnetic stimulation (TMS) is a treatment method that uses electric currents in the region of the brain via electromagnetic stimulation. In this method, a magnetic field generator is applied to produces electric currents near the head of the patient who has tremor disorder [38].

2.6 TREMOR CONTROL

Control of tremor as a human body vibration is an important problem for researchers. There are two different kinds of tremor control that are called passive tremor control and active tremor control.

2.6.1 Passive vibration (tremor) control

Passive vibration control is a kind of control method which is used to control and reduce the vibration. There are some mechanical devices that are used for tremor reductions in passive technology. This equipment contains added inertia, viscous damping, and gyroscopic stabilization. This method is used by many researchers who are interested in passive vibration control [39, 40].

Passive control of the rest tremor of the human arm in Parkinson's disease is studied in 2004 [41]. In this study a vibration absorber was added to the tremulous arm to lessen the tremor amplitude. The added system included a second mass-spring-damper grouping. The energy of vibration was transferred to the added mass by the spring in the vibration absorber. Also, a viscous damper is applied in the structure to eliminate the vibration energy and decrease the amplitude of the added mass. As the tremor frequencies for different Parkinson's patients are not same, it is essential that the designed vibration absorber attenuate the tremor at a particular frequency range. The Proposed vibration absorber for the arm with two degrees of freedom is presented in Figure 2-2.

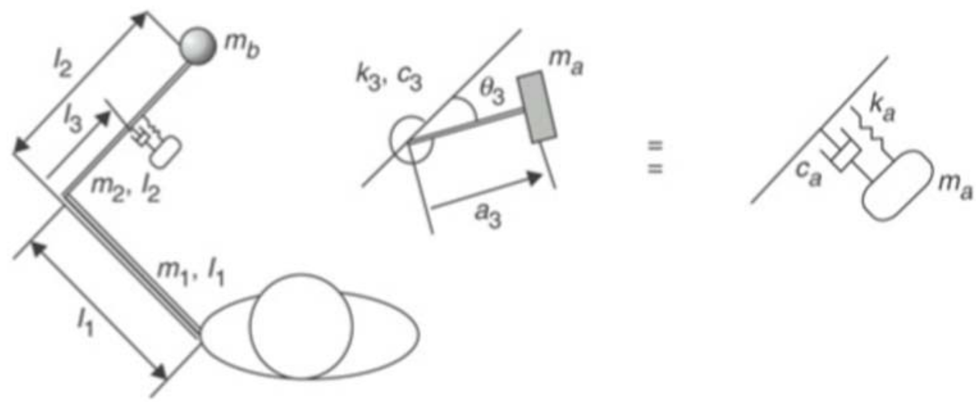

Figure 2-2. Vibration absorber for a 2-DOF arm model [41]

Using passive technology for tremor reduction was not successful as there were some drawbacks for this method. One of the main problems in this method is supressing all voluntary and involuntary movement rather than involuntary motion. Also using passive equipment cause loss of muscle strength and also fatigue in the human body [40].

2.6.2 Active vibration (tremor) control

Active vibration control or active force control is an alternate way to control and supress the vibration. In this method a counter force which is equal to the original vibration force but in the opposite direction (as it is out of phase) is applied to the vibrating structure to decrease the vibration. As a result, the vibration of structures will be stopped as two equal and opposite forces cancel each other [24]. Active Vibration control is famous as an effective method for vibration control in a dynamical system [42, 43]. This technique as a system that improves vibration reduction in the structures is studied by many researchers [44, 45]. Hewit proposed an active force control (AFC) scheme in the early 80's.The system is known as a flexible and effective system as it remains stable even in the presence of identified and unidentified disturbances. Mailah et al used AFC schemes on robotic manipulator and investigate the effect of AFC on robot control [46, 47].

In previous works, some researchers used AFC method for tremor attenuation in human body parts [4, 5, 24]. In these studies, a 4-DOF mass-spring-damper model of the human hand was used. Using AFC technique for postural tremor suppression was investigated by Suhail et al. They used a piezoelectric actuator in an AFC system to control human hand tremor [24]. The general form of the AFC system is shown in Figure 2-3.

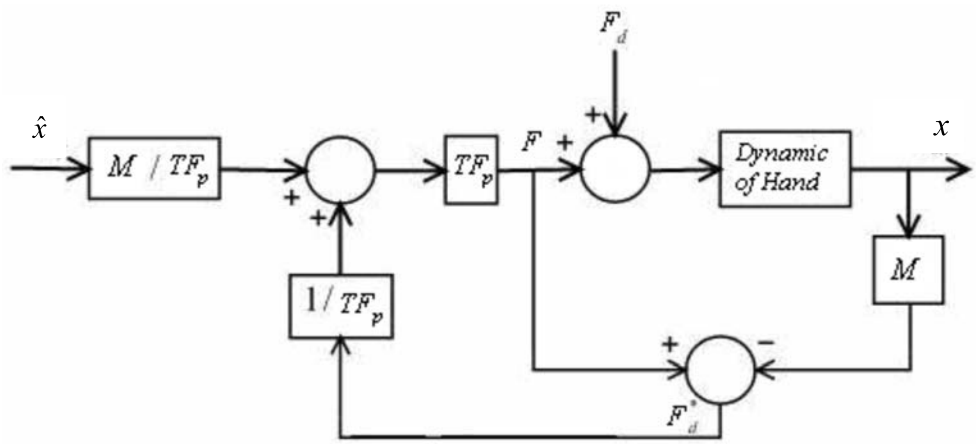

Figure 2-3. Typical AFC system [24]

The typical form of the AFC system is shown in Figure 2-3. In this Figure, F_d is disturbance, F is actuator force and TFP is transfer function of the actuator. M is the mass of the system. x is the desired position, $\hat{x}$ is the actual position AFC system [24].

2.7 Wearable Tremor Suppressing Orthosis

Using a wearable orthosis which is developed to improve the user's physical performance and help the disabled to have better body movement has been of interest to many researchers [48, 49]. Wearable orthosis are categorized in two main areas; exoskeletons which are made from hard material and soft exosuits that are made from soft material. The main difference between these two categories is the kind of materials for designing [50].

There are some assistive devices such as HONDA Walking Assist Device and Hybrid Assistive Limb (HAL), which were developed to support patients who suffer from hemiplegia or muscular weakness [48, 49]. WOTAS that stands for wearable orthosis for tremor assessment and suppression was a wearable robot which was developed for movement measurement and suppression from an upper limb for patients with disorders such as tremor [51]. Figure **2-4** shows a patient wearing the WOTAS on the right upper limb for tremor suppression. This orthosis covers the patient's elbow and wrist joints to attenuate tremor in elbow flexion-extension, wrist flexion-extension and wrist pronation-supination [52].

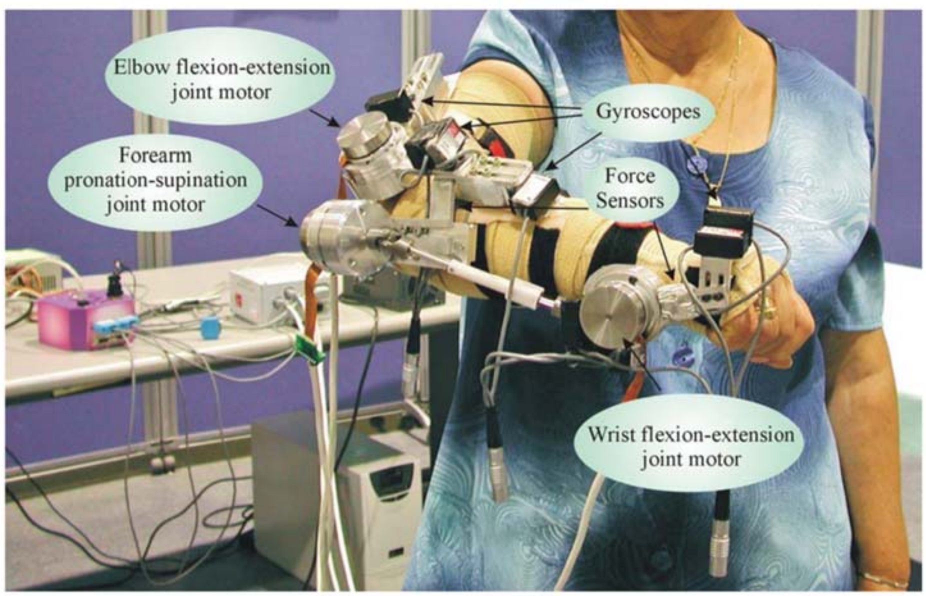

Figure 2-4. Patient using the WOTAS orthosis affixed on the right upper limb [52]

Today, using soft wearable device is growing worldwide. The major benefit of these products compared to firm exoskeletons is the light weight that motivates patients to use them easily.

A soft wearable hand robot is shown in Figure 2-5. The robot that is called the Exo-Glove is practical for the patient who suffers from paralysis of the hands due to a spinal cord injury. Using this glove, the patient is able to grasp objects of various shapes. A soft tendon routing system was used in the robot which was inspired by the human musculoskeletal system. The patients who have a problem in opening or closing their fingers but can use joints of upper limb such as the elbow, wrist, and shoulder joints were the best group for using this Exo-Glove [53].

Figure 2-5. The Exo-Glove allows the disabled to perform everyday tasks, greatly improving their quality of life [53]

2.8 ACTIVE VIBRATION CONTROL USING PIEZOELECTRIC ACTUATORS

In recent years, piezoelectric materials are used to control vibration of structures. The origin of “piezo” comes from a Greek word meaning pressure. Piezoelectric materials which are known as smart materials are used as sensors and actuators in different structures. These materials represent a reversible effect. Applying an electric voltage to piezoelectric material produces mechanical energy, i.e., vibrations or displacements as these materials convert electrical energy into mechanical energy. Also, displacements or vibrations are measurable with measuring output voltage [54-56]. There are different materials in the nature such as ammonium phosphate, quartz, paraffin, bone and wood that have piezoelectric properties. Also, piezoelectricity exists in some synthetic materials such as, barium titanate, lead zirconate titanate (PbZrTiO3–PbTiO3, known as PZT), lead lanthinum zirconate titanate (PLZT), lithium sulfate, barium strontium titanate (BaSTO), and polyvinylidene fluoride (PVDF) and PVDF copolymers [57].

Piezoelectric materials are used in many applications, such as accelerometers, signal filters and ultrasonic transducers and microphones. Also these materials are used in scanning force microscopy to move the microcantilever beam for applications such as small mass and biochemical sensing [58]. Also, it has become common recently to use these materials in medical applications such as microsurgery devices to cancel the physiological vibration of the human hand [1, 2, 59]. A tremor cancelation in a handheld microsurgical instrument is developed to sense its own motion, identify between intended and unintended motion, and deflect its tip to cancel the unwanted motion in real-time. An adaptive zero-phase notch filter is used to model and filter the tremor. Also the intraocular shaft manipulator that is a 3-DOF piezoelectric actuated mechanism driven by a feedforward controller is used [2].

Also, these smart materials have interested many researchers to use them for tremor suppressing of the human body in active force control method [60-62]. In fact, piezoelectric materials are used as a smart actuator in the active force control system to control and reduce the hand tremor.

Many researchers have used piezoelectric material to control the vibration of beam models [63]. Using the Euler–Bernoulli or thin beam theory and also Timoshenko theory to analyse the effect of piezoelectric material on vibration reduction has interested many researchers. In the Euler–Bernoulli or thin beam theory, the rotation of cross sections of the beam is neglected compared to the translation. In addition, the angular distortion due to shear is considered negligible compared to the bending deformation. The thin beam theory is applicable to beams for which the length is much larger than the depth (at least 10 times), and the deflections are small compared to the depth. Timoshenko theory or thick beam theory considers the effect of shear deformation, in addition to the effect of rotary inertia, to describe the behavior of thick beams [64].

Based on the Euler–Bernoulli beam theory, the long and thin beam which coupled with the piezoelectric layer as an actuator is studied and its equation of motion is derived [65]. Daqaq et. al studied the nonlinear vibrations and frequency response analysis of microcantilevers actuated with a piezoelectric material [66]. Also, the analytical solution for nonlinear-free vibration of viscoelastic microcantilevers covered with a piezoelectric actuator has been studied [54]. The cantilever is a Euler–Bernoulli beam and a layer of the piezoelectric actuator is bonded to its surface. Nonlinear-forced vibrations of piezoelectrically actuated viscoelastic Euler Bernoulli beam was studied with the method of Multiple Scales, and the governing equation of motion was derived for this beam [67]. Analytical solution for the nonlinear free and forced response of a viscoelastic piezoelectric cantilever beam resting on a nonlinear elastic foundation to external harmonic excitation has been investigated. This work is of high importance as it can be used in real-world applications since many engineering structures rest on an elastic foundation. Also biological sensor for post-surgery monitoring of heart wall motion is one of the interesting applications of this study [68]. Also, Mareishi et al. studied analytical solution for free and forced vibration response of smart laminated nano-composite beams resting on a nonlinear elastic foundation that is under external harmonic excitation [69]. Additionally, dynamic stability of the slender laminated composite Euler Bernoulli beam is investigated in the beam that has a piezoelectric layer and is subjected to axial periodic loads [70, 71]. The free and forced vibration of a functionally graded beam was studied within the framework of Euler-Bernoulli beam theory. The Galerkin procedure is used to obtain a second-order nonlinear ordinary differential equation for this beam which has cubic and quadratic nonlinear terms. The natural frequencies are obtained for a nonlinear problem and also, forced vibration of the system in primary resonance has been studied [72].

Nonlinear vibration response of a microcantilever, which has a piezoelectric actuator and subjected to tip-sample interaction, had been studied. The effects of the geometric dimensions of the piezoelectric actuator on the response of the system had been considered [73].

Free vibration analysis of multi-span Timoshenko beams was investigated with using the assumed mode method [74]. The equation of motion of the structure is derived to obtain natural frequency and free vibration responses of the multi-span beams. Also, the interpolation functions were used to modify the mode shapes of the beams.

Vibration analysis of a rotating Timoshenko beam with finite element method was considered, and the stiffness and mass matrices of a rotating twisted beam element were developed [75]. Also, the first four natural frequencies and mode shapes were calculated in bending-bending mode.

A functionally graded piezoelectric Timoshenko smart beam was proposed to describe the electro-mechanical static response of the beam [76]. Mechanical loads and electric potential are applied to the beam, and a multiquadric radial basis function method was used to analysis the behavior of the smart beam.

In addition to that, the buckling behavior of piezoelectric nanowires using the Timoshenko beam theory was investigated [77]. A distributed transverse load was applied to the structure, and analytical relations for the critical force of axial buckling of nanowires were given. Thermo-Electrical Loads was used to study the behavior of Piezoelectric functionally graded material (FGM) Timoshenko beams [78]. The exact solution was presented for the nonlinear response of FGM Timoshenko beams.

Forced vibration analysis of the beam which is covered with a piecewise piezoelectric layer as an actuator in terms of harmonic mechanical excitation is of great significance as it can be employed in practical conditions such as constructing sensors for vibration measurements and actuators for developing robotic systems. Also using flexible piezoelectric systems for energy harvesting is one of the interesting applications in this area [79].

2.9 ACTIVE VIBRATION CONTROL USING PAIRED SENSOR-ACTUATOR

Recently using smart materials such as piezoelectric material has been considered by many researchers. Using these materials as a sensor and actuator helps to control the vibration in different dynamic structures. These kinds of structures use smart sensor and actuator called ‘smart structures’ or ‘smart adaptive structures’. Using piezoelectric sensor and actuator for vibration control causes the structure to sense the vibration and automatically react to control it [80]. Designing a system which has an accurate electromechanical interface between the structure and piezoelectric materials is essential for active vibration control [70].

The dynamic stability behaviour of the laminated composite beam was investigated in 2002 [70]. The model was a slender beam which had two layers of piezoelectric; one layer as a sensor on top and another layer as an actuator on the bottom surface of the beam. An axial periodic compressive load was applied to the beam which was fixed at both ends and finally the dynamic stability of the beam was investigated. Dynamic response of the beam was controlled using a closed control algorithm which employed the direct and converse piezoelectric effects. Also the effect of control gain on the beam response in the active control loop was studied.

Li et al. [81] studied active vibration control of a pyramidal lattice sandwich beam using a piezoelectric sensor and actuator which were attached on the top and bottom surfaces of the beam. The piezoelectric materials are to act as the actuator and sensor. In the structural modelling, the discrete lattice truss core is converted to an equivalent homogenized continuum material. Hamilton’s principle was used to derive the dynamical model of the structure. The vibration of system was reduced using velocity feedback control method. The responses of the system were found to investigate the control effects on the sandwich beam. The numerical result from simulation showed that the velocity feedback control methods are effective for vibration suppression.

A new strategy was developed by Li et al. to actively control the vibration of an elastic beam to which piezoelectric actuators and sensors were bonded to its surfaces periodically.

The equations of motion of the structure are derived using Hamilton's principle to study the beam behaviour. Stability of the system was increased by using a negative proportional feedback control system. The control voltages that induced the piezoelectric actuators were in sensible ranges and finally the vibration of the elastic beam was tuned by the periodically placed piezoelectric layers [82].

A one-dimensional theory for a beam which had layers of piezoelectric material as sensors and actuators is developed to study the beam behaviour in active control system. The equations of motion of the associated boundary conditions are derived for the vibrations of a piezoelectrically actuated beam to find the relations between longitudinal deflection and bending deflection [83].

Active vibration control of a lightly damped T-beam is studied to control the torsional and bending modes of the beam. Piezo ceramic actuators and sensors and also a linear quadratic Gaussian controller were used in the active control system. The simulation results showed that the control system has a very significant effect on vibration control [80].

Aldraihem et al. investigated the vibration attenuation of a laminated beam as a smart structure and derived the equation of motion of the beam. The piezoelectric material was bonded on the beam surface as a sensor and actuator. They studied the effect of active vibration on both Euler-Bernoulli and Timoshenko beam using finite element method. The results showed that using Euler-Bernoulli beam model can lead to instability because of the unconsidered modes [84].

Active Vibration Suppression of a composite cantilevered Euler–Bernoulli beam which includes an elastic piezoelectric sensor and actuator were examined by Djojodihardjo et al in 2015. Analytical solution for beam response was defined when the beam carried a spring loading at its tip. Hamilton's principle was used to derive the equation of motion of the beam and Galerkin based finite element Analysis was used to solve the problem. The result of the study is practical in the light-weight structures in space applications, such as robot's arms, solar panels and antennas [85].

The vibration control of a rotating composite thin-walled beam is studied by Choi et al. The beam response was found using a single cell composite beam and the piezoelectric effect was considered to derive the equations. A feedback control algorithm was used to supress the vibration of the structure [86].

A velocity feedback control algorithm was used for vibration control of an aircraft wing. Fiber reinforced and piezo-composite was used in the thin-walled beam model to develop a smart structure. The beam response was found using Hamilton's principle and the effect of different parameters such as size and position of piezoelectric actuator were studied [87].

In this research human hand and forearm were modelled in discrete and continuous formats to investigate the effect of the control system on the tremor reduction and suppression.

2.10 Tremor Classification

Defining human body's tremor and finding tremor characteristics is one of the research area of interest for many researchers. Developing any kind of tremor treatment needs to define the severity of tremor in the patients as the range of tremor amplitude and frequency is different for patients. Detecting tremor behaviour is essential in recommending a suitable therapy to decrease its psychological, physical and social impact.

Cheraghizanjani et al. developed a tremor test rig which measured the level of tremor in some patients with neurological diseases. They investigated two kinds of tremor, postural and rest tremor in the hand in horizontal and vertical directions using laser displacement sensors. Finally they analysed and classified the tremor using programming [3].

A smartphone-based application was developed to identify Parkinson's and Essential postural tremors using discrete wavelet transforms and support vector machines with a high accuracy, about 96%. This research is of great significance as discriminating between Parkinson's and essential tremor is difficult in many situations. In this study a novel method was proposed that used attention and distraction during tremor recording. The result showed that using attention and distraction has a significant effect on identification of Parkinson's and essential tremor [88].

Camara et al. used local field potentials (LFP) to record data in the subthalamic nucleus of 7 Parkinsonian patients. They used some inserted electrodes of a deep brain stimulation (DBS). This kind of data recording is effective as there is a proper access to sub-cortical data which led to the use of the recorded results into real medical devices. Artificial intelligence techniques were used to select appropriate feature and detect tremor types [89]. A comparative analysis between Support Vector Machines and neural networks was done in 2012 to classify tremor using imbedded microelectrode in the brain of a PD patient. The performance of a Support Vector Machine (SVM) was compared with a Multiple Layer Perceptron (MLP) and a Radial Basis Function Network (RBN) which are two famous artificial neural network classifiers. The results showed using SVM provide more appropriate result for tremor classification specially in Parkinson's disease (PD) data [90].

Tremor type was identified using pattern analysis of sEMG signals in 2010. In this study sEMG sensors were attached to the patient's body in different positions and patients were asked to do some special task. A classifier system was developed to recognize the tremor type in the automatic process. The designed model was appropriate to identify the best attachment point for sEMG electrodes and most proper features to get to the practical results in the process of classification [91].

In another research the analysis of sEMG was presented for Parkinson's disease. EMG signal was analysed by histogram and crossing rate (CR) method. In this study EMG signals were recorded from 25 patients and 22 healthy subjects and the proposed method was used to discriminate patients from healthy subjects [92].

Jeon et al. applied machine learning to classify tremor severity in PD with High-accuracy automatic. A wearable device of the wristwatch-type and also a gyroscope and accelerometer were used to record data from 85 Parkinsonian patients. During the experiment they were asked to do four tasks and tremor was recorded in the resting, postural and intention task position. Recorded data was analysed to extract appropriate features for classification. Also using accelerometer data, displacement and angle signals were found. The results specified the proposed system is as a practical tool for identifying tremor severity in PD [93].

Also, acceleration of hand tremor in PD and essential tremor were recorded for 25 subject and a novel method was used to process the data set and identify tremor type in two different groups. SVM and singular value decomposition (SVD) was applied to extract the features and analyse the data set. The results illustrated that proposed method was effective for tremor classification with high accuracy [94].

In another research a new feature was developed to classify tremor in essential tremor (ET) and PD. Tremor in PD is seen in the resting position of the hand but in the ET it is higher during action task. In this study tremor was recorded using a triaxial gyroscope sensor. The sensor was attached to the subject's finger during resting and action task. Finally the SVM was used as a classifier to distinguish PD tremor from ET [95].

Wearable motion and audio sensors were used to record data signal from PD to classify tremor severity in three level; mild, moderate and severe. Empirical Wavelet transform (EWT) and empirical wavelet packet transform (EWPT) were used to break down recorded data to different levels. Amplitudes and frequencies of signals were identified to extract the best features for the classification process. Three classifiers were used for data analyses which were called extreme learning machine (ELM), K-nearest neighbour (KNN) and probabilistic neural network (PNN). Experimental results established that the proposed method was an effective system to discriminate PD from healthy subjects and also showed the tremor severity in PD with classification accuracies of more than 90% [96].

2.10.1 Electromyography

During movement, human's muscles generate electrical signals which are called electromyography (EMG) or myoelectric signal (MES). Recording and analysing these signals help many researchers to identify movement characteristics. Also recording EMG signals from people who have some movement disorders are of interest to many researchers as they can analyse the signals to provide the best treatment. The electric signal which is generated in the muscle relates to the concept of a motor unit (MU).This human motor system supports a wide range of human movements and muscle contraction [97].

Simplified human motor system and role of MU in human movement is shown in Figure 2-6.

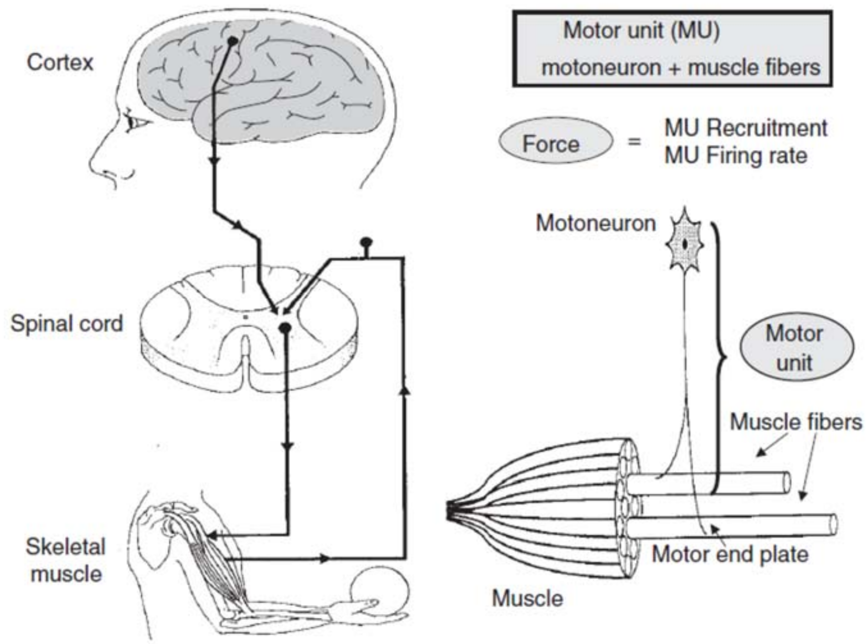

Figure 2-6. A simplified diagram of motor control system and motor unit [97]

Powerful signals are generated by the human cortex which take effect on the motoneurons of the human spinal cord. When the motorneuron which is a part of MU is activated, the muscle fibres are innervated. There are different numbers of MUs for different kinds of muscles. Depending on the size of muscle, for small hand muscle to large muscles, the number of MUs are approximately between 100 to 1000 or more. Also each MU is able to produces a wide range of force [98, 99].

The EMG signal is a stochastic or random signal whose amplitude can range from 0 to 1.5 mV (root mean square) and also it is from 0 to 10 mV (peak-to-peak). The frequency of energy above the electrical noise level is between 0 to 500 Hz and the main energy of the noise is in from 50 to150 Hz [100]. EMG signals are associated with noise and distinguishing the actual EMG signal is difficult due to these noises. There are different properties which have effect on EMG signals such as individual form of skin, the velocity of blood flow, tissue structure and skin temperatures. These properties cause the generation of a different kind of noise which has an effect on the signal qualification. The main noise resources in EMG recording are inherent noise in the electrode, movement artifact, electromagnetic noise, cross talk, internal noise inherent instability of the signal [101].

Using a differential amplifier is one of the effective ways for noise reduction in EMG recording. An electronic circuit is used to remove the existence signal of two electrodes in the differential amplifier and also amplify the difference. Finally, the actual EMG signals will be amplified, and noise signals will be detached. During the data recording, the noise generated by motion artefacts occur which has two main sources; cable movement which connect electrode to the amplifier and also connection between electrode surface and skin [100].

2.10.2 Electromyography pattern recognition

Todays, researchers use EMG signal as a valuable source for developing rehabilitation devices to help disable people. They use recorded EMG signal to control human movement such as developing devices for hand or leg rehabilitation. There are two ways for using EMG signals for movement control; EMG-based pattern recognition and non-pattern recognition system [102].

EMG signals are classified to different classes, based on the EMG-based pattern recognition (EMG-PR) but in non-pattern recognition (EMG-non-PR) human movements are analysed from movement characteristics view such as angle of movement or produced force from muscle activity. Figure 2-7 illustrates the principle steps in EMG-PR system.

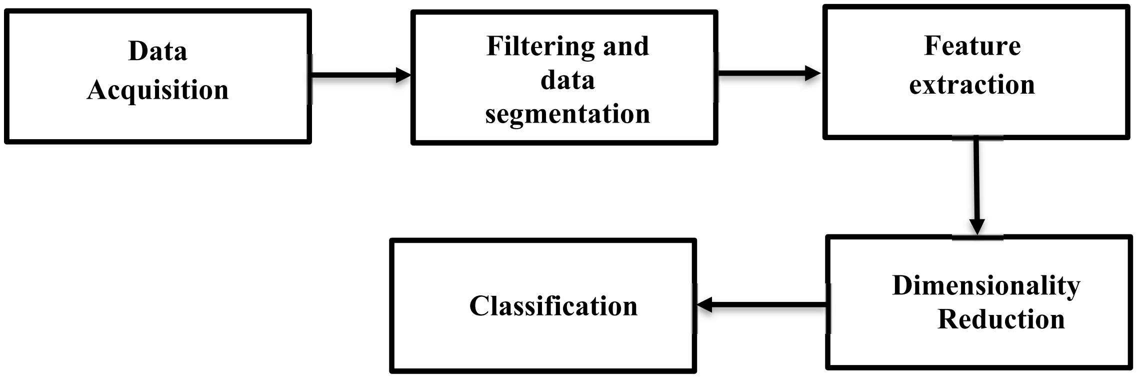

Figure 2-7. EMG pattern recognition system

First, EMG electrodes are attached to the skin and EMG signals are recorded from muscle activity. Then some pre-processing steps are done on the dataset to identify different classes for EMG dataset. The main pre-processing step on the EMG data can be divided into four main stages; filtering and data segmentation, feature extraction, feature reduction and classification as shown in Figure 2-7.

2.10.2.1 Filtering

One of the pre- processing steps in EMG analysis is noise filtering which tries to attenuate noises from recorded data. A high-pass filter with cut-off frequency near 10–20 Hz and a low-pass filter with a cut-off frequency near 400–450 Hz can be applied to the dataset to reduce unwanted noises. Due to movement artifacts and also electrode–skin interface instability the EMG signals include unwanted noise in the frequency range 0 to 20 Hz. In this case, the high-pass filter with a cut-off frequency in the 15 to 20 Hz range will be used. Also, a notch filter can be used to remove the noise with the frequency of 50 Hz or 60 Hz. Using a notch filter is not recommended in all cases as it removes some frequency band from high-power density EMG signals and also causes phase rotation in some frequencies [97].

2.10.2.2 Data segmentation

The EMG data is recorded and considered in the special period for feature extraction. This period is called segment. The process of pattern recognition is performed based on the data in this period. The processing time of generating control commands for classification plus a neighbouring segment length should be equal to or less than 300 ms because of real-time restrictions. Also the segment length must be chosen large enough as features variance increases when the length of segment reduces and this will have a negative effect on classification [103, 104].

There are two different ways for data segmentation in the classification process. The first one is disjoint or overlapped windowing which is only associated with the window length and shown in Figure 2-8 [103].

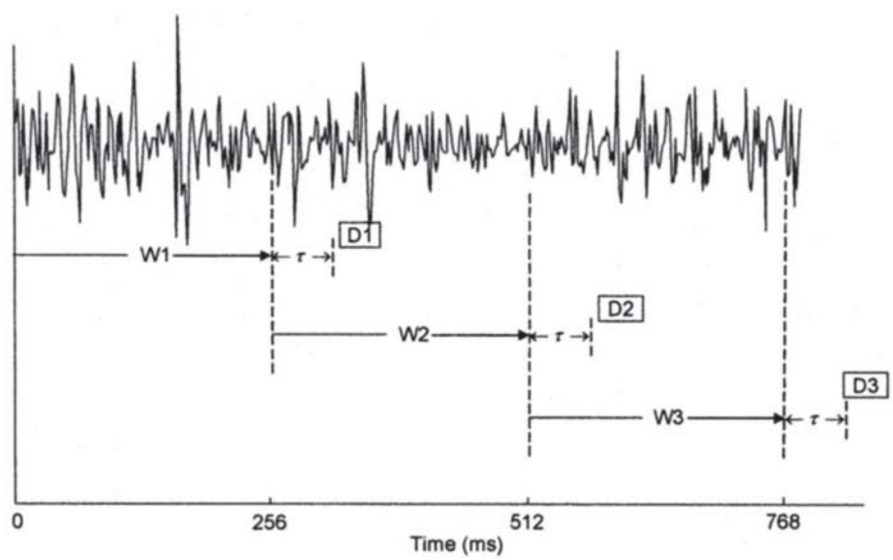

Figure 2-8. Disjoint windowing in data segmentation [103]

The second way is the overlapped windowing which is associated with the window length and window increment. The overlapped windowing is illustrated in Figure 2-9 . The time period between two continuous windows is called the window increment [103].

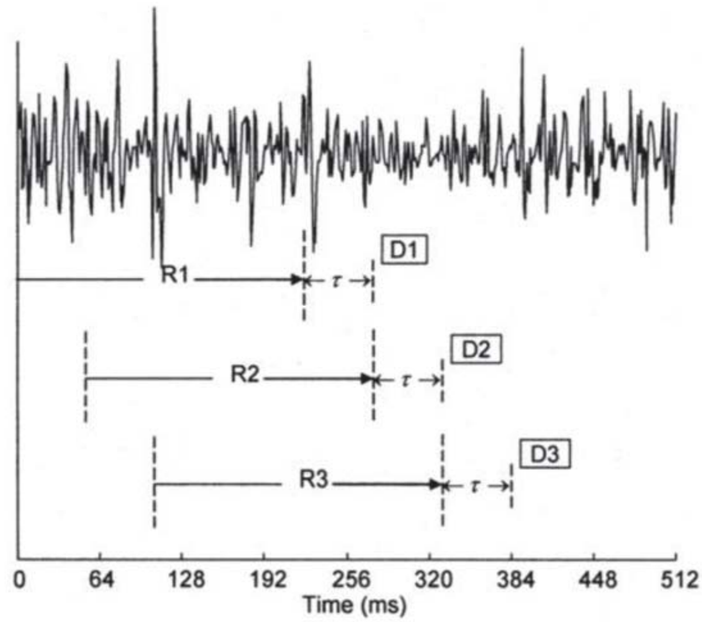

Figure 2-9. Overlapped windowing in data segmentation. Sequence of ms records (R1, R2, and R3) are used to make decisions at times D1, D2, and D3 [103].

Another concept that has direct effect on the EMG pattern recognition is transient and steady state of the EMG signals. In the muscle contraction process, when the contraction is started from rest position transient state is considered. On the other hand, if the contraction is maintained in the special level (EMG level in that position), the steady state is considered. In the majority of EMG pattern recognition, the steady state response is considered to increase the accuracy of classification. Figure 2-10 shows the classification error for transient and steady state of the EMG signals [103].

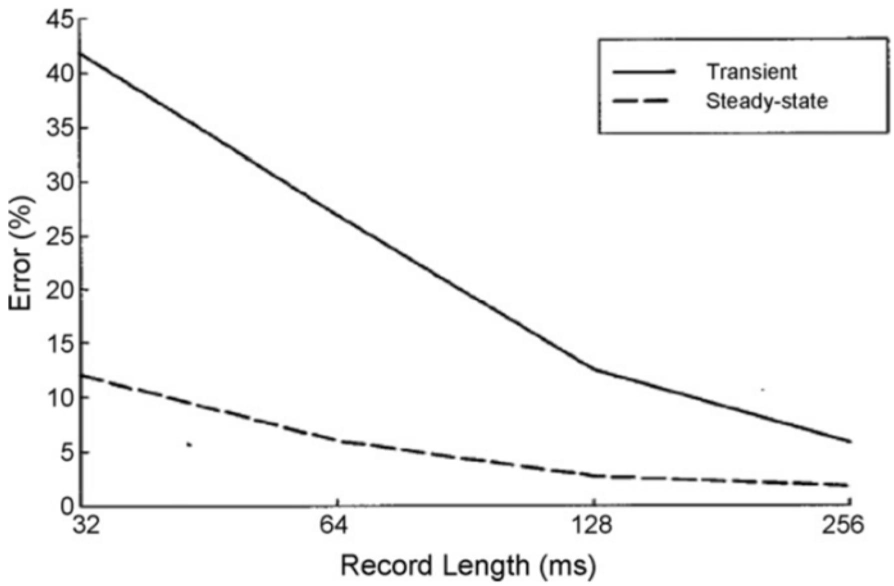

Figure 2-10. Classification error [103]

2.10.2.3 Feature extraction

As it is seen in the Figure 2-7, one of the main steps in EMG pattern recognition is feature extraction. In the Feature extraction useful information in EMG signal are extracted and the useless EMG signals are removed [105]. An effective and practical feature should have three properties which include maximum class separability, robustness, and complexity [106, 107].

If the feature has maximum class separability the misclassification rate will be in the lowest possibility. The second condition is robustness. Also the feature will maintain its class separability in real-time situation if it has robustness Also if the feature complexity is kept in the lowest possibility, it is applied in real-time environment [100].

There are three different kind of EMG features in different domains; time domain, frequency domain and time-frequency domain features.

2.10.2.3.1 Time domain (TD) features

Time domain features are one of the groups of interest to researchers for EMG classification as in time domain, there is no need for any transformation and calculation on the EMG data and using these groups of features are easy and quick. EMG signals have a non-stationary property in that the statistical properties change during time, but TD features undertake the data as a stationary signal. This is the main drawback of TD features. Generally, this group of features are used extensively for their reasonable performances when there is not much noise in the environments. Here are some of the most used features in EMG classification [105].

1. Integrated EMG (IEMG)

(IEMG) is as a summation of absolute values of the EMG signal amplitude. This feature is used in clinical application and as an onset detection index in EMG non-pattern recognition and it is defined as [105]:

$$\text{IEMG} = \sum_{n=1}^{N} |x_n| \qquad \text{Equation 2-1}$$

2. Mean absolute value (MAV)

MAV is one of the popular features which is used in detection of the surface EMG signal for the limb control. MAV is an average of the absolute value of the amplitude of the EMG signal in a specific segment. It is defined as [105]:

$$\text{MAV} = \frac{1}{N} \sum_{n=1}^{N} |x_n| \qquad \text{Equation 2-2}$$

3. Modified mean absolute value type 1

In this feature the effect of weighted window function w_n is considered in the feature equation to increase the accuracy of MAV feature. It is shown as[105]:

$$\mathrm{MAV1} = \frac{1}{N}\sum_{n=1}^{N} w_n \left| X_n \right|$$
$$w_i = \begin{cases} 1 & 0.25N \le n \le 0.75N \\ 0.5 & \text{otherwise} \end{cases}$$ Equation 2-3

4. Zero crossings (ZC)

In this feature the number of times which the signal crosses the zero is counted. To reduce the effect of noise, threshold condition is considered around zero crossing. ZC is represented as [105]:

$$\mathrm{ZC} = \sum_{n=1}^{N-1} \left[\mathrm{sgn}(x_n \times x_{n+1}) \cap \left| x_n - x_{n+1} \right| \ge \text{threshold} \right]$$
$$\mathrm{sgn}(x) = \begin{cases} 1 & x \ge \text{hreshold} \\ 0 & \text{otherwise} \end{cases}$$ Equation 2-4

5. Waveform length (WL)

Waveform length is a feature which considers cumulative length of the EMG signal along a segment and it is given as [105]:

$$\mathrm{WL} = \sum_{n=1}^{N-1} \left| x_{n+1} - x_n \right|$$ Equation 2-5

6. Autoregressive (AR) features

This feature tries to make the non-stationary signal as a stationary Gaussian process in a segment. This feature defines each sample of the EMG signal as a linear combination of the previous samples x_{i-p} plus a white noise error term t_i. Also, coefficients of the AR model a_p is as a feature vector. It is given by [105]:

$$x_i = \sum_{p=1}^{P} a_p x_{i-p} + t_i \qquad \text{Equation 2-6}$$

where P is the order of the AR model.

7. Slope sign changes (SSC)

SSC counts the number of times that the sign of slope changes. This feature is define by [105]:

$$\text{SSC} = \sum_{n=2}^{N-1} f\left[(x_n - x_{n-1}) \times (x_n - x_{n+1})\right]$$
$$f(x) = \begin{cases} 1 & x \geq \text{threshold} \\ 0 & \text{otherwise} \end{cases} \qquad \text{Equation 2-7}$$

8. Hjorth time domain parameters (HTD)

This time domain feature introduced by Hjorth in 1970 for Electroencephalography (EEG) activity and it can be applied to EMG signals too. The parameters for this feature are Activity, Mobility, and Complexity [100].

$$\text{Activity}: m_0 = \text{var}(x(t))$$
$$\text{Mobility}: m_1 = \sqrt{\frac{m_0(\frac{dx(t)}{dt})}{m_0(x(t))}} \qquad \text{Equation 2-8}$$
$$\text{Complexity}: m_2 = \frac{m_1(\frac{dx(t)}{dt})}{m_1(x(t))}$$

2.10.2.3.2 Frequency domain (FD) features

FD features, which are also called spectral domain features, are of more interest in fatigue analysis. These Features are generally attained from power spectral density (PSD). Mean frequency (MNF) and median frequency (MDF) are two variables of the PSD which are used commonly. There are different FD features which some of them are of more interest to researchers [105].

1. Peak frequency (PKF)

The frequency which includes the maximum power is PKF and it is defined as [105]:

$$\text{PFK} = \max(P_i), \quad i = 1, \ldots, N \qquad \text{Equation 2-9}$$

2. Mean frequency (MNF)

MNF is an average frequency that is attained from the sum of the frequency product and its power spectrum divided by the total power spectrum summation and it is shown as [105]:

$$\text{MNF} = \frac{\sum_{n=1}^{N} f_n P_n}{\sum_{n=1}^{N} P_n} \qquad \text{Equation 2-10}$$

3. Median frequency (MDF)

MDF is defined as a frequency that divides the spectrum into two regions with equal amplitude; it is expressed as [105]:

$$\sum_{n=1}^{\text{MDF}} P_n = \sum_{n=\text{MDF}}^{N} P_n = \frac{1}{2}\sum_{n=1}^{N} P_n \qquad \text{Equation 2-11}$$

4. Mean power (MNP)

Average power of the EMG power spectrum is MNP which is defined as [105]:

$$\text{MNP} = \frac{\sum_{n=1}^{N} P_n}{N} \qquad \text{Equation 2-12}$$

2.10.2.3.3 Time-frequency domain (TFD)

Using TFD features provides a description of the physical properties with higher accuracy than TD or FD features as TDF considers the energy of the EMG signals in time and frequency domains. On the other hand, using this group of features is not of interest and practical as they need lots of calculation [108].

2.10.2.4 Dimensionality reduction

As it is seen in Figure 2-7, the next step after feature selection is feature reduction. In feature extraction step, all features are extracted from EMG data to make a large feature set. In the feature extraction process the raw EMG signals are displayed as a feature vector and are used as an input to the classifier. Raw EMG signals are not practical as they are random and also directly feed to the classifier. In classification process, features are reduced in the dimension to avoid overloading the classifier where the classifier can work accurately in different scenario. Dimensionality Reduction is achieved by using different dimension reduction methods [101].

Two popular methods of dimensionality reduction are feature selection (FS) and feature projection (FP). FS selects a feature subgroup from initial features to decrease dimension of features but the FP transforms the initial features to a new feature space which has a smaller dimension. For EMG signals classification, the FP is more interesting than the FS as FP has large variance of the EMG signals [108].

There are two different classes for feature projection which are called supervised and unsupervised method. Linear discriminant analysis (LDA) is one example of the supervised method which contains the class knowledge into the projection [109]. Principle component analysis (PCA) which is a sample of the unsupervised method projects the feature space into a new space without any class information [110].

2.10.2.4.1 Linear discriminant analysis (LDA)

The vectors which best discriminate between the classes is searched for in the LDA rather than searching for vectors that have best description of feature. In fact LDA maximize the *between-class* scatter matrix while minimizing the *within-class* scatter matrix [100]. The within-class scatter matrix is defined as:

$$S_w = \sum_{i=1}^{C}\sum_{i=1}^{N_j}(x_i^j - \mu_j)(x_i^j - \mu_j)^T$$ Equation 2-13

where C is the number of classes, Nj is the number of samples in class j, x_i^j as a matrix is the ith sample of class j and μ_j is the mean of the class j. The *between-class* scatter matrix is described as:

$$S_b = \sum_{i=1}^{c}(\mu_j - \mu)(\mu_j - \mu)^T$$ Equation 2-14

2.10.2.4.2 Principle component analysis (PCA)

PCA extracts and maintains the main and most significant information and causes the size of dataset to be compressed. In fact, PCA calculates the main calculated components from the linear combination in initial dataset [100].

If there is a feature set in the form of $X = (x_1, \ldots, x_N)$ that X is a matrix with t-dimensional space and N shows the number of samples, a linear transformation that transform t-dimensional space of features onto m-dimensional space can be found by PCA [100]. A new feature can be expressed as:

$$y_i = P_l^T X_i \qquad i = 1, \ldots, N$$ Equation 2-15

which P_l shows the linear transformation for features which transfer from t to m-dimensional space with $m \ll t$.

The singular value decomposition method (SVD) is used to find the eigenvalues. P_l consists of columns that are the eigenvectors e_i.

$$\lambda_i e_i = Q_c e_i$$
$$Q_c = XX^T$$ Equation 2-16

where λ_i is the eigenvalue associated with the eigenvector e_i and Q_c is the covariance matrix [100].

2.10.2.5 EMG classification

The next step in EMG classification after feature selection and feature reduction, is classification, Figure 2-7. The main aim of classifier is classifying the extracted and reduced features to special classes. There are various kinds of classifiers for EMG classification process such as Fuzzy classifier , Self-Organizing Map (SOM), Artificial Neural Network (ANN) , Support Vector Machines (SVM))[105, 111], Linear Discriminant Analysis (LDA)[112], Multilayer Perceptron (MLP) [113], Hidden Markov Model (HMM) [114] , Feed-Forward Neural Networks (FNN) [115], K-Nearest Neighbour (KNN) [116] .

Extreme learning machine **(**ELM) is a new classifier which was invented by the ANN and is of interest to many researchers in this area [104, 117, 118]. As this classifier is famous and it is used in many EMG application, the following section will explain it in more detail.

2.10.2.5.1 Extreme learning machine (ELM)

Essentially, ELM is as a single-hidden-layer feed-forward networks (SLFNs). The schematic concept of ELM is shown in Figure 2-11.

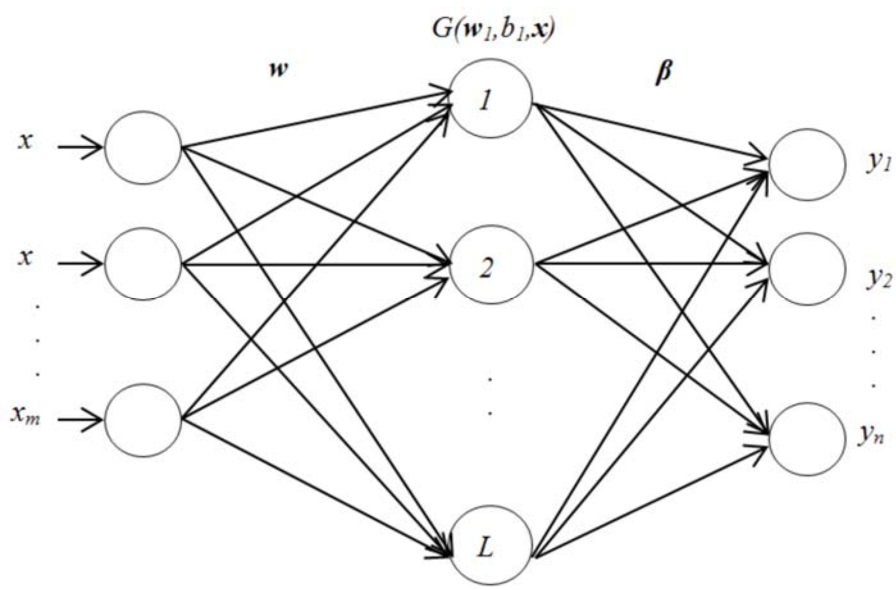

Figure 2-11. Single feed-forward networks for extreme learning machine [100]

When there is input $x_j = [x_{j1}, x_{j2}, \ldots, x_{jm}]^T \in R^m$ and target $y_j = [y_{j1}, y_{j2}, \ldots, y_{jn}]^T \in R^n$ for N different sample of (xj, yj), the output of a standard SLFN with *L* hidden neurons is given as:

$$f_j(x) = \sum_{i=1}^{L} \beta_{jL} g(w_i x_j + b_i) = H\beta \quad j = 1, \ldots, N$$ Equation 2-17

where $\beta_{jL} = [\beta_{j1}, \beta_{j2}, \ldots, \beta_{jL}]^T$ represents the weight vector of j*th* hidden and output neuron, g(x) denotes the activation function of the hidden node, $w_i = [w_{i1}, w_{i2}, \ldots, w_{im}]^T$ shows the vector of the weight for the i*th* hidden and input neurons , b_i is the threshold for the i*th* hidden neuron and H is the hidden layer output matrix and is defined as:

$$H = \begin{bmatrix} g(w_1 x_1 + b_1) & \ldots & g(w_L x_1 + b_L) \\ \vdots & & \vdots \\ g(w_1 x_N + b_1) & \cdots & g(w_L x_N + b_L) \end{bmatrix}$$ Equation 2-18

Also β in right side of Equation 2-15 is given as:

$$\beta = \begin{bmatrix} \beta_1^T \\ \vdots \\ \beta_1^T \end{bmatrix}$$ Equation 2-19

The aim of the ELM is not only to minimize the training error, it also minimizes the norm of the output weights, which is:

$$\min_{w_i, b_i, \beta} : \left\| H(w_1, \ldots, w_L, b_1, \ldots, b_L)\beta - T \right\|^2$$ Equation 2-20

Equation 2-20 can be written in new form as in the ELM, the input weights w_i and biases b_i are allocated randomly.

$$\min_{\beta} : \left\| H\beta - T \right\|^2$$ Equation 2-21

Considering the minimum norm, the least-square solution of Equation **2-21** is given as:

$$\beta : H^{*}T$$ Equation 2-22

as T shows the target and is defined as:

$$T = \begin{bmatrix} y_1^T \\ \vdots \\ y_1^T \end{bmatrix}$$ Equation 2-23

and H^* shows the Moore–Penrose generalized inverse of the matrix *H.*

Finally, the optimization of the ELM training can be written as follows:

$$\text{Minimize}: \mathrm{L}_{\mathrm{P}_{\mathrm{ELM}}} = \frac{1}{2}\left\|\beta\right\|^2 + c\frac{1}{2}\sum_{i=1}^{N}\left\|\zeta_i\right\|^2$$
$$g(x_i)\beta = t_i^T - \zeta_i^T \qquad i = 1,...,$$ Equation 2-24

where c is a user-specified parameter and $\zeta_i^T = [\zeta_{i,1}, \zeta_{i,2}, \ldots, \zeta_{i,n}]^T$ is the output vector error.

The training of ELM is the solution of Equation 2-23 the dual optimization problem based on Karush-Khun-Tucker (KKT) theorem. Then:

$$\mathrm{L}_{D_{\mathrm{ELM}}} = \frac{1}{2}\left\|\beta\right\|^2 + c\frac{1}{2}\sum_{i=1}^{N}\left\|\zeta_i\right\|^2 - \sum_{i=1}^{N}\sum_{j=1}^{n}\alpha_{i,j}(g(x_i)\beta_j - t_{i,j} + \zeta_{i,j})$$ Equation 2-25

as $g(x_i)$ is a feature mapping (hidden layer output vector), β_j is the output weight linking the hidden layer and the j*th* output node. Also $\beta_j = \left[\beta_1,...,\beta_n\right]$. Taking partial differentiation of $\mathrm{L}_{D_{\mathrm{ELM}}}$ over ζ_i and making it equal to zero gives:

$$\frac{\partial L_{D_{ELM}}}{\partial \zeta_i} = 0 \rightarrow \{\alpha_i = c\zeta_j \qquad \text{Equation 2-26}$$

Also taking partial differentiation of $\mathrm{L}_{D_{\mathrm{ELM}}}$ over α_i and making it equal to zero is defined as:

$$\frac{\partial L_{D_{ELM}}}{\partial \alpha_i} = 0 \rightarrow \{g(x_i)\beta - t_i^T + \zeta_i^T = 0 \qquad \text{Equation 2-27}$$

And finally taking partial differentiation of $\mathrm{L}_{D_{\mathrm{ELM}}}$ over β_j and making it equal to zero is given as follows:

$$\frac{\partial L_{D_{ELM}}}{\partial \beta_j} = 0 \rightarrow \begin{cases} \beta_j = \sum_{j=1}^{N} \alpha_{i,j} g(x_i)^T \\ \beta = H^T \alpha \end{cases} \qquad \text{Equation 2-28}$$

as $\alpha = [\alpha_1, \alpha_2, \ldots, \alpha_N]$ and $\alpha_i = [\alpha_{i,1}, \alpha_{i,2}, \ldots, \alpha_{i,n}]$.

Substituting Equation 2-26 and Equation 2-27 into Equation 2-28 gives:

$$(\frac{1}{c} + HH^T)\alpha = T \qquad \text{Equation 2-29}$$

as T is given as follow:

$$T = \begin{bmatrix} t_1^T \\ \vdots \\ t_N^T \end{bmatrix} = \begin{bmatrix} T_{11} & \cdots & T_{1n} \\ \vdots & & \vdots \\ T_{N1} & \cdots & T_{Nn} \end{bmatrix} \qquad \text{Equation 2-30}$$

Using Equation 2-22 and Equation 2-30:

$$\beta = H^T(\frac{1}{c} + HH^T)T \qquad \text{Equation 2-31}$$

Equation 2-17 can be written as:

$$f(x) = g(x)\beta = g(x)H^T(\frac{1}{c} + HH^T)^{-1}T$$ Equation 2-32

The output of the ELM can be rewritten as follows if the training data is very large (as it is demonstrated in [117]):

$$f(x) = g(x)\beta = g(x)H^T(\frac{1}{c} + HH^T)^{-1}H^T T$$ Equation 2-33

g(x) is defined as:

$$g(x) = [Q_n(w_1, b_1, x), \ldots, Q_n(w, b_1, x)]$$ Equation 2-34

where Q_n is a non-linear piecewise continuous function and it can be defined as one of the following functions [100]:

- Sigmoid function

$$Q_n(w, b, x) = \frac{1}{1 + \exp(-(wx + b))}$$ Equation 2-35

- Gaussian function

$$Q_n(w, b, x) = \exp(-b\|x - w\|^2)$$ Equation 2-36

- Multi-quadratic function

$$Q_n(w, b, x) = (\|x - w\|^2 + b^2)^{1/2}$$ Equation 2-37

- Hard-limit function

$$Q_n(w, b, x) = \begin{cases} 1 & (wx - b) \geq 0 \\ 0 & \text{otherwise} \end{cases}$$ Equation 2-38

Chapter 3: Active Force Control Method for Tremor Suppression in Human Hand and Forearm

3.1 Introduction

Because tremor as a neurological disorder might affect the patients' life, investigating to find an effective way to attenuate the tremor is essential for affected people. In this chapter active force control (AFC) system is proposed to analyse the behaviour of upper limb tremor in the human body. A single piezoelectric actuator is embedded in the developed AFC system for controlling the behavior of PD controller. Tremor is applied to the AFC as a disturbance and the proposed design tries to make a constant output close to zero. As a result, tremor in the upper limb will be supressed in the developed system during a special time. The proposed AFC system can be used in the rehabilitation device for tremor suppression as it can attenuate just involuntary movement. Also using AFC for assistive device is reasonable due to proper and user-friendly equipment. Three different models which include a 4-DOF biomedical model of the hand, a 1-DOF musculoskeletal model of the elbow joint and a 3-DOF musculoskeletal model of the wrist joint are used to investigate the effect of AFC method on tremor suppression.

3.2 Active Force Control (AFC) Method

AFC is a robust controller that is introduced by Hewit [42]. In fact, AFC introduces a cancelling "anti-vibration" wave through an appropriate array of secondary sources. These secondary sources are interconnected through an electronic system using a specific signal processing algorithm for the particular cancellation scheme [119].

Today's active vibration control is a very effective research area that has different application in many technologies. A typical active vibration control system has mechanical and electronic components in the control system. The principle components of any active vibration control system are the mechanical structure influenced by disturbance, sensors for measuring the vibration, controllers, and actuators for suppressing the influence of the disturbance on the structure [120].

The typical form of the AFC system is shown in Figure 3-1 where F_e is the disturbance, F_a is the actuator force K and A(s) are the gain and transfer function of the actuator and s is the Laplace variable. M and M' are the mass and estimated mass of the system, respectively. x is the desired position, $\hat{x}$ is the actual position, ε is the system error and $G(s) = A^{-1}(s)$ [121].

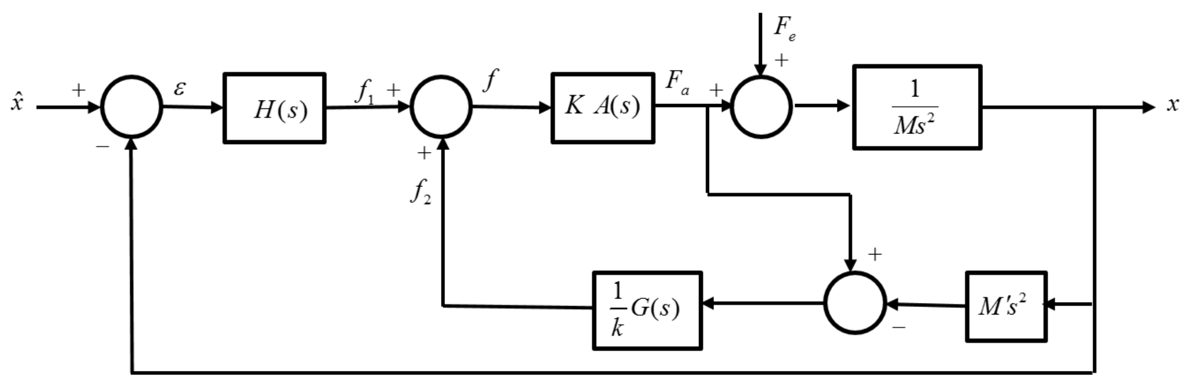

Figure 3-1. Block diagram of the AFC system

For suppressing the hand tremor with use of the AFC scheme, Figure 3-2 is suggested. As it is shown in Figure 3-2, the aim of the proposed design is to make constant output with respect to the disturbance on the system. Actually, this design is an effective control system if the output of the system is invariant. In this figure, *TF* is the transfer function of the piezoelectric actuator, u is the desired position, q is the actual position of the hand. In this

AFC system, a PD controller controls the piezoelectric actuator for damping hand tremor. From Newton's second law of motion, the main AFC equation will be expressed as:

$$F_e^{'} = F_a - M^{'}\ddot{q} \qquad \text{Equation 3-1}$$

where, $F_e^{'}$ is estimated disturbance force, F_a is actuator force, $M^{'}$ is estimated vibratory mass and $\ddot{q}$ is measured acceleration signal [4].

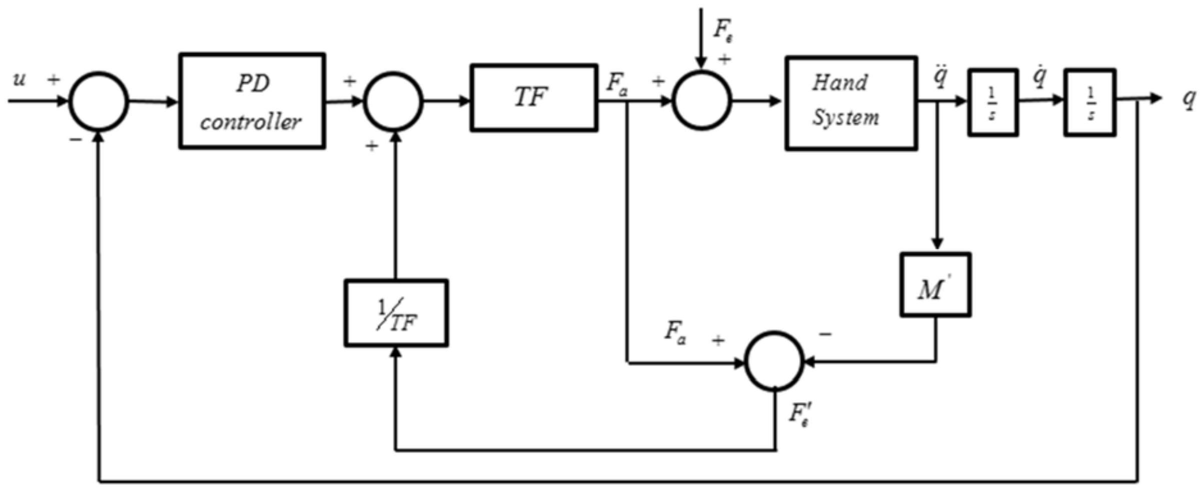

Figure 3-2. A plot of proposed design for active force control system of the human hand

3.2.1 Transfer function of piezoelectric actuator

As one of the main parts of the proposed AFC system which was shown in Figure 3-2, is the piezoelectric actuator, this section provides some information about piezoelectric characteristics which is considerable for piezoelectric actuators.

The word "Piezo" is derived from the Greek word known as pressure [122]. When a piezoelectric material receives an input force, it can induce an electrical charge (as sensor) and when it receives electrical charge it can convert this electrical charge into mechanical energy (as actuator). Therefore, piezoelectric materials have considerable importance working in the field of a smart structure. Smart structures can sense external disturbance with sensors and respond to that with active control that is associated with actuator and

controllers in real time to maintain the mission requirements of these smart structures. Thus, it can be said a smart structure needs four significant ingredients: the structure, sensor, actuator and controller. Piezoelectric actuators and sensors are widely used in various applications and are integrated with the main structure. Piezoelectric actuators have an effective role in today's technology. These actuators have been used in many applications and fields. One of these areas is active vibration control. Piezoelectric devices have some beneficial characteristics for being used in active control systems. This kind of actuators have small dimension and weight and can be simply driven by voltage. Furthermore these actuators are easily controlled and provide fast response [24, 122].
Piezoelectric characteristic can be expressed by Equation **3-2** [123].

$$F_a = \frac{2w_c h_c}{l_c} \cdot \frac{d_{31}}{S_{11}} V_c \qquad \text{Equation 3-2}$$

where F_a is maximum force of piezoelectric actuator [N], w_c is cantilever width [m], h_c is cantilever thickness [m], l_c is cantilever length [m], d_{31} is piezoelectric constant [mv^{-1}], S_{11} is elastic constant of piezoelectric material [m^2N^{-1}], V_c is input voltage [V].

For this simulation study, the parameters used for piezoelectric actuator transfer function are; $w_c = 0.0318m$, $h_c = 0.005m$, $l_c = 0.0635m$, $d_{31} = 190 \times 10^{-12} mv^{-1}$, $S_{11} = 1.613 \times 10^{-11} m^2 N^{-1}$ [24] .

3.2.2 Controller

An AFC system needs to have a controller in the system as it was shown in Figure 3-2. A proportional–integral–derivative controller (PID controller) is a control loop feedback mechanism generally used in industrial control systems. A PID controller continuously calculates an error value as the difference between a measured process variable and a desired set point. The controller attempts to minimize the error over time by adjustment of a control variable of the system. For having a desired result with these controllers, finding appropriate parameters for the PID controller is essential. A general form of a classic PID controller is described in Equation 3-3:

$$\text{output}(t) = K_p e(t) + K_i \int_0^t e(t)dt + K_d \frac{de(t)}{dt} \qquad \text{Equation 3-3}$$

where $output(t)$ is the controller output and $e(t)$ is the error. K_p, K_i and K_d are the proportional, integral and derivative gain, respectively. Some applications may require using only one or two terms to provide the appropriate system control. This is achieved by setting the other parameters to zero. A PID controller will be called a PI, PD, P or I controller in the absence of the respective control actions [124]. In this study, a PD controller is used and heuristic method can be used for determining the PD parameters.

3.3 Biodynamic Human Hand Model

As one of the main parts of AFC is mechanical structure influenced by disturbance, three different models of human hand and forearm are used to analyse the effect of AFC system on tremor suppression. The disturbance on these models in AFC system is tremor. These three models consist of a 4-DOF biomedical model of the hand, 1-DOF musculoskeletal model of the elbow joint and a 3-DOF musculoskeletal model of the wrist joint. Investigation of proposed AFC system on these three models represent the effectiveness of the proposed system on tremor suppression as these models cover a main part of hand and forearm in the human body.

3.3.1 A four degrees of freedom (4-DOF) biomedical model of the hand

There are a number of mechanical equipollent models that have been developed to specify the characteristics of biodynamic response of the human hand and arm under vibration[125]. For study about human hand tremor, it is necessary to determine the biodynamic response of the human hand to apperceive the relation between force and motion of human tremor. In this study, a 4-DOF biodynamic model of the hand is used.

Reynolds et al. proposed 4-DOF linear model of the human hand system [126]. This model is the combination of mass-spring-damper system. Figure 3-3 shows the 4-DOF model. In this figure, masses m_1, m_2, m_3, and m_4 indicate the mass of epidermis, dermis, subcutaneous tissue and the muscle of the human hand, respectively. The coupling between epidermis and dermis tissue is shown with k_1 and c_1 that represent the visco-elastic properties of these tissues. There is strong coupling between the dermis and the subcutaneous tissue of the hand and k_2 and c_2 indicate this coupling. On the other hand, the elements k_3 and c_3 are considered to show weak coupling between the subcutaneous tissue and the muscle. The coupling between muscle and the bones has been related to element k_4 and c_4. Hence, in the simulation 4-DOF model, a disturbance is needed for study about hand tremor. As the reason of human hand tremor is the damage on the human brain, this disturbance is a kind of internal force and the best place for the source of force should be at the muscle [4]. The result of this section was published in [60].

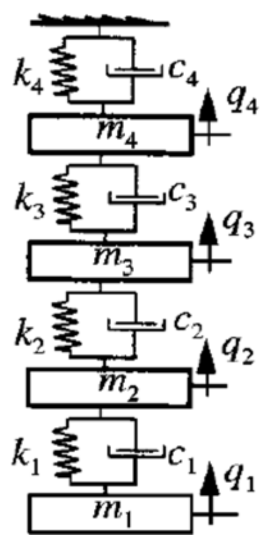

Figure 3-3. Four DOF palm model [125]

The dynamic equations of motion of 4-DOF model at the palm can be described by Equation 3-4 as a coupled differential equation:

$$m_i\ddot{q}_i + F_{Ki} + F_{Di} = F_{Oi}; \qquad i = 1,2,..,n$$ Equation 3-4

where m_i is mass, $\ddot{q}$ is the acceleration of the system and n is the number of DOF. F_{ki}, F_{Di} and F_{Oi} are restoring, dissipative and excitation forces acting on mass i, respectively. If it is assumed that the stiffness and damping coefficient is linear, the restoring and dissipative force will be as below:

$$F_{Ki} = \begin{cases} k_i(\mathrm{q}_i - q_{i+1}); & i = 1 \\ k_{i-1}(\mathrm{q}_i - q_{i-1}) + k_i(\mathrm{q}_i - q_{i+1}); & i = 2,...,n-1 \\ k_{i-1}(\mathrm{q}_i - q_{i-1}) + k_i q_i; & i = n \end{cases}$$ Equation 3-5

$$F_{Di} = \begin{cases} c_i(\dot{\mathrm{q}}_i - \dot{q}_{i+1}); & i = 1 \\ c_{i-1}(\dot{\mathrm{q}}_i - \dot{q}_{i-1}) + c_i(\dot{\mathrm{q}}_i - \dot{q}_{i+1}); & i = 2,...,n-1 \\ c_{i-1}(\dot{\mathrm{q}}_i - \dot{q}_{i-1}) + c_i\dot{q}_i; & i = n \end{cases}$$ Equation 3-6

$$F_{Oi} = \begin{cases} 0; & i \neq 4 \\ F_{input}; & i = 4 \end{cases}$$ Equation 3-7

where k_i and c_i are linear stiffness and damping coefficients which are characteristics of the springs and dampers of the system.

Using Equation 3-4 to Equation 3-7, the equations of motion for the 4-DOF palm model can be express as,

$$m_1\ddot{q}_1 + c_1\dot{q}_1 - c_1\dot{q}_2 + k_1q_1 - k_1q_2 = 0$$ Equation 3-8

$$m_2\ddot{q}_2 - c_1\dot{q}_1 + (c_1 + c_2)\dot{q}_2 - c_2\dot{q}_3 - k_1q_1 + (k_1 + k_2)q_2 - k_2q_3 = 0$$ Equation 3-9

$$m_3\ddot{q}_3 - c_2\dot{q}_2 + (c_2 + c_3)\dot{q}_2 - c_3\dot{q}_4 - k_2q_2 + (k_2 + k_3)q_3 - k_3q_4 = 0$$ Equation 3-10

$$m_4\ddot{q}_4 - c_3\dot{q}_3 + (c_3 + c_4)\dot{q}_4 - k_3q_3 + (k_3 + k_4)q_4 = F_{input}$$ Equation 3-11

The parameters used to emulate the 4-DOF hand tremor are given in Table 3-1.

Table 3-1. Parameters of skin anatomy at human hand model [71]

Skin layer	Epidermis (m_1)	Dermis (m_2)	Subcutaneous Tissue (m_3)	Muscle (m_4)
Mass (kg)	0.0043	0.105	0.566	4.3
Damper (Ns/m)	88.8	1.5	0.1	3.99
Spring (N/m)	678	185	23.9	34.9

3.3.1.1 Simulation of control system for (4-DOF) biodynamic model of the hand

As it is discussed in this section, human hand is modelled as 4-DOF system. To control and supress the human hand tremor, a control scheme is proposed in Figure 3-2. In this control system, AFC method was used. A PD controller and piezoelectric actuator were embedded in this control system. For study about the result of control system the human hand is simulated in MATLAB-Simulink. In this simulation a harmonic force is applied for the palm excitation. Then displacements plots show the hand behaviour in this control system. MATLAB- Simulink simulation for the control of human hand model with AFC is included in Appendix A.

3.3.1.2 Results and conclusion

As it was mentioned before, the proposed system is simulated in MATLAB to investigate the effect of AFC control system to reduce the hand tremor. The sinusoidal disturbance is applied to the dynamic system of hand model with amplitude of 10 N and frequency of 10 Hz.

The displacement signal for hand tremor is illustrated in Figure 3-4 for 10 sec. From this figure, it can be seen that the displacement is between -3mm to +4 mm which is the target range since the actual human hand postural tremor in Parkinson disease is about ±5mm [13, 24].

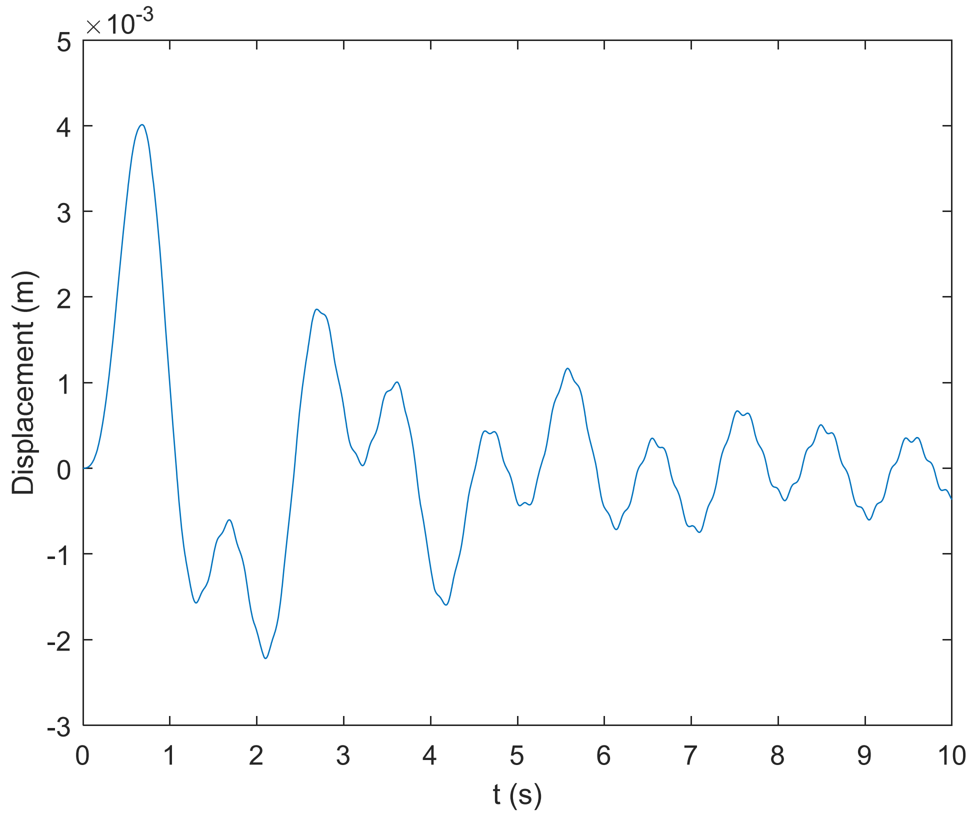

Figure 3-4. Displacement result for the 4-DOF hand model from MATLAB simulation

The result for the hand model with AFC method is shown in Figure 3-5 for 40 seconds to describe the efficiency of the system for tremor disappearing after a while. As shown in this figure, during simulation time, the hand tremor decreases considerably and is between -1.5×10^{-9} m to $+1.5\times10^{-9}$ m. It is clear that the AFC control system with PD controller and piezoelectric actuator is a very effective system for suppressing the hand tremor.

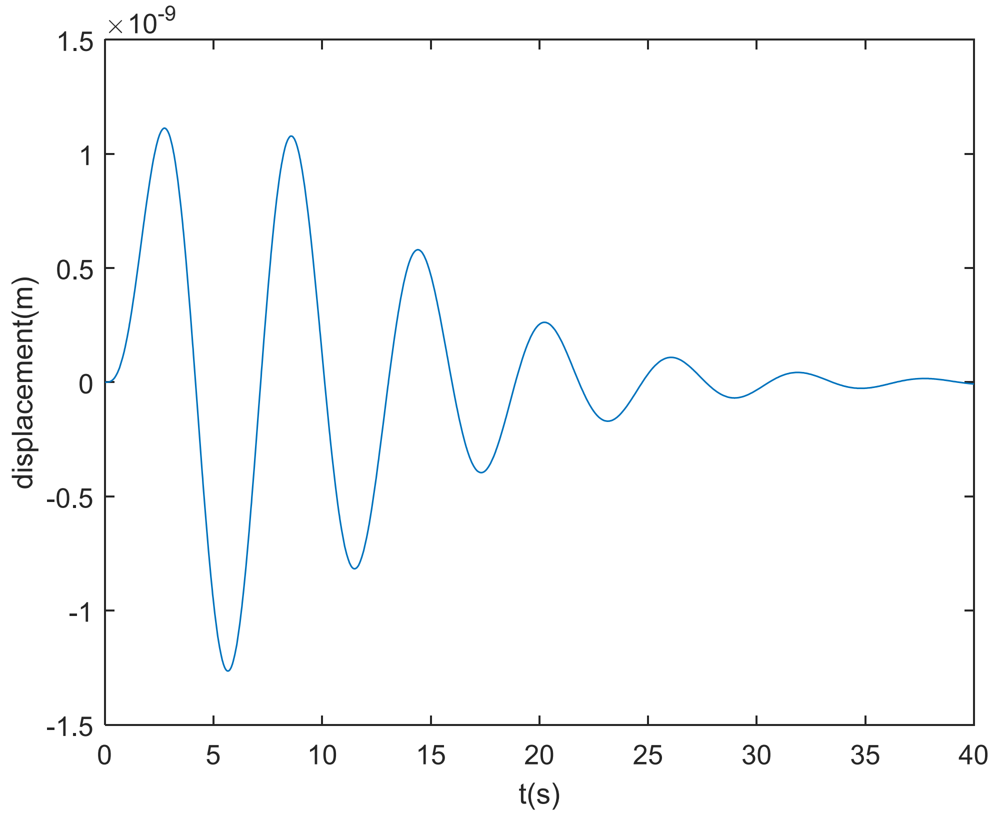

Figure 3-5. Displacement result for the 4-DOF hand model from MATLAB simulation with AFC control system

Figure 3-6 shows the simulation displacement result for 4-DOF hand model for both uncontrolled and controlled system. It is clear that the result significantly improve with the use of AFC method for tremor suppression. In uncontrolled system tremor amplitude is between -3×10^{-3} m to $+4\times10^{-3}$ m and in controlled system amplitude of hand tremor is between -1.5×10^{-9} m to 1.5×10^{-9} m.

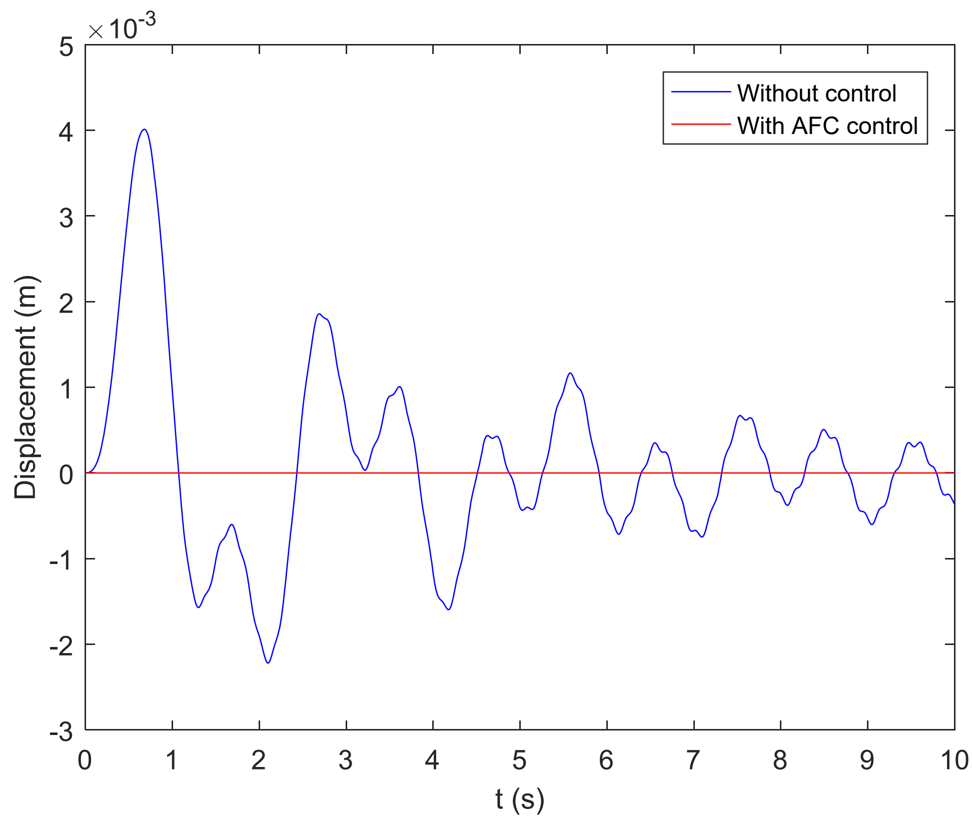

Figure 3-6. Displacement result for the 4-DOF hand model from MATLAB simulation with and without AFC control system

3.3.2 A one degree of freedom (1-DOF) biomedical model of the elbow joint

In this study, a two-dimensional (2D) model of the arm with one degree of freedom (elbow flexion-extension) in a 2D plane is adopted. This model includes two muscles, biceps, and triceps. These two muscles are a pair of antagonist muscles functioning as flexor and extensor of the elbow joint. The biceps has two heads: long head and short head. The triceps muscle group has three heads: lateral, medial and long heads [127]. Since the tremor control in a single joint in a 2D plane is considered in this part, only uniarticular muscles of elbow joint are taken into account in the analysis. Therefore, biceps long head (LH) and triceps lateral head (LtH) are selected for simulation of tremor. Figure 3-7 shows a simplified musculoskeletal model [127]. The result of this section was published in [61].

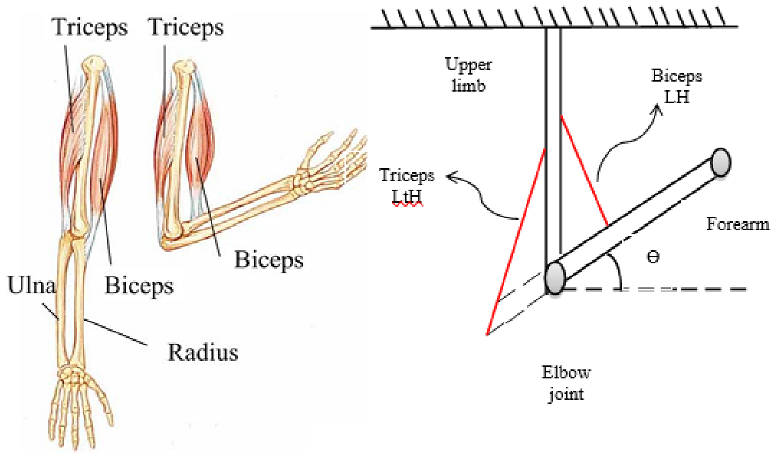

Figure 3-7. Left figure is the physiological model of the elbow joint [127]. Right figure is the simplified musculoskeletal model

The forearm is considered only and is modelled as a pendulum. The dynamic equation of motion of the elbow with tremor is:

$$T_t + T_p = (\frac{1}{4}ml^2 + I)\ddot{\theta} + \frac{1}{2}mgl\cos\theta n \qquad \text{Equation 3-12}$$

where T_t is the moment that a muscle generates through active electrical stimulation, T_p is the internal passive moment, m is the forearm mass, I is the moment of inertia, l is the forearm length, and g is the gravitational constant. The value of the related parameters used in the calculation is listed in Table 3-2 [127].

Table 3-2. Parameter values for forearm model [127]

m (kg)	**I (kgm^2)**	**l (m)**
1.6	0.013	0.32

3.3.2.1 Muscle model

The muscle model is developed from the classic Hill-type muscle model [128, 129]. In this model, the muscle response to a stimulation signal is composed of two parts: activation dynamics and contraction dynamics. The muscle model is illustrated in Figure 3-8.

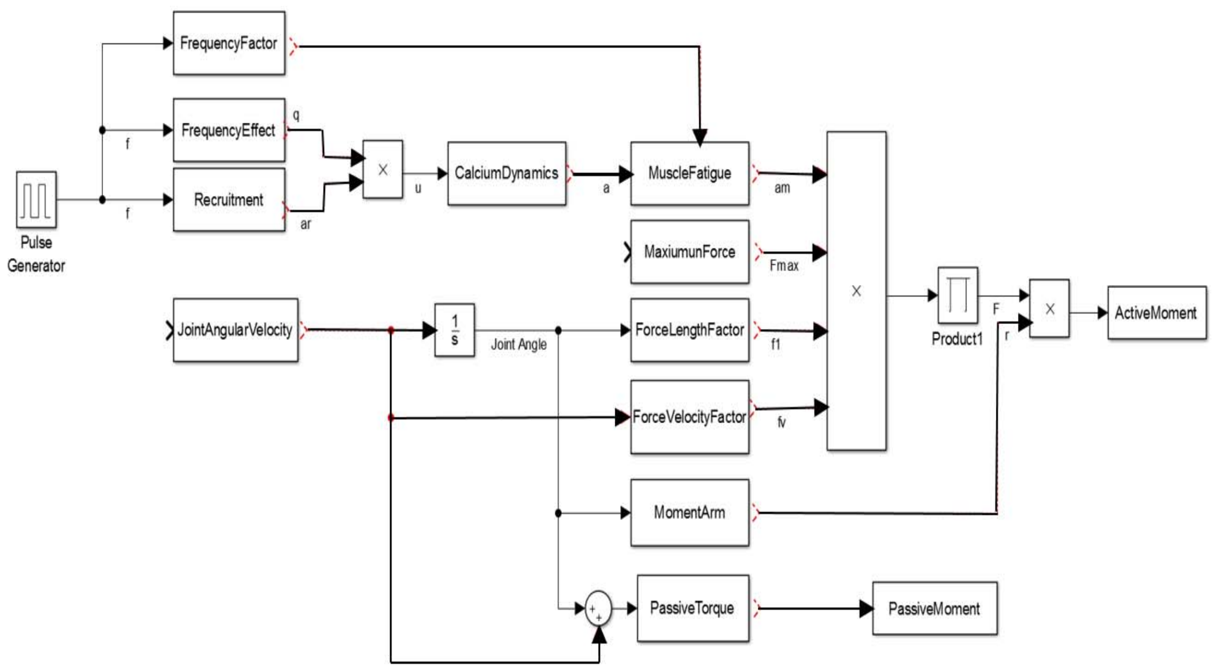

Figure 3-8. Simulink model of a muscle model [130]

3.3.2.1.1 Muscle contraction dynamics

Muscle contraction property is derived from the mechanical structure of the muscle.

a) Active Force: The force which is generated by a muscle through the stimulation is called the active force as:

$$F = F_{\max} \times f_l \times f_v \times a_m \qquad \text{Equation 3-13}$$

where F_{max} is the muscle maximum isometric force, f_l is the force-length factor, f_v is the force-velocity factor, and a_m is the muscle activation with fatigue. $a_m = a.p$, where p is the muscle fatigue factor and a is the muscle activation without fatigue.

The active moment for 1-DoF elbow joint in flexion-extension is:

$$T_t = \sum_{i=1}^{2} F_i r_i \qquad \text{Equation 3-14}$$

where F_i is the muscle force, r_i is the moment arm, and i indicates the number of muscles, biceps LH and triceps LtH.

b) Muscle length factor*:* Changing muscle length forcefully affects the active force. A Gaussian-like function is used to describe the relationship between the muscle force and muscle fibre length as follow:

$$f_l = \exp\left[-\left(\frac{\bar{l}-1}{\varepsilon}\right)^2\right] \qquad \text{Equation 3-15}$$

where f_l is a normalized factor, $\bar{l}$ is the normalized muscle length with respect to the optimal muscle length; $\bar{l} = l_m / l_{opt}$ and $l_m = r(\theta - \theta_r)$.

c) Force -Velocity Factor: The muscle velocity has also an effect on the muscle force, and the factor f_v is used to describe this relationship as:

$$f_v = 0.54 \arctan(5.69\bar{v} + 0.51) + 0.745 \qquad \text{Equation 3-16}$$

where $\bar{v}$ is the normalized muscle velocity with respect to the maximum contraction (shortening) velocity v_{max} of the muscle; $\bar{v} = v_m / v_{max}$ and $v_m = r\dot{\theta}$. Table 3-3 shows the parameters for two muscles [131, 132].

Table 3-3. Parameter values for muscles

Muscles	l_{opt} (m)	v_{max} (m/s)	F_{max} (N)	r(m)
BICEPS	0.136	0.68	900	0.03
TRICEPS	0.084	0.42	900	-0.03

d) The Passive Torque: The passive torque is derived from the passive element (PE) in the muscle model. For the elbow joint, it is given as [133]:

$$T_p = 0.2\dot{\theta} - 7.8\,\mathrm{sgn}(\theta - \pi/2)\left[\exp(36/\pi\left|\theta - \pi/2\right|) - 1\right] \times 10^{-7} \qquad \text{Equation 3-17}$$

where *sgn*() is the signum function specifying the sign of its argument.

3.3.2.1.2 Muscle activation dynamics

When the muscle is stimulated by the electrical pulses, there is a dynamic process for the muscle to generate the force. This electrical characteristic of the muscle is referred to as activation dynamics [130].

a. **Muscle Recruitment Curve:** This property can be modelled by a piecewise function with three values: a threshold pulse width (PW_d), a saturation pulse width (PW_s) and the pulse width of the electrical pulse (z). The normalized muscle recruitment curve, a_r, can be described in the following way:

$$a_r = \begin{cases} 0 & z \le PW_d \\ \dfrac{1}{PW_s - PW_d}(z - PW_d) & PW_s \le z \le PW_d \\ 1 & z \ge PW_s \end{cases} \qquad \text{Equation 3-18}$$

b. **Frequency Characteristics:** When the frequency of stimulation pulse varies, it also affects the force produced by the muscle. This force-frequency characteristic can be defined by:

$$q(f)=\frac{(af)^2}{1+(af)^2}$$ Equation 3-19

where f is the stimulation frequency, $q(f)$ is the characteristic factor and a is the muscle activation without fatigue.

Calcium Dynamics: The muscle cannot be activated and relaxed simultaneously, and there always exists a time delay. Calcium dynamics can be modelled as a first order differential equation.

$$\dot{a}=\frac{1}{\tau_{ac}}(u-ua)+\frac{1}{\tau_{ad}}(u-a)$$ Equation 3-20

where a is the muscle activation without fatigue, $u = a_r q$; τ_{ac} is activation time constant, and τ_{da} is the de-activation time constant.

c. **Muscle Fatigue:** It depends on the activation level, a, and frequency f of the stimulation.

$$\dot{p}=\frac{a\lambda(p_{\min}-p)}{\tau_{fat}}+\frac{(1-p)(1-a\lambda)}{\tau_{rec}}$$ Equation 3-21

$$\lambda=1-\beta_s+\beta_s(\frac{f}{100})$$ Equation 3-22

where p is the fatigue, τ_{fat} is the fatigue time constant, τ_{rec} is the recovery time constant, p_{min} is the minimum fitness, λ is the frequency factor on fatigue, and β_s is the shaping factor. Table 3-4 shows the parameter values related to contraction and activation dynamics [132, 134].

Table 3-4. Parameter values for the elbow musculoskeletal model

PW_s (μs)	PW_d (μs)	τ_{ac} (ms)	τ_{da} (ms)	τ_{fat} (ms)	τ_{rec} (ms)	β_s $(-)$	ε $(-)$	$p_{\min}$ $(-)$

100	500	40	70	18	30	0.6	0.4	0.4

3.3.2.2 Simulation of control system for (1-DOF) biomedical model of the elbow joint

As was discussed in previous parts, in this part, the elbow joint is modelled as a 1-DOF musculoskeletal model that consists of two muscles and one skeleton. As we need to control the joint tremor, a control scheme is proposed, Figure 3-9. In this loop, a proportional–derivative (PD) controller controls the piezoelectric actuator for damping joint tremor.

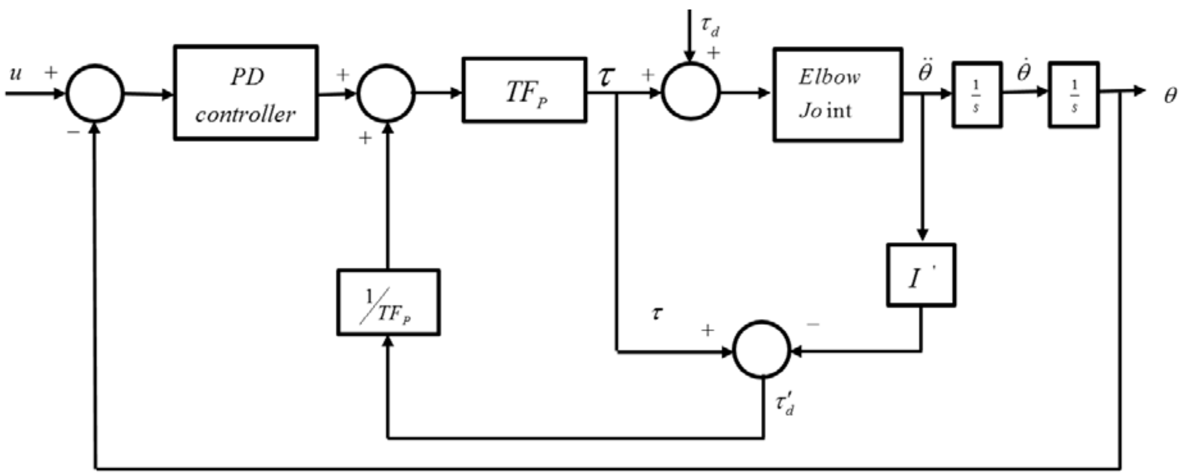

Figure 3-9. A plot of proposed design for active force control system of the elbow joint

From Newton's second law of motion, the equation for 1-DOF elbow joint will be expressed as:

$$\tau_d' = \tau - I'\ddot{\theta} \qquad \text{Equation 3-23}$$

where, τ_d' is estimated disturbance torque, τ is actuator torque, I' is the estimated vibratory inertia and $\ddot{\theta}$ is measured angular acceleration signal [4].

To study the result of the control system, the elbow joint is simulated in MATLAB-Simulink. MATLAB–Simulink simulation block for AFC system for 1-DOF musculoskeletal model of elbow joint is included in the Appendix B. Upper limb (elbow joint) tremor can be achieved when tremulous stimulation activates the related muscles. Artificial electrical pulses can be applied to the muscle via functional electrical stimulation (FES) technique to generate the artificial tremor. Three variables of electrical pulse can be regulated, i.e. pulse width, pulse frequency, and pulse amplitude. Pulse width (PW) is the only controlled variable here which is considered 300 μs to achieve the elbow joint tremor which is about -6 to +6 degrees [127]. The other two variables are set as constants; pulse frequency which is 20 Hz and pulse amplitude which is 25 *mA*. Then displacements plots show the joint behaviour in this control system.

3.3.2.3 Results and conclusion

As it was declared previously, the proposed system was simulated in MATLAB to investigate the effect of an AFC control system to reduce the elbow joint tremor with the help of a piezoelectric actuator and a PD controller.

The displacement signal for the tremor of the elbow joint without any control system is illustrated in Figure 3-10 for 5 seconds. From the figure, it can be found that the elbow joint tremor is between -8 degrees to +8 degrees which is close to the target range as the actual human hand tremor in Parkinson’s disease is about ±6 degrees [13, 24].

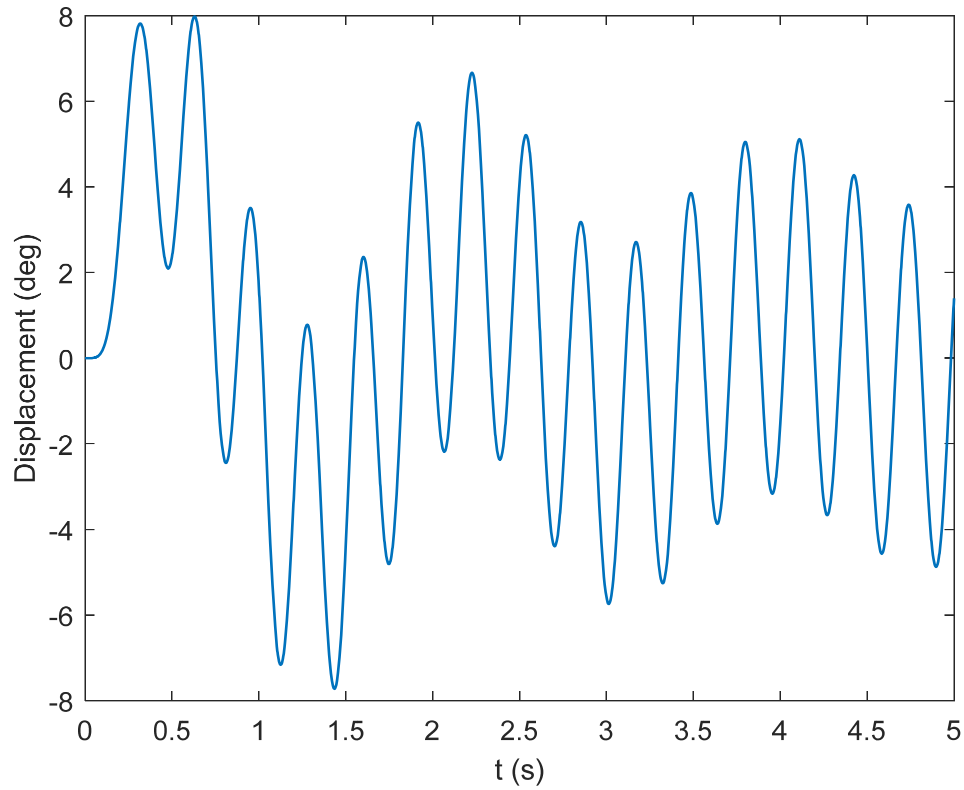

Figure 3-10. Displacement result for tremor of a 1-DOF musculoskeletal model of the elbow joint from MATLAB simulation

The results for the displacement of the elbow joint with an AFC method and a piezoelectric actuator is shown in Figure 3-11. As this figure shows, during simulation time, the tremor decreases considerably and is between -1×10^{-2} degrees to $+1.5\times10^{-2}$ degrees which is much smaller than joint angle without an AFC system. It is clear that an AFC control system with a PD controller and a piezoelectric actuator is a very effective system for suppressing tremor.

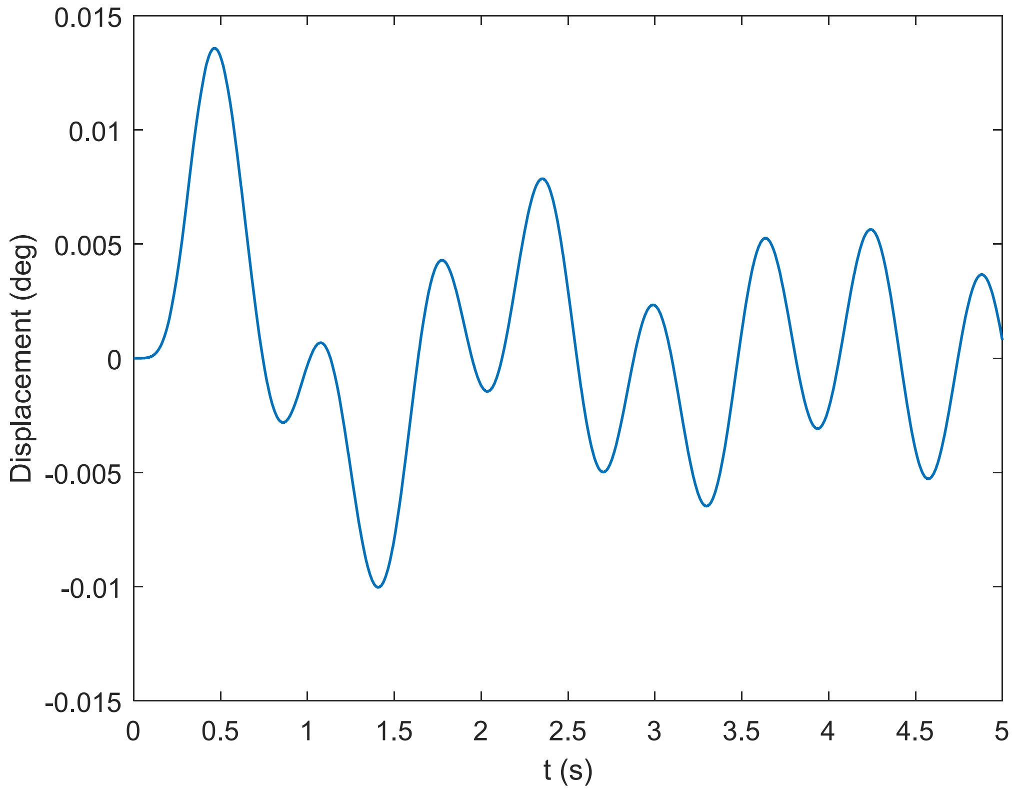

Figure 3-11. A plot of Displacement result for the 1-DOF musculoskeletal model of the elbow joint from MATLAB simulation with AFC control system

Figure 3-11 shows the simulation displacement result for 1-DOF musculoskeletal model of the elbow joint for the system before and after control. From Figure 3-12 the result significantly improves with use of AFC method for tremor suppression in elbow joint. In the system with AFC, angle of elbow joint tremor is between -1×10^{-2} degrees to $+1.5\times10^{-2}$ degrees which is very small compare to elbow joint tremor without AFC (between -8 degrees to +8 degrees).

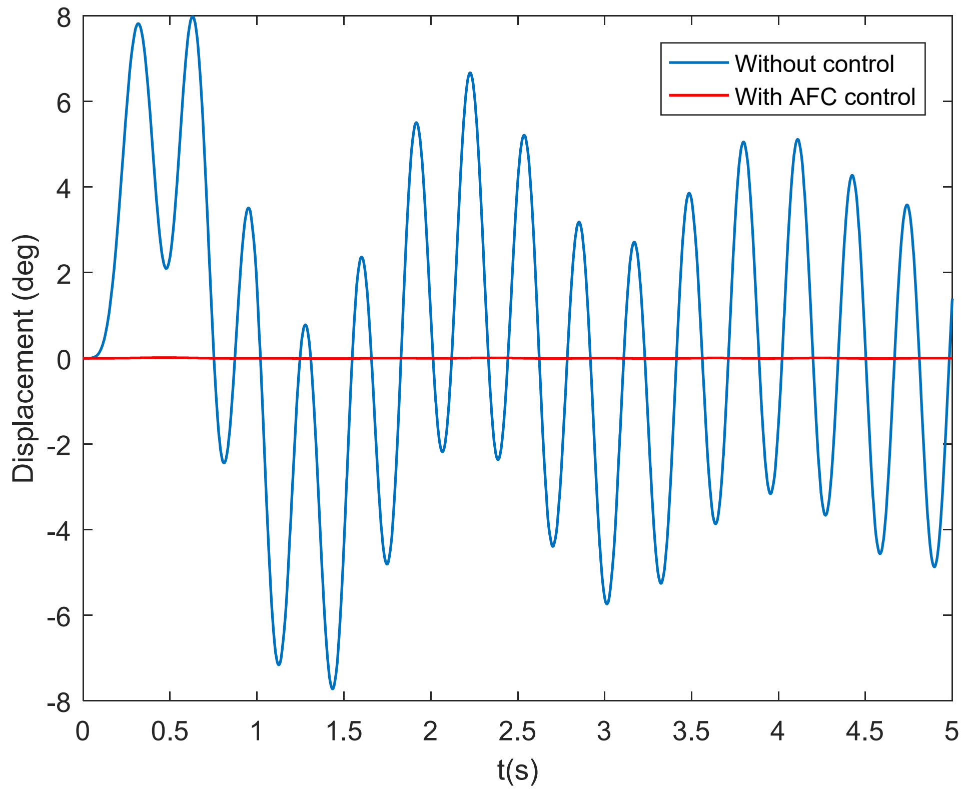

Figure 3-12. A plot of displacement result for the 1-DOF musculoskeletal model of the elbow joint from MATLAB simulation with and without AFC control system

3.3.3 A three degrees of freedom (3-DOF) musculoskeletal model of wrist joint

In this part, the wrist joint movement in 3-DOF with four main muscles that contribute to wrist movement is considered. These four muscles are extensor carpi radialis longus (ECRL), extensor carpi ulnaris (ECU), flexor carpi radialis (FCR) and flexor carpi ulnaris (FCU). These four muscles contribute in flexion-extension (FE) and radial ulnar deviation (RUD) and pronation-supination (PS) of the wrist joint. Figure 3-13 shows these four muscles. The result of this section was published in [62].

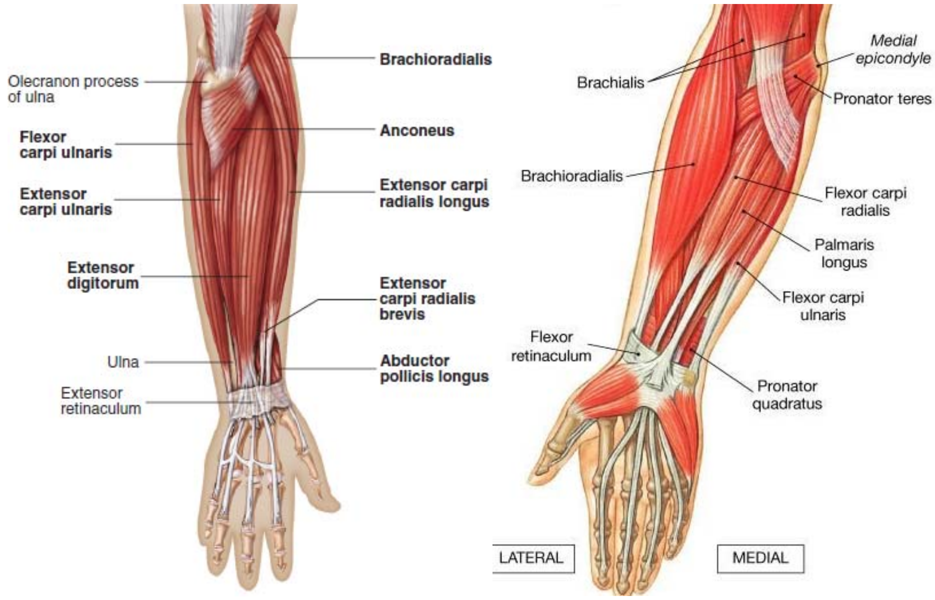

Figure 3-13. Muscles in the forearm

If the wrist is considered as a 1-DOF join, it is modeled as a pendulum. The equation of motion of the 1-DOF wrist joint is:

$$T_t - T_p + T_g = J_z\ddot{\theta} \qquad \text{Equation 3-24}$$

where T_t is the generated moment by muscle through active electrical stimulation, T_p denotes the internal passive moment, T_g is the moment caused by gravity that is written as:

$$T_g = mgl\cos\theta \qquad \text{Equation 3-25}$$

where *m* indicates the hand mass, *l* is the distance between the mass center of hand and wrist joint, and *g* signifies the gravitational constant.

If wrist FE, RUD and PS are considered as the wrist joint movement, the equation of motion for 3-DOF wrist joint can be written as:

$$\begin{aligned} T_{t1} - T_{p1} &= J_1\ddot{\theta}_1 \\ T_{t2} + T_g - T_{p2} &= J_2\ddot{\theta}_2 \\ T_{t3} - T_{p3} &= J_3\ddot{\theta}_3 \end{aligned} \qquad \text{Equation 3-26}$$

where T_1, T_2 and T_3 are the muscle moments that are generated through active electrical stimulation in FE, RUD and PS directions respectively. Θ_1, Θ_2 and Θ_3 are the joint angles in FE, RUD and PS directions respectively. Also, J_1, J_2 and J_3 are the wrist inertia in 3-DOF.The value of the related parameters used in the calculation is listed in Table 3-5.

Table 3-5. The parameter values for the hand

m(g)	**l(cm)**	**J_1 (gm^2)**	**J_2 (gm^2)**	**J_3 (gm^2)**
445.3	8.6	1.305	0.871	1.784

The parameters in Table 3-5 are for a specific subject that has the weight of 73.0kg and height of 1.741m [130].

3.3.3.1 Muscle model

The muscle model that is used for wrist joint tremor is developed from the classic Hill-type muscle model [128, 129]. Figure 3-8 shows the block diagram of the muscle model. As is discussed in section 3.3.3.1, the muscle response to stimulation signal is composed of two parts: activation dynamics and contraction dynamics. The equation for muscle activation dynamics, Equation 3-18 to Equation 3-22, for the wrist joint is the same as for the elbow joint.

For muscle contraction dynamics, the equation for active force, active moment of wrist joint and muscle length factor are the same as in Equation 3-13 , Equation 3-14 and Equation 3-15.

As the rest joint is considered as a 3-DOF model, for wrist flexion-extension (FE), radial-ulnar deviation (RUD), and pronation-supination (PS), the active moment can be written as Equation 3-27:

$$\begin{bmatrix} T_1 \\ T_2 \\ T_3 \end{bmatrix} = r \begin{bmatrix} F_{ECRB} \\ F_{ECU} \\ F_{FCR} \\ F_{FCU} \end{bmatrix} \qquad \text{Equation 3-27}$$

where the r is moment arm matrix as Equation 3-28 [130]:

$$r = \begin{bmatrix} -0.016 & -0.006 & 0.015 & 0.015 \\ -0.014 & 0.025 & -0.007 & 0.018 \\ 0.0025 & 0.0002 & 0.0042 & 0.0024 \end{bmatrix} \qquad \text{Equation 3-28}$$

Also in 3-DOF the velocity of each muscle in Equation 3-16 can be rewritten as Equation 3-29:

$$\begin{bmatrix} v_{m1} \\ v_{m2} \\ v_{m3} \\ v_{m4} \end{bmatrix} = r^T \begin{bmatrix} \dot{\theta}_1 \\ \dot{\theta}_2 \\ \dot{\theta}_3 \end{bmatrix} \qquad \text{Equation 3-29}$$

Table 3-6 shows the parameters for four muscles in Equation 3-16 [130-132].

Table 3-6. The parameters of wrist muscles

Muscles	l_{opt} **(m)**	v_{max} **(m/s)**	F_{max}**(N)**
ECRB	0.0585	10	122.9
ECU	0.0622	10	117
FCR	0.0628	10	59.7
FCU	0.0509	10	102.6

Also the passive torque for the wrist joint is given as Equation 3-30 [133]:

$$T_p = B_p\dot{\theta} + +K_p\theta + M_p \qquad \text{Equation 3-30}$$

where M_P is:

$$M_p = k_2 \frac{\exp(k_1(\theta / \mathrm{k}_3))}{\exp(k_1)} - k_2 \frac{\exp(k_1(-\theta / \mathrm{k}_3))}{\exp(k_1)} \qquad \text{Equation 3-31}$$

Table 3-7. The constant parameters in Equation **3-31**[133]

	$\mathbf{K_p}$	$\mathbf{B_p}$	$\mathbf{k_1}$	$\mathbf{k_2}$	$\mathbf{k_3}$
Flexion-	0.4	0.3	6	0.3	0.8

extension					
Radial ulnar deviation	0.3	0.3	6	0.1	0.3
Pronation-supination	0.4	0.3	6	0.03	1

The value of constant parameters for Equation 3-31 is given in Table 3-7.

3.3.3.2 Results and conclusion

AFC control system is used to analyse the effect of a control system with a piezoelectric actuator and a PD controller on human wrist joint tremor in 3-DOF in MATLAB-Simulink. The electrical stimulation is applied to related muscles to attain wrist joint tremor. Artificial tremor can be generated as artificial electrical pulses applied to the muscles via functional electrical stimulation (FES) technique. Three variables of electrical pulse can be regulated, i.e. pulse width, pulse frequency, and pulse amplitude. Pulse width (PW) is the only controlled variable here while another two variables are set as constants; pulse frequency which is 20 Hz and pulse amplitude which is 15 *mA*. Then displacements plots show the joint behaviour in this control system. The electrical stimulation is applied to ECRB and FCU with pulse width of 300 μs and 400 μs respectively to achieve the wrist joint tremor which is about -5 to +5 degrees [133].

In this part the effect of AFC system on the displacement signal for the tremor of the wrist joint in 3-DOF, flexion-extension (FE), radial-ulnar deviation (RUD), and pronation-supination (PS), is studied.

Figure 3-14 shows the tremor of the wrist joint in flexion-extension before and after using AFC method for 5 seconds. In this figure, the upper graph is for wrist tremor angle that is about -5 degrees to +5 degrees. AFC system is applied to the wrist joint to supress the tremor. The lower graph shows the tremor angle after using control system that is about -1×10^{-2} degrees to 1×10^{-2} degrees.

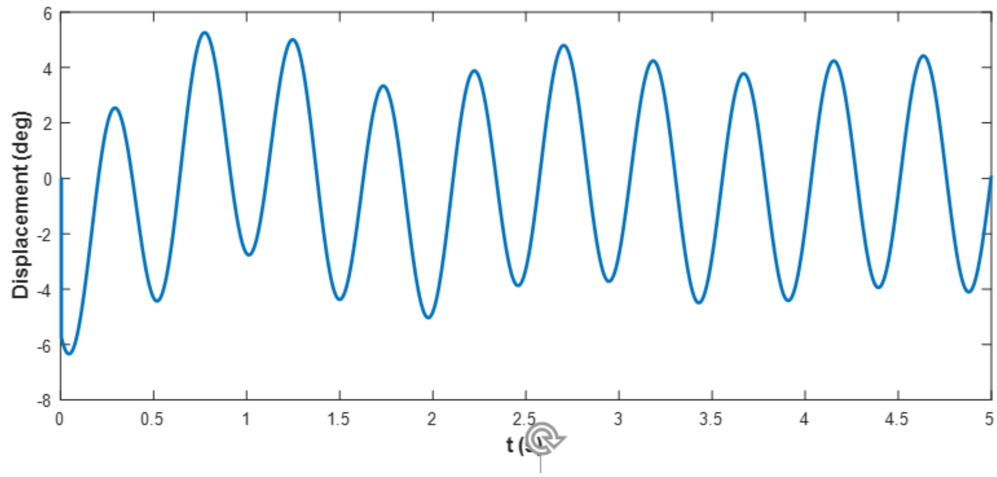

(a)

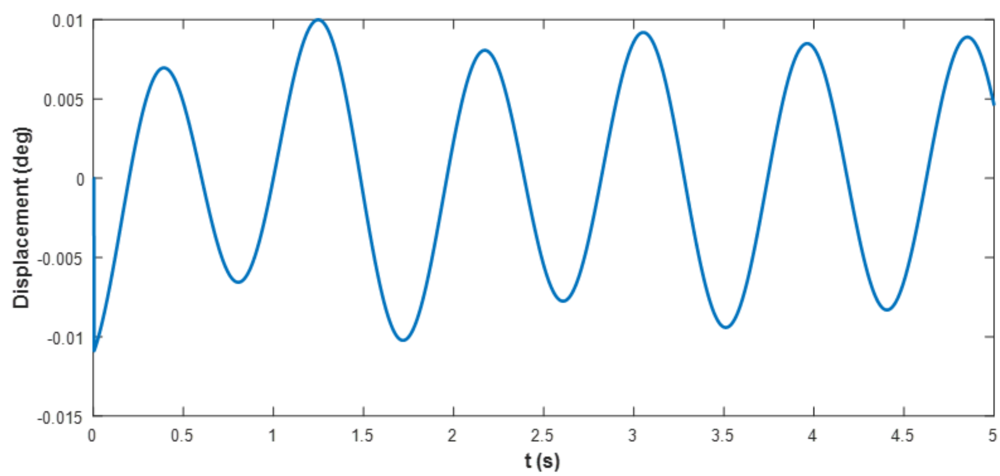

(b)

Figure 3-14. Displacement results for a 3-DOF musculoskeletal model of the wrist joint in FE from MATLAB simulation without control system (a), with an AFC control system (b).

The tremor of the wrist joint in radial-ulnar deviation is shown in Figure 3-15 for 5 seconds. In this figure, the upper graph is for wrist tremor angle without AFC system that is about -5 degrees to +7 degrees. Also, the lower graph shows the result after using control system for wrist joint that is about -6×10^{-3} degrees to 7×10^{-3} degrees.

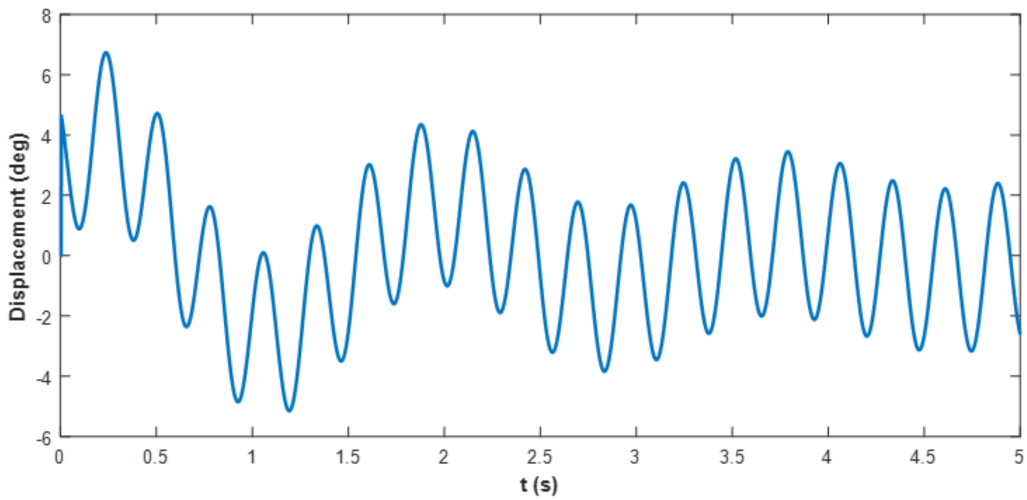

(a)

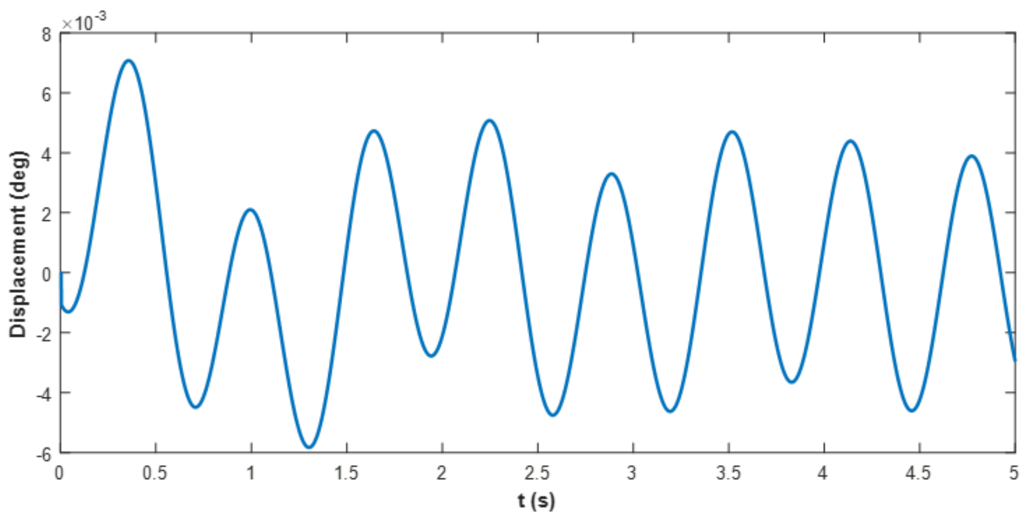

(b)

Figure 3-15. Displacement results for a 3-DOF musculoskeletal model of the wrist joint in RUD from MATLAB simulation without control system (a), with an AFC control system (b).

Figure 3-16 illustrates the effect of AFC system on tremor reduction of the wrist joint in pronation-supination. In this figure, the upper graph shows the wrist tremor angle which is about -2 degrees to +3 degrees. AFC system is applied to the wrist joint to supress the tremor. The lower graph shows the tremor angle after using control system that is about -1.5×10^{-2} degrees to 1.2×10^{-2} degrees.

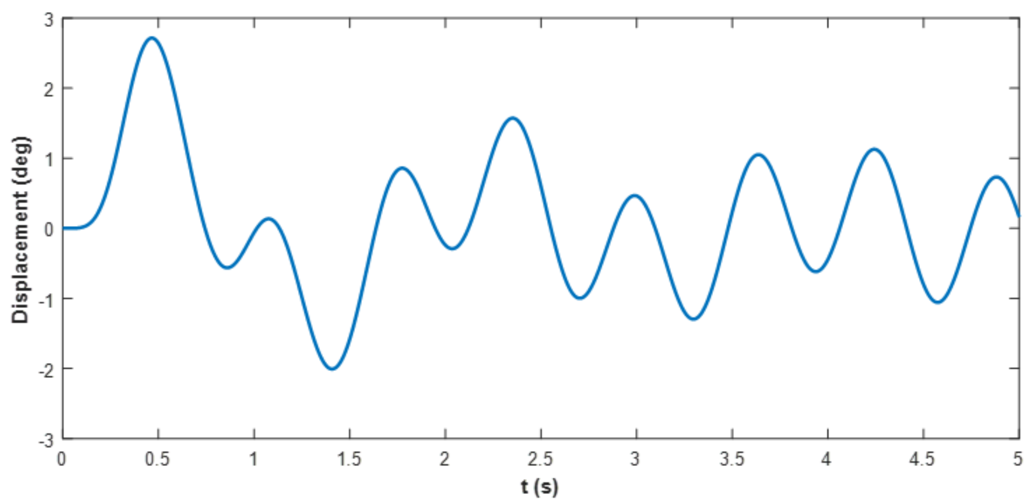

(a)

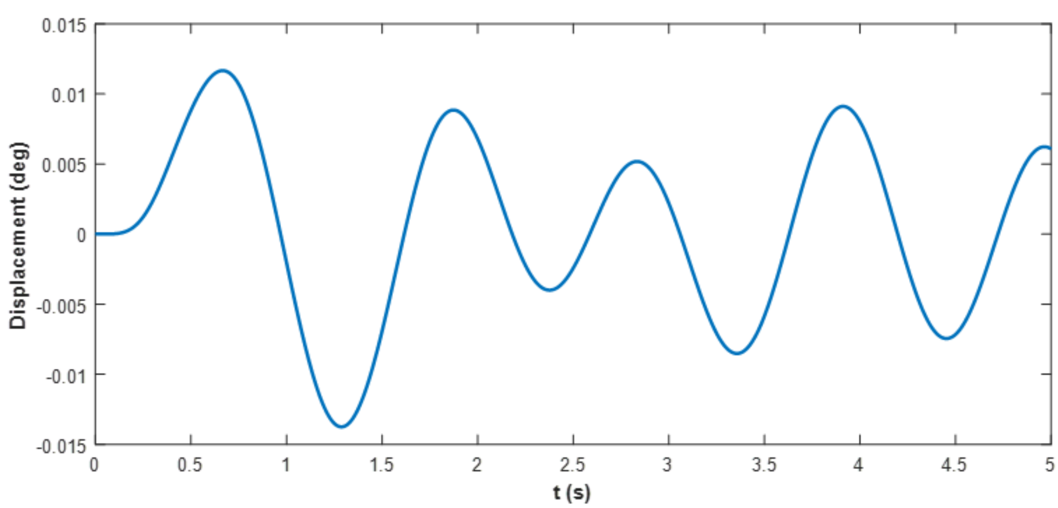

(b)

Figure 3-16. Displacement result for a 3-DOF musculoskeletal model of the wrist joint in PS from MATLAB simulation without control system (a), with an AFC control system (b).

The result of the effect of AFC system on tremor reduction in Figure 3-14 to Figure 3-16 shows that this control system that uses a piezoelectric actuator as an actuator and a PD controller is a very effective system for tremor attenuation. After applying the control system to the musculoskeletal of the wrist joint, wrist joint tremor reduced in flexion-extension (FE), radial-ulnar deviation (RUD), and pronation-supination (PS).

3.4 CONCLUSION

The effect of the AFC system on tremor suppression in PD was investigated in this chapter. In the proposed AFC system, a piezoelectric actuator controls the behavior of the PD controller to get to the desireable result. The behaviour of three different models including 4-DOF biomedical model of the hand, a 1-DOF musculoskeletal model of the elbow joint and a 3-DOF musculoskeletal model of the wrist joint were studied. Matlab simulink was used to simulate the AFC system. Results showed that after using the AFC system on all three models, the tremor was supressed effectively which means the proposed AFC system is a practical tool for tremor control.

Chapter 4: Analytical Solution for Vibration of Human Forearm Beam Model

4.1 Introduction

Analytical solution for the vibration of human forearm which is modelled as a beam, is studied in this chapter. The investigation aim is based on the analysis of the effect of a piezoelectric material as a sensor and actuator on vibration control. To achieve this purpose, the human forearm is modelled as a continuous beam and it is analysed in two different ways.

In the first part of this chapter, in section 4.2.1, the human forearm is modelled as a Timoshenko beam which has a layer of piezoelectric actuator on its top surface as an actuator and forced vibration of the model is investigated. Timoshenko beam theory is considered for thick beams. As the dimension of a real hand is close to the thick beam, the proposed beam model complies with Timoshenko beam theory and the effect of both rotary inertia and shear deformation are considered for its analysis. Hamilton principle is used to obtain the equation of motion of the beam. Thus, by employing the Galerkin procedure, the governing equation of motion which is a second order ordinary differential equation in time is derived. An external force is applied by a sinusoidal force to the beam to test the beam behaviour. The response of the system to the force stimulation gives the analytical relations for natural frequency and amplitude of the vibration. Using the obtained analytical relations, the effects of different factors and material properties including density and modulus of elasticity of the piezoelectric actuator and the piezoelectric coefficient on the vibration of this beam are investigated. The results indicate that the piezoelectric layer as an actuator provides an effective tool for active control of vibration. The result of this section was submitted and it was published in [135].

In the second part of this chapter, as stated in section 4.2.2, the human forearm is modelled as a continuous beam that has two layers of piezoelectric material as a sensor and actuator.

In this part of the study, the model is simplified and the effects of rotary inertia and shear deformation are neglected and the Euler–Bernoulli theory is used for analysis. The aim of this part is to analyse the effect of active vibration control on human forearm tremor. The beam model that has a piezoelectric sensor on its bottom surface and a piezoelectric actuator on its top surface will be analysed in the closed loop control system to suppress the human forearm tremor. As human tremor is a sinusoidal movement, this tremor is applied to the model by a harmonic force. Then the equation of motion of the beam is obtained using Hamilton principle. Also, the second order ordinary differential equation of motion is derived by employing the Galerkin procedure. Finally, the effect of active force control is investigated on the beam model to see the effect of piezoelectric sensor and actuator on human forearm tremor control.

4.2 MODELLING AND FORMULATION

4.2.1 Piezoelectrically actuated Timoshenko beam model

In this part, the human forearm is modelled as a Timoshenko beam which has a piezoelectric actuator on its top surface and analytical solution for force vibration of this model is investigated. As the beam model conforms to Timoshenko beam theory, the effect of both rotary inertia and shear deformation are considered for analysis.

A uniform flexible continuous beam which is covered with a layer of piezoelectric actuator on its top surface as an actuator is studied. The beam is initially straight, and it is free at one end and has a pin joint and a rotational spring at the other end to resists against beam torsion.

. The piecewise piezoelectric is as an actuator as shown in Figure 4-1.

The beam model has a length of l and thickness h_b, while the length and thickness of the piezoelectric layer are $(l2 - l1)$ and h_p respectively. Also, it is assumed that the piezoelectric width is the same as the beam width (w_b=w_p). The piezoelectric actuator is perfectly bonded to the beam at a distance $l1$, measured from the pin joint support.

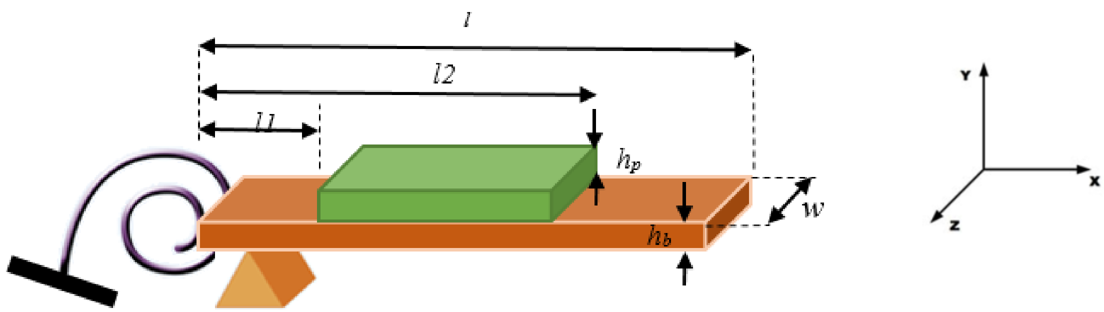

Figure 4-1. Beam model covered with a piezoelectric actuator

Timoshenko theory considers the effects of both rotary inertia and shear deformation. Also, this theory is used for thick beams [64]. The equations of motion for the transverse vibration of the beam is derived with Hamilton principle. The equation of motion for the Timoshenko beam without piezoelectric layer is:

$$-\frac{\partial}{\partial x}\left[KAG\frac{\partial}{\partial x}\left(\frac{\partial y}{\partial x}-\phi\right)\right]+\rho A\frac{\partial^2 y}{\partial t^2}=f(x,t) \quad \text{Equation 4-1}$$

$$-\frac{\partial}{\partial x}(EI)\frac{\partial\phi}{\partial x}-KAG\left(\frac{\partial y}{\partial x}-\phi\right)+\rho I\frac{\partial^2\phi}{\partial t^2}=0 \quad \text{Equation 4-2}$$

where K is the shear correction factor, A is the area of cross-section, G is the shear modulus, y is the lateral displacement and $Ø$ denotes the angle of rotation of the cross section due to bending, ρ is the density of the beam, $f(x,t)$ is the external force on the beam, E is the modulus of elasticity of the beam and I denote the second moment of inertia.

4.2.1.1 Beam properties

As Hamilton principle is used to derive the equation of motion of the beam model, beam properties are given in this part. The mass and the polar moment of inertia of the beam are presented as:

$$m(x) = w_b\left[\rho_b h_b + \left(H_{l1} - H_{l2}\right)\rho_p h_p\right] \qquad \text{Equation 4-3}$$

$$J\left(x\right) = \frac{1}{12} w_b\left[\rho_b h_b^3 + \left(H_{l1} - H_{l2}\right)\rho_p h_p^3\right] \qquad \text{Equation 4-4}$$

$$H_{l1} = H(x - l1), \qquad H_{l2} = H(x - l2) \qquad \text{Equation 4-5}$$

J(x) and *m(x)* are the polar moment of inertia and mass of the beam respectively. *H(x)* is the Heaviside function. Also, w and h represent the width and thickness of the beam and piezoelectric layer, ρ is the density of the beam. In this section, the sub/superscripts b and p show the properties of beam and piezoelectric respectively.

As shown in Figure 4-1, the piezoelectric layer on top of the beam is piecewise. Therefore the neutral surface for each part of the beam is different. For $x < l2$ and $x > l1$, the neutral surface is the geometric center of the beam while for the part that has the piezoelectric layer the neutral surface is as Equation 4-6 [54]:

$$z_n = \frac{E_p h_p (h_p + h_b)}{2(E_p h_p + E_b h_b)} \qquad \text{Equation 4-6}$$

where E indicates modulus of elasticity.

4.2.1.2 Piezoelectric equations

For piezoelectric materials, the electrical field displacement and the mechanical stress-strain relations are as follows [68]:

$$\sigma = E\varepsilon - hD \qquad \text{Equation 4-7}$$

$$Q = -h^T \varepsilon + \beta D \qquad \text{Equation 4-8}$$

As σ is the stress vector, E is the elasticity coefficient matrix, ε is the strain vector, h is the coupling coefficients matrix, D is the displacement vector, and Q is the electrical field vector and β is impermittivity coefficients matrix.

The one-dimensional electrical field is considered for this problem, and the electrical displacement relation for this problem is as Equation 4-9 [67]:

$$D = \begin{bmatrix} 0 \\ 0 \\ D_3(s,t) \end{bmatrix}$$ Equation 4-9

Then, the coupling of stress and electrical field for the one-dimensional piezoelectric actuator takes the forms of:

$$\sigma_{11}^{P} = E_P \varepsilon_{11}^{P} - h_{31} D_3$$ Equation 4-10

$$Q_3 = -h_{31}\varepsilon_{11} + \beta_{33} D_3$$ Equation 4-11

Therefore, Equation 4-12 shows the coupling relation for a one-dimensional piezoelectric actuator is:

$$\sigma_{11}^{P} = E_P \varepsilon_{11}^{P} - E_p d_{31} \frac{p(t)}{h_p}$$ Equation 4-12

where d_{31} is the piezoelectric constant that relates the mechanical tension to the electrical displacement, $p(t)$ is the voltage applied to the piezoelectric actuator, and sub/superscript p denotes piezoelectric.

4.2.1.3 Equation of motion

As previously mentioned, a beam model has been developed for human forearm model to investigate the tremor behaviour. The proposed model has a piezoelectric actuator on its top surface. In this section the equation of motion of the beam is obtained from Hamilton principle.

4.2.1.3.1 Kinetic energy

The kinetic energy of the Timoshenko beam with a layer of piezoelectric actuator on its top surface can be expressed by Equation 4-13:

$$T = \frac{1}{2}\int_0^l m(x)\left(\frac{\partial y}{\partial t}\right)^2 dx + \frac{1}{2}\int_0^l J(x)\left(\frac{\partial \phi}{\partial t}\right)^2 dx \qquad \text{Equation 4-13}$$

where *y* is the lateral displacement, and *Ø* denotes the angle of rotation of the cross section due to bending. Also, *J(x)* and *m(x)* are the polar moment of inertia and mass of the beam respectively

Then,

$$\delta T = \int_0^l m(x)\left(\frac{\partial y}{\partial t}\right)\delta\left(\frac{\partial y}{\partial t}\right)dx + \int_0^l J(x)\left(\frac{\partial \phi}{\partial t}\right)\delta\left(\frac{\partial \phi}{\partial t}\right)dx \qquad \text{Equation 4-14}$$

As the beam is a Timoshenko beam, the effect of shear deformation in addition to the effect of rotary inertia, is considered.

4.2.1.3.2 Potential energy

As the beam has a layer of piezoelectric actuator on its top, the potential energy for the section of the beam that has a layer of actuator is different to other parts. The potential energy for the beam is derived for three sections as follow:

For $0<x<l1$: In this section there is no piezoelectric layer on the beam. The potential energy for this part is as in Equation 4-15:

$$\delta U1 = \int_v E_b \varepsilon_1 \delta\varepsilon_1 dv + \int_v \tau_{xz}\delta\gamma_{xz} dv \qquad \text{Equation 4-15}$$

where strain equation for this part of the beam is:

$$\varepsilon_1 = -z\frac{\partial\phi}{\partial x} \quad when \quad 0 < x < l1$$ Equation 4-16

and τ_{xy} is shear stress and γ_{xy} is shear strain for Timoshenko beam as:

$$\tau_{xy} = K_b G_b(\frac{\partial y}{\partial x} - \phi),$$
$$\gamma_{xy} = (\frac{\partial y}{\partial x} - \phi)$$ Equation 4-17

Finally, with substituting Equation 4-17 into Equation 4-15, the potential energy for *0<x<l1* is obtained based on *y* as the lateral displacement and *Ø* as the angle of rotation of the cross section due to bending:

$$\begin{aligned}\delta U1 &= w_b\int_0^{l1}\int_{-h_b/2}^{h_b/2} E_b(-z\frac{\partial\phi}{\partial x})\delta(-z\frac{\partial\phi}{\partial x})dzdx \\ &+ w_b\int_0^{l1}\int_{-h_b/2}^{h_b/2} K_bG_b(\frac{\partial y}{\partial x}-\phi)\delta(\frac{\partial y}{\partial x}-\phi)dzdx \\ &= \int_0^{l1}\frac{w_bE_bh_b^3}{12}(\frac{\partial\phi}{\partial x})\delta(\frac{\partial\phi}{\partial x})dx \\ &+ w_bh_b\int_0^{l1}K_bG_b(\frac{\partial y}{\partial x}-\phi)\delta(\frac{\partial y}{\partial x})dx \\ &- w_bh_b\int_0^{l1}K_bG_b(\frac{\partial y}{\partial x}-\phi)\delta(\phi)dx\end{aligned}$$ Equation 4-18

For *l1<x<l2*: In this section there is a layer of piezoelectric actuator on the beam that acts as an actuator. In this case the potential energy of the actuator is considered too. The potential energy for this part is as follow where the third part of the Equation 4-19 is the potential energy of the piezoelectric actuator layer:

$$\delta U2 = \int_v E_b\varepsilon_1\delta\varepsilon_1 dv + \int_v \tau_{xz}\delta\gamma_{xz}dv + \int_v(\sigma_p\delta\varepsilon_p + e_3\delta D_3)dv$$ Equation 4-19

where strain equation for this part of the beam due to the presence of piezoelectric layer is as:

$$\varepsilon_1 = -(z - z_n)\frac{\partial\phi}{\partial x} \qquad when \qquad l1 < x < l2$$ Equation 4-20

Using Equation 4-10, Equation 4-11 and Equation 4-17 the potential energy for this part of the beam is:

$$\begin{aligned}
&\delta U2 = w_b \int_0^{l1} \int_{-h_b/2}^{h_b/2} E_b(-(z-z_n))(\frac{\partial\phi}{\partial x})\delta(-(z-z_n)\frac{\partial\phi}{\partial x})dzdx \\
&+w_b \int_{l1}^{l2} \int_{-h_b/2}^{h_b/2} (K_b G_b + K_p G_p)(\frac{\partial y}{\partial x} - \phi)\delta(\frac{\partial y}{\partial x} - \phi)dzdx \\
&+w_p \int_{l1}^{l2} \int_{-h_b/2}^{h_b/2+h_p} \Big[(E_p(-(z-z_n)\frac{\partial\phi}{\partial x}) - h_{31}D_3)\delta(-(z-z_n)\frac{\partial\phi}{\partial x}) \\
&+(-h_{31}(-(z-z_n)\frac{\partial\phi}{\partial x}) + \beta_{33}D_3)\,\delta D_3 \Big] dzdx \\
&= \int_{l1}^{l2} \frac{E_b w_b h_b^3}{12}(\frac{\partial\phi}{\partial x})\delta(\frac{\partial\phi}{\partial x})dx \\
&+\int_{l1}^{l2} \Big[((E_b w_b h_b z_n^2 + \frac{E_p w_p}{3}(h_p^3 + 3h_p(\frac{h_b}{2} - z_n)^2 \\
&+3h_p^2(\frac{h_b}{2} - z_n)))(\frac{\partial\phi}{\partial x})\delta(\frac{\partial\phi}{\partial x}) \\
&+\beta_{33} w_p h_p D_3 \delta D_3 + (h_{31} w_p h_p (h_p + h_b - 2z_n)/2)(\frac{\partial\phi}{\partial x})\delta D_3 \\
&+(h_{31} w_p h_p (h_p + h_b - 2z_n)/2) D_3\, \delta D_3 \Big] dx \\
&+(w_b h_b + w_p h_p)\int_{l1}^{l2} (K_b G_b + K_p G_p)(\frac{\partial y}{\partial x} - \phi)\delta(\frac{\partial y}{\partial x})dx \\
&-(w_b h_b + w_p h_p)\int_{l1}^{l2} (K_b G_b + K_p G_p)(\frac{\partial y}{\partial x} - \phi)\delta(\phi)dx
\end{aligned}$$ Equation 4-21

For *l2<x<l*: In this part of the beam there is not piezoelectric layer. The potential energy for this part using Equation 4-16 and Equation 4-17 is:

$$\begin{aligned}
\delta U3 &= w_b \int_{l2}^{l} \int_{-h_b/2}^{h_b/2} E_b(-z\frac{\partial\phi}{\partial x})\delta(-z\frac{\partial\phi}{\partial x})dzdx \\
&+ w_b \int_{l2}^{l} \int_{-h_b/2}^{h_b/2} K_b G_b(\frac{\partial y}{\partial x}-\phi)\delta(\frac{\partial y}{\partial x}-\phi)dzdx \\
&= \int_{l2}^{l} \frac{w_b E_b h_b^3}{12}(\frac{\partial\phi}{\partial x})\delta(\frac{\partial\phi}{\partial x})dx \\
&+ w_b h_b \int_{l2}^{l} K_b G_b(\frac{\partial y}{\partial x}-\phi)\delta(\frac{\partial y}{\partial x})dx \\
&- w_b h_b \int_{l2}^{l} K_b G_b(\frac{\partial y}{\partial x}-\phi)\delta(\phi)dx
\end{aligned} \qquad \text{Equation 4-22}$$

Also as there is a rotational spring in the beam model, the potential energy for the spring is considered and it is as:

$$U_{spring} = \frac{1}{2}k_s(\frac{\partial y}{\partial x}(0,t))^2 \qquad \text{Equation 4-23}$$

which,

$$\delta U_{spring} = k_s\frac{\partial y}{\partial x}\delta(\frac{\partial y}{\partial x}) \qquad \text{Equation 4-24}$$

as k_s is spring stiffness.

Finally, the total potential energy of the beam with a piezoelectric actuator on the top surface of it can be written as:

$$\delta U_{Total} = \int_0^l \Big\{ P(x)(\frac{\partial \phi}{\partial x})\delta(\frac{\partial \phi}{\partial x}) + \beta_{33} w_p h_p D_3(x,t)\delta D_3$$
$$+(h_{31} w_p h_p (h_p + h_b - 2z_n)/2)\frac{\partial \phi}{\partial x}\delta D_3$$
$$+(h_{31} w_p h_p (h_p + h_b - 2z_n)/2) D_3 \delta(\frac{\partial \phi}{\partial x}) \Big\} dx$$
$$+\int_0^l S(x)(\frac{\partial y}{\partial t} - \phi)\delta(\frac{\partial y}{\partial t} - \phi)dx + k_s \frac{\partial y}{\partial x}\delta(\frac{\partial y}{\partial x})$$

Equation 4-25

where:

$$P(x) = \frac{E_b w_b h_b^3}{12} + (H_{l1} - H_{l2}) E_b w_b h_b \, z_n^2$$
$$+(H_{l1} - H_{l2})\frac{E_p w_p}{3} . \left[h_p^3 + 3h_p (\frac{h_b}{2} - z_n)^2 + 3h_p^2 (\frac{h_b}{2} - z_n) \right]$$

Equation 4-26

$$S(x) = (1 - (H_{l1} - H_{l1}))K_b A_b(x) G_b$$
$$+(H_{l1} - H_{l1})(K_b A_b(x) G_b + K_p A_p(x) G_p)$$

Equation 4-27

External force on the beam is modeled as a distributed transverse load *f(x,t)*. The work done by this load is as Equation 4-28:

$$W = \int_0^l (f(x,t).y)dx$$

Equation 4-28

Also due to the input voltage to the piezoelectric patch, there is a virtual electrical work that is expressed as:

$$\delta W_{electrical} = w_p \int_0^l V_a(x,t)\delta D_3(x,t)dx$$

Equation 4-29

$V_a(x,t)$ is the applied voltage to the piezoelectric actuator and D is the displacement vector.

The Hamilton principle is used to find the equation of motion of the beam. The Hamilton principle is defined as follows:

$$\delta H = \int_{t1}^{t2} (\delta L + \delta W) = 0 \qquad \text{Equation 4-30}$$

where $\delta L = \delta T - \delta U$

The equation of motion of the proposed model for forearm is obtained by Hamilton principle using Equation 4-13, Equation 4-25, Equation 4-28 and Equation 4-29 as:

$$\begin{aligned}
&\int_{t1}^{t2} \Big[\int_0^l m(x)(\frac{\partial y}{\partial t})\delta(\frac{\partial y}{\partial t})dx + \int_0^l J(x)(\frac{\partial \phi}{\partial t})\delta(\frac{\partial \phi}{\partial t})dx \\
&-\int_0^l \Big\{ P(x)(\frac{\partial \phi}{\partial x})\delta(\frac{\partial \phi}{\partial x}) + \beta_{33} w_p h_p D_3(x,t)\delta D_3 \\
&+(h_{31} w_p h_p (h_p + h_b - 2y_n)/2)\frac{\partial \phi}{\partial x}\delta D_3 \\
&+(h_{31} w_p h_p (h_p + h_b - 2y_n)/2) D_3 \delta(\frac{\partial \phi}{\partial x}) \Big\} dx \\
&-\int_0^l S(x)(\frac{\partial y}{\partial t} - \phi)\delta(\frac{\partial y}{\partial t} - \phi)dx - k_s \frac{\partial y}{\partial x}\delta(\frac{\partial y}{\partial x}) \\
&+\int_0^l f(x,t)\delta y dx + w_p \int_0^l V_a(x,t)\delta D_3(x,t)dx \Big] dt = 0
\end{aligned} \qquad \text{Equation 4-31}$$

Using integration by parts;

$$\begin{aligned}
&\int_{t1}^{t2}\Big[\ \int_0^l [(-m(x)(\frac{\partial^2 y}{\partial t^2})+\frac{\partial}{\partial x}(S(x)(\frac{\partial y}{\partial x}-\phi))\delta y \\
&+\int_0^l(-J(x)(\frac{\partial^2\phi}{\partial t^2})+\frac{\partial}{\partial x}((h_{31}w_p h_p(h_p+h_b-2y_n)/2)D_3) \\
&+\frac{\partial}{\partial x}(P(x)\frac{\partial\phi}{\partial x})+S(x)(\frac{\partial y}{\partial x}-\phi))\delta\phi \\
&+(-(h_{31}w_p h_p(h_p+h_b-2y_n)/2)\frac{\partial\phi}{\partial x}-\beta_{33}w_p h_p D_3+w_p V_a)\delta D_3\big]dx \\
&-(P(x)\frac{\partial\phi}{\partial x}+(h_{31}w_p h_p(h_p+h_b-2y_n)/2)D_3)\delta\phi\Big|_0^l \\
&-(S(x)(\frac{\partial y}{\partial x}-\phi))\delta w\Big|_0^l\ \Big]dt=0
\end{aligned} \quad \text{Equation 4-32}$$

Finally the equation of motion of the proposed model which is a Timoshenko beam covered with a piezoelectric actuator on it is obtained as follows:

$$m(x)\frac{\partial^2 y}{\partial t^2}-\frac{\partial}{\partial x}S(x)(\frac{\partial y}{\partial x}-\phi)=f(x,t) \quad \text{Equation 4-33}$$

$$J(x)\frac{\partial^2\phi}{\partial t^2}-\frac{\partial}{\partial x}(P(x)(\frac{\partial\phi}{\partial x}))-\frac{\partial}{\partial x}((h_{31}w_p h_p(h_p+h_b-2y_n)/2)D_3)-S(x)(\frac{\partial y}{\partial x}-\phi)=0 \quad \text{Equation 4-34}$$

$$\beta_{33}w_p h_p D_3(x,t)+(h_{31}w_p h_p(h_p+h_b-2y_n)/2)\frac{\partial\phi}{\partial x}=w_p V_a(x,t) \quad \text{Equation 4-35}$$

From Equation 4-31, the boundary condition of the beam is as follows:

$$\begin{aligned}
&\left[P(x)(\frac{\partial\phi}{\partial x})+(h_{31}w_p h_p(h_p+h_b-2y_n)/2)D_3\right]\partial\phi\Big|_0^l=0 \\
&S(x)(\frac{\partial y}{\partial t}-\phi)\delta(\frac{\partial y}{\partial t}-\phi)\delta y(x,t)\Big|_0^l=0 \\
&k_s\frac{\partial y}{\partial x}\delta(\frac{\partial y}{\partial x})\Big|_{x=0}=0
\end{aligned} \quad \text{Equation 4-36}$$

From Equation 4-35 the dielectric displacement can be written as:

$$D_3(x,t)=(w_pV_a(x,t)-(h_{31}w_ph_p(h_p+h_b-2y_n)/2)\frac{\partial\phi}{\partial x})/\beta_{33}w_ph_p \qquad \text{Equation 4-37}$$

Substituting the dielectric displacement from Equation 4-37 into Equation 4-34 gives:

$$\begin{aligned}&J(x)\frac{\partial^2\phi}{\partial t^2}-\frac{\partial}{\partial x}(R(x)(\frac{\partial\phi}{\partial x}))\\&-S(x)(\frac{\partial y}{\partial x}-\phi)=\frac{\partial}{\partial x}(((h_{31}w_p(h_p+h_b-2y_n)/2)/\beta_{33})V_a(x,t))\end{aligned} \qquad \text{Equation 4-38}$$

as;

$$R(x)=P(x)-((h_{31}(h_p+h_b-2y_n)/2)^2/\beta_{33}$$

For laminar piezoelectric actuator, it is assumed that there is a uniform input voltage at the place that the actuator is attached on the beam, and naturally zero input voltage in another place. This voltage can be expressed as [57]:

$$V_a(x,t)=V_a(t)H(x) \qquad \text{Equation 4-39}$$

Using Equation 4-33, Equation 4-38 and Equation 4-39 the equation of motion of the beam model is reduced to:

$$m(x)\frac{\partial^2 y}{\partial t^2}-\frac{\partial}{\partial x}S(x)(\frac{\partial y}{\partial x}-\phi)=f(x,t) \qquad \text{Equation 4-40}$$

$$\begin{aligned}&J(x)\frac{\partial^2\phi}{\partial t^2}-\frac{\partial}{\partial x}(R(x)(\frac{\partial\phi}{\partial x}))\\&-S(x)(\frac{\partial y}{\partial x}-\phi)=((h_{31}w_p(h_p+h_b-2y_n)/2)/\beta_{33})V_a(t)H'(x)\end{aligned} \qquad \text{Equation 4-41}$$

Galerkin approximation has been used to solve the partial differential equation and obtain the natural frequency and mode shapes of the Timoshenko beam.

Transverse deflection, y, and bending angle ϕ can be expressed as:

$$y(x,t)=\sum_{i=1}^{\infty}Y_i(x)q_i(t) \qquad \text{Equation 4-42}$$

$$\phi(x,t)=\sum_{i=1}^{\infty}\varphi_i(x)q_i(t) \qquad \text{Equation 4-43}$$

where q(t) is the time-dependent function and *Y(x)* and $\varphi(x)$ are the fundamental vibration mode shapes [136].

$$\begin{aligned}Y(x)&=C_1\cosh(b\alpha x)+C_2\sinh(b\alpha x)\\&+C_3\cos(b\beta x)+C_4\sin(b\beta x)\end{aligned} \qquad \text{Equation 4-44}$$

$$\begin{aligned}\varphi(x)&=D_1\sinh(b\alpha x)+D_2\cosh(b\alpha x)\\&+D_3\sin(b\beta x)+C_4\cos(b\beta x)\end{aligned} \qquad \text{Equation 4-45}$$

where C_1 to C_4 and D_1 to D_4 are constants and can be obtained from boundary conditions of the beam. Also,

$$\begin{aligned}C_1&=\frac{l\alpha}{b(\alpha^2+s^2)}D_1, C_2=\frac{l\alpha}{b(\alpha^2+s^2)}D_2\\C_3&=-\frac{l\beta}{b(\beta^2-s^2)}D_3, C_4=-\frac{l\beta}{b(\beta^2-s^2)}D_4\end{aligned} \qquad \text{Equation 4-46}$$

b is the dimensionless frequency of the beam. Also, α , β and s are as follow:

$$\alpha=\left[\frac{1}{2}\left[-(r^2+s^2)+((r^2-s^2)^2+\frac{4}{b^2})^{0.5}\right]\right]^{0.5} \qquad \text{Equation 4-47}$$

$$\beta=\left[\frac{1}{2}\left[(r^2+s^2)+((r^2-s^2)^2+\frac{4}{b^2})^{0.5}\right]\right]^{0.5} \qquad \text{Equation 4-48}$$

$$\begin{aligned}s^2&=EI/(KAGl^2)\\r^2&=I/(Al^2)\end{aligned} \qquad \text{Equation 4-49}$$

As the beam is free at one end and has a pin joint and a rotational spring at the other end, the boundary conditions of the beam are:

$$\begin{aligned} &Y(x=0)=0 \\ &M(x=0)=k_s\psi(x=0) \\ &V(x=l)=0 \\ &M(x=l)=0 \end{aligned}$$

Equation 4-50

where Y is vertical deflection, M is bending moment, V is shear force and ψ is the bending slope of the beam.

The boundary condition of the beam in the form of a matrix is as:

$$\begin{bmatrix} \dfrac{l\alpha}{b(\alpha^2+s^2)} & 0 & -\dfrac{l\beta}{b(\beta^2-s^2)} & 0 \\ \dfrac{EI\beta\alpha}{l} & -k_s & \dfrac{EI\beta b}{l} & -k_s \\ \dfrac{KAGs^2}{(\alpha^2+s^2)}\sinh(b\alpha) & \dfrac{KAGs^2}{(\alpha^2+s^2)}\cosh(b\alpha) & -\dfrac{KAGs^2}{(\beta^2-s^2)}\sin(b\beta) & -\dfrac{KAGs^2}{(\beta^2-s^2)}\cos(b\beta) \\ \dfrac{EIb\alpha}{l}\cosh(b\alpha) & \dfrac{EIb\alpha}{l}\sinh(b\alpha) & \dfrac{EIb\beta}{l}\cos(b\beta) & -\dfrac{EIb\beta}{l}\sin(b\beta) \end{bmatrix} \times \begin{bmatrix} C_1 \\ C_2 \\ C_3 \\ C_4 \end{bmatrix} = \begin{bmatrix} 0 \\ 0 \\ 0 \\ 0 \end{bmatrix}$$

Equat ion 4-51

For a nontrivial solution of the constants *C1* and *C4*, the determinant made by coefficients of boundary condition matrix is set equal to zero [64].

Substituting y(x,t) and $\phi(x,t)$ from Equation 4-42 and Equation 4-43 into Equation 4-40 and Equation 4-41 the equation of motion of the beam model can be written as:

$$\sum_{i=1}^{\infty} m(x)Y_i(x)\ddot{q}_i(t) - \left(\sum_{i=1}^{\infty} S(x)\frac{\partial^2 Y_i(x)}{\partial x^2} - \sum_{i=1}^{\infty} S(x)\frac{\partial \varphi_i(x)}{\partial x}\right)q_i(t) = f(x,t$$

Equation 4-52

$$\sum_{i=1}^{\infty} J(x)\varphi_i(x)\ddot{q}_i(t) - \sum(R(x)(\frac{\partial^2\varphi_i(x)}{\partial x})q_i(t)$$
$$-(\sum_{i=1}^{\infty} S(x)\frac{\partial Y_i(x)}{\partial x} - \sum_{i=1}^{\infty} S(x)\varphi_i(x))q_i(t)$$
$$= ((h_{31}w_p(h_p + h_b - 2y_n)/2)/\beta_{33})H'(x)V_a(t)$$
Equation 4-53

$y(x,t)$ and $\phi(x,t)$ satisfy the free vibration of the beam as they are the beam mode shapes:

$$-m(x)Y_i(x)\omega_i^2 - S(x)(\frac{\partial^2 Y_i(x)}{\partial x^2} - \frac{\partial\varphi_i(x)}{\partial x}) = 0$$
Equation 4-54

$$-J(x)\varphi_i(x)\omega_i^2 - R(x)(\frac{\partial^2\varphi_i(x)}{\partial x}) - S(x)(\frac{\partial Y_i(x)}{\partial x} - \varphi_i(x)) = 0$$
Equation 4-55

Substituting Equation 4-54 and Equation 4-55 into Equation 4-52 and Equation 4-53:

$$\sum_{i=1}^{\infty} m(x)Y_i(x)\ddot{q}_i(t) + \sum_{i=1}^{\infty}\omega_i^2 m(x)Y_i(x)q_i(t) = f(x,t)$$
Equation 4-56

$$\sum_{i=1}^{\infty} J(x)\varphi_i(x)\ddot{q}_i(t) + \sum_{i=1}^{\infty}\omega_i^2 J(x)\varphi_i(x)q_i(t)$$
$$= ((h_{31}w_p(h_p + h_b - 2y_n)/2)/\beta_{33})H'(x)V_a(t)$$
Equation 4-57

There is an orthogonality conditions between different mode shapes of the beam as:

$$\int_0^l m(x).Y_i(x).Y_j(x) = \begin{cases} 1 & i = j \\ 0 & i \neq j \end{cases}$$
Equation 4-58

$$\int_0^l J(x).\varphi_i(x).\varphi_j(x) = \begin{cases} 1 & i = j \\ 0 & i \neq j \end{cases}$$
Equation 4-59

Then multiplying Equation 4-56 by $Y_i(x)$ and Equation 4-57 by $\varphi_i(x)$ and integrating from 0 to l leads to:

$$\sum_{i=1}^{\infty}\int_{0}^{l} Y_i(x)m(x)Y_i(x)\ddot{q}_i(t)dx + \sum_{i=1}^{\infty}\int_{0}^{l} Y_i(x)\omega_i^{\,2}m(x)Y_i(x)q_i(t)dx$$
$$= \int_{0}^{l} Y_i(x)f(x,t)dx \qquad \text{Equation 4-60}$$

$$\sum_{i=1}^{\infty}\int_{0}^{l} \varphi_i(x)J(x)\varphi_i(x)\ddot{q}_i(t)dx + \sum_{i=1}^{\infty}\omega_i^{\,2}\int_{0}^{l} \varphi_i(x)J(x)\varphi_i(x)q_i(t)dx$$
$$= ((h_{31}w_p(h_p + h_b - 2y_n)/2)/\beta_{33})\int_{0}^{l} \varphi_i(x)H'(x)V_a(t) \qquad \text{Equation 4-61}$$

Finally, with adding Equation 4-60 and Equation 4-61, and using Equation 4-58 and Equation 4-59 the equation of motion of the Timoshenko beam which has a piezoelectric actuator on its top surface is derived as:

$$\ddot{q}_i(t) + \omega_i^2 q_i(t) = F_i(t) + P_i(t)$$
$$F_i(t) = \int_{0}^{l} f(x,t)Y_i(x)$$
$$P_i(t) = (\frac{1}{2}w_p(t_p + t_b - 2y_n)\frac{h_{31}}{\beta_{33}})V_a(t)\int_{0}^{l}\frac{d}{dx}(H_{l1} - H_{l2})\varphi_i(x)dx$$
$$= (\frac{1}{2}w_p(t_p + t_b - 2y_n)\frac{h_{31}}{\beta_{33}})V_a(t)(\varphi_i(l_1) - \varphi_i(l_2)) \qquad \text{Equation 4-62}$$

Here, it is assumed that the external force and the applied voltage to the piezoelectric actuator are harmonic as follows:

$$f(x,t) = F(x)\sin(\omega_1 t)$$
$$F(x) = 5x \qquad \text{Equation 4-63}$$

$$V(t) = V.\sin(\omega_2 t) \qquad \text{Equation 4-64}$$

Using Equation 4-62 to Equation 4-64 the vibration of the Timoshenko beam with a layer of piezoelectric as an actuator on its top surface is expressed as:

$$q(t) = A.\cos(\omega t) + B.\sin(\omega t) + \frac{\left[(\int_0^l f(x,t)\varphi(x)) / \sin(\omega_1 t) \right]}{\omega^2 - \omega_1^2}.\sin(\omega_1 t)$$
$$+ \frac{\left[(\frac{1}{2} w_p (t_p + t_b - 2y_n) \frac{h_{31}}{\beta_{33}}).V_a(t).(\varphi_n(l_1) - \varphi_n(l_2)) \right]}{\omega^2 - \omega_2^2}.\sin(\omega_2 t)$$

Equation 4-65

ω is the natural frequency of the beam. Also, the constants A and B can be found from the initial condition of the beam. Finally, the vibration of the proposed beam model which helps to analyse the effect of the piezoelectric actuator on vibration control of the forearm model is obtained as:

$$q(t) = \frac{\left[-(\int_0^l f(x,t)\varphi(x)) / \sin(\omega_1 t) \right] \omega_1}{\omega} \sin(\omega t)$$
$$- \frac{\left[(\frac{1}{2} w_p (t_p + t_b - 2y_n) \frac{h_{31}}{\beta_{33}}).V_a(t).(\varphi_n(l_1) - \varphi_n(l_2)) \right] \omega_2}{\omega} \sin(\omega t)$$
$$+ \frac{\left[(\int_0^l f(x,t)\varphi(x)) / \sin(\omega_1 t) \right]}{\omega^2 - \omega_1^2}.\sin(\omega_1 t)$$
$$+ \frac{\left[(\frac{1}{2} w_p (t_p + t_b - 2y_n) \frac{h_{31}}{\beta_{33}}).V_a(t).(\varphi_n(l_1) - \varphi_n(l_2)) \right]}{\omega^2 - \omega_2^2}.\sin(\omega_2 t)$$

Equation 4-66

4.2.1.4 Results

In this section, the results of forced vibration for the human forearm which is modelled as a Timoshenko beam with an actuator layer on its top surface is presented. As the main aim of this section is vibration control on the human forearm, analytical expressions for vibration of the beam model are derived. The effects of different parameters including piezoelectric strain constant, voltage of piezoelectric actuator, density and modulus of elasticity of piezoelectric actuator on the vibration of the beam are discussed to see the effect of each property on the vibration control of the beam. The external force for the analysis is considered as $f(x,t) = 5.x.\sin(5t)$ and the voltage of the actuator is $V(t) = 10.\sin(10t)$. The effects of these properties on the vibration of the beam are presented in Figure 4-2 to Figure 4-6. All figures illustrate the vibration of the beam with the physical properties of the beam and piezoelectric actuator which are listed in Table 4-1 and are drawn based on Equation 4-66 around the first mode of vibration. The beam properties are chosen in a way to get to the closest real human forearm properties.

Table 4-1. Physical properties of the beam model covered with a piezoelectric actuator

$l = 300mm$	$E_p = 104GPa$
$l_1 = 100mm$	$E_b = 14GPa$
$l_2 = 200mm$	$\rho_b = 1810kgm^{-3}$
$w_b = 70mm$	$\rho_p = 6390kgm^{-3}$
$w_p = 70mm$	$G_b = E_b / 2.5$
$h_b = 50mm$	$G_p = E_p / 2.5$
$h_p = 50mm$	$K = 0.833$
$d_{31} = 11pCN^{-1}$	

4.2.1.4.1 Analytical results

Figure 4-2 shows two plots of the vibration of the beam with and without a piezoelectric layer. The system response decreases almost three times faster when the beam is covered with a piezoelectric layer as can be found from the comparison of the two plots. In fact, adding the piezoelectric layer to the beam model causes the total stiffness of the beam model to increase resulting in reduction of the vibration amplitude. It should also be noted that because the frequency of the external force and the frequency of the applied voltage to the piezoelectric actuator is 5 and 10 rad/s, respectively, the beam vibrates with a combination of these frequencies.

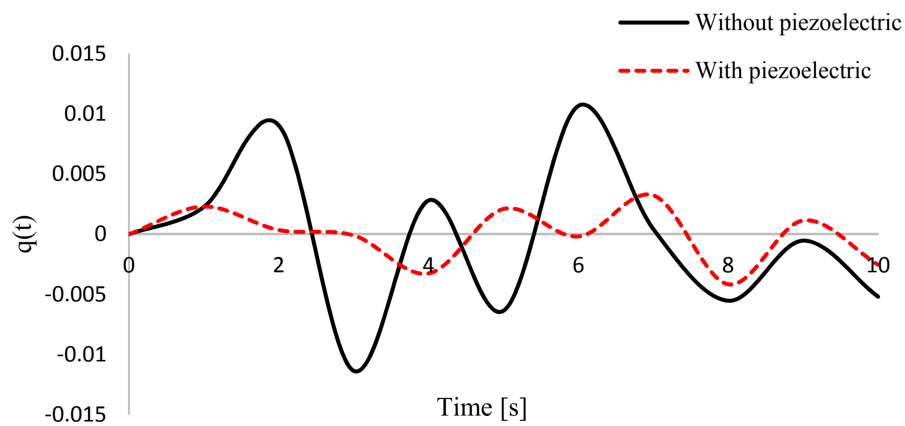

Figure 4-2. The vibration of the beam without and with a piezoelectric layer

The effect of the piezoelectric strain constant, d_{31}, which is related to the presence of piezoelectric actuation on the vibration of the beam is investigated. The piezoelectric strain constant is changed from 11×10^{-12} C/N to 11×10^{-10} C/N and the result for vibration of the beam is shown in Figure 4-3. As seen, the absolute value of the maximum amplitude of vibration increases with d_{31}. Obviously, for a given applied electric field, a higher piezoelectric strain constant creates a larger mechanical stress or displacement.

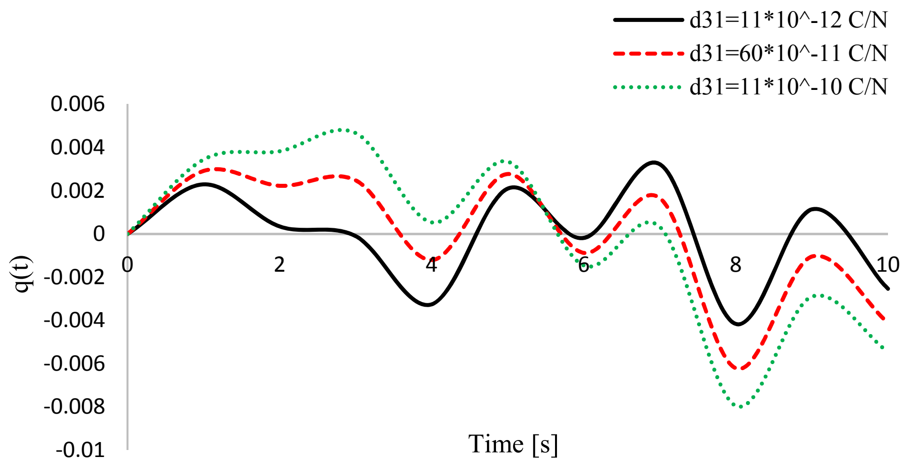

Figure 4-3. The vibration of the Timoshenko beam with a piezoelectric layer for different d_{31}

Figure 4-4 depicts the effect of different voltage amplitudes of the piezoelectric actuator on the beam vibration while the other parameters are kept fixed. The voltage of the piezoelectric actuator was shown in Equation 4-64. As seen in Figure 4-4, the absolute value of the maximum amplitude of vibration increases as the applied voltage increases. The absolute values of the maximum amplitude of vibration for applied voltages of 10 v, 25 v, and 45 v are 0.004, 0.005, and 0.006, respectively.

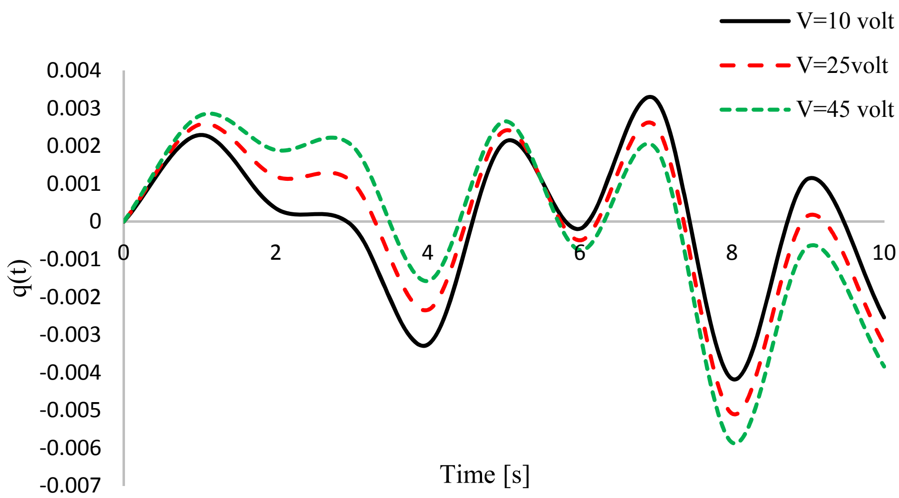

Figure 4-4. The vibration of the Timoshenko beam with a piezoelectric layer for different voltage of piezoelectric actuator.

The effect of changing the piezoelectric density from 6390 to 7700 kg/m^3 on the vibration of the beam is shown in Figure 4-5. As the density of the piezoelectric actuator increases, the absolute value of the maximum amplitude of vibration increases. The absolute values of the maximum amplitude of vibration for densities of 6390, 7000, and 7700 kg/m^3 are 0.003, 0.004, and 0.005, respectively. A higher density means a more flexible structure while the other parameters remain unchanged resulting in a larger amplitude of vibration.

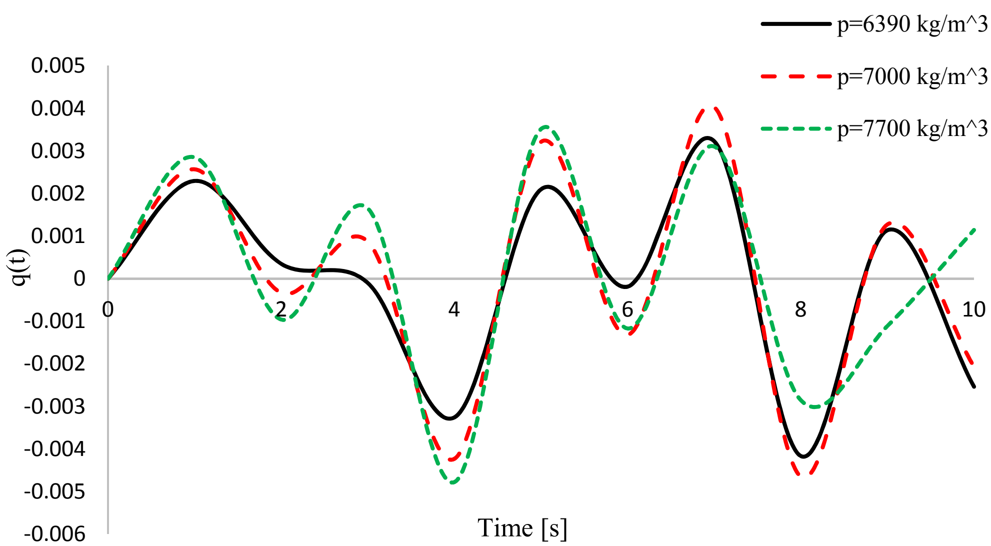

Figure 4-5. The vibration of the Timoshenko beam with a piezoelectric layer for different density of piezoelectric actuator

The effect of the modulus of elasticity of the piezoelectric actuator, *Ep*, is presented in Figure 4-6. As the modulus of elasticity increases, the amplitude of the vibration decreases. This is due to the fact that higher a modulus of elasticity gives a stiffer structures resulting in a smaller amplitude of vibration. The maximum amplitude of vibration for modulus of elasticity of 104 GPa, 350 GPa, and 800 GPa is 322×10^{-5}, 271×10^{-5}, and $178e^{-5}$ respectively.

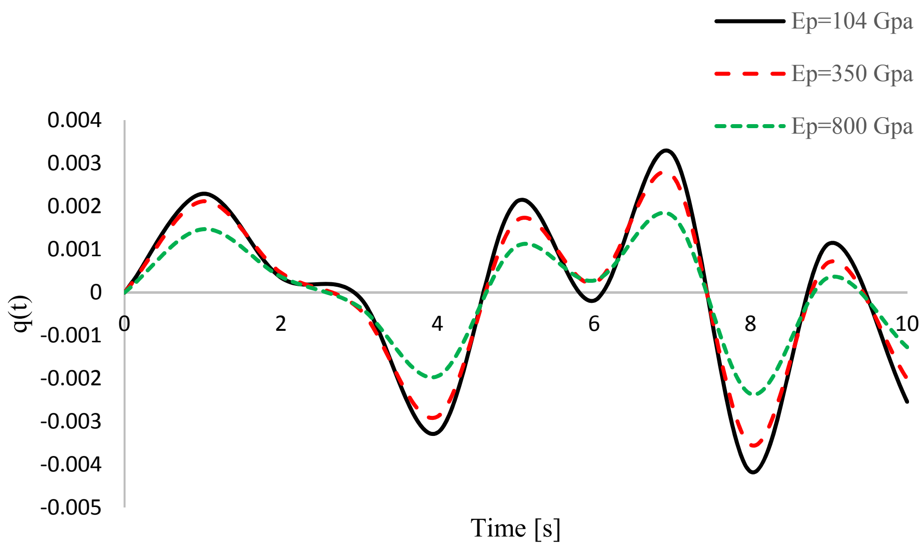

Figure 4-6. The vibration of the Timoshenko beam with a piezoelectric layer for different modulus of elasticity of piezoelectric actuator

4.2.1.4.2 Finite element result

Finite element analysis (FEA) using ABAQUS was performed to verify the results obtained from the analytical solution. An 8-node linear piezoelectric brick element (C3D8E) and an 8-node linear brick element (C3D8) were used to mesh the piezoelectric and substrate parts, respectively. Figure 4-7 illustrates the meshed beam model.

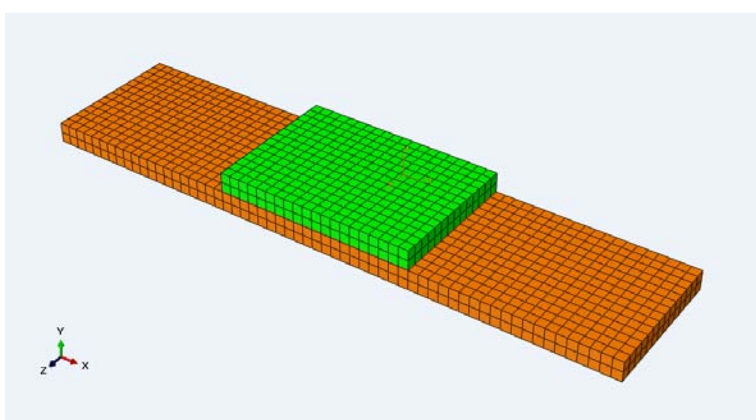

Figure 4-7. Mesh configuration of FE model of the beam

Figure 4-8 shows the result for vibration of the beam without piezoelectric layer for both analytical and FE result. As it is seen in the figure the result of FE for the beam model is very close to the analytical result. The correlation coefficient between the analytical and numerical results is 0.99.

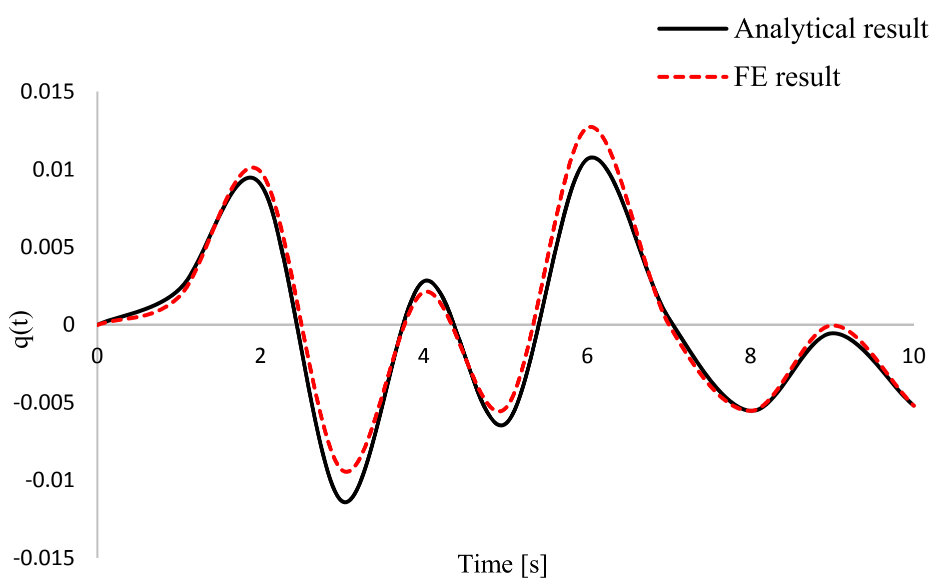

Figure 4-8. Analytical and FE result for vibration of the beam without piezoelectric layer

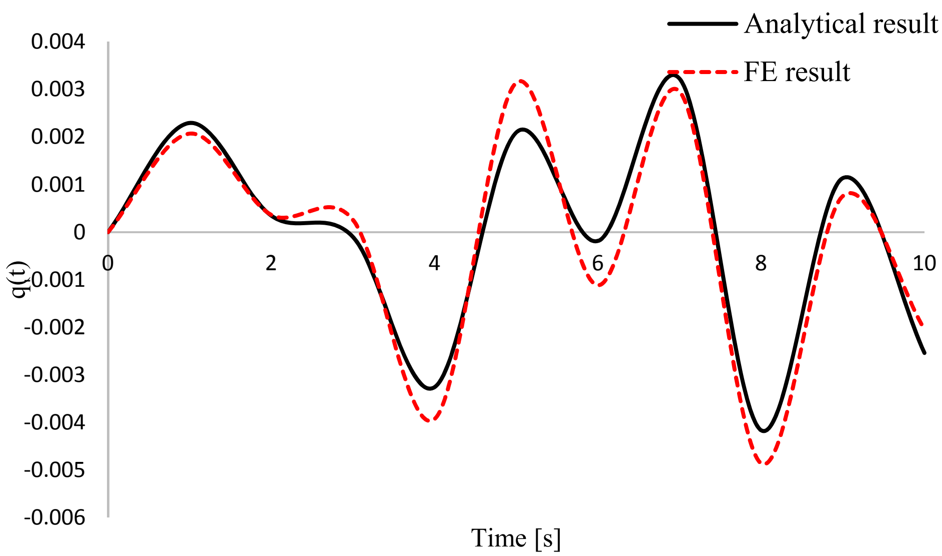

Figure 4-9. Analytical and FE result for vibration of the beam with the piezoelectric layer.

Figure 4-9 shows the result for vibration of the beam with the piezoelectric layer for both analytical and FE result. The correlation coefficient between the analytical and numerical results is 0.97.

4.2.2 Active vibration control in human forearm model

In this part, an active vibration control (AVC) for investigating the human forearm tremor is proposed. The control system uses the piezoelectric sensor and actuator pair to control and suppress the forearm tremor which is the main aim of the proposed active control system. Human forearm is modelled as an Euler-Bernoulli beam that is a uniform flexible continuous beam and is covered with a layer of piezoelectric sensor on its bottom surface and a piezoelectric actuator on its top surface. The beam is initially straight, and it is free at one end and has a pin joint and a rotational spring at the other end. The human forearm beam model is shown in Figure 4-10.

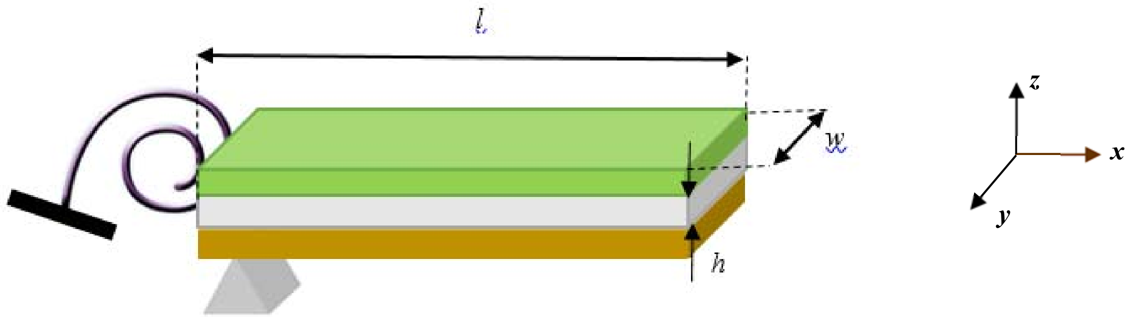

Figure 4-10. Human forearm beam model covered with a piezoelectric sensor and actuator

As human forearm tremor is a kind of sinusoidal movement, an external harmonic force is applied to the beam model as tremor. A closed loop control system is used to actively control the tremor on the model as the aim is reducing the tremor in the model. Analytical solution for the vibration of beam model is investigated to analyse the effect of piezoelectric sensor and actuator on tremor reduction. As the beam is the Euler–Bernoulli, the rotation of cross sections of the beam is neglected compared to the translation and the angular distortion caused by shear is considered negligible compared to the bending deformation [64].

As it can be seen in the Figure 4-10, the beam model has a length of l , width of w_b and thickness of h_b. The piezoelectric sensor and actuator are perfectly bonded to the beam and it is assumed that the length, width and thickness of piezoelectric sensor and actuator is the same as the beam; ($l=l_b=l_a=l_s$), ($w=w_b=w_a=w_s$) and ($h=h_b=h_a=h_s$).

4.2.2.1 Equation of motion

Hamilton principle is used to derive the equation of motion of the beam model.

4.2.2.1.1 Kinetic energy

The kinetic energy of the beam model with a layer of piezoelectric as a sensor in bottom layer and another piezoelectric layer as an actuator on its top surface can be expressed in Equation 4-67 as:

$$T=\frac{\rho_b}{2}\int_{vb}(\frac{\partial\chi}{\partial t})^2 dv_b+\frac{\rho_a}{2}\int_{va}(\frac{\partial\chi}{\partial t})^2 dv_a+\frac{\rho_s}{2}\int_{vs}(\frac{\partial\chi}{\partial t})^2 dv_s \qquad \text{Equation 4-67}$$

as χ is the lateral displacement, ρ_b , ρ_a and ρ_b are mass density of beam, piezoelectric actuator and piezoelectric sensor. Also, v_b , v_a and v_s are volume of the beam, actuator and sensor respectively.

$$\begin{aligned}T&=\frac{1}{2}\int_0^l[\rho_b h_b w_b+\rho_a h_a w_a+\rho_s h_s w_s](\frac{\partial\chi}{\partial t})^2 dx\\&=\frac{1}{2}\int_0^l[m_b+m_a+m_s](\frac{\partial\chi}{\partial t})^2 dx\end{aligned} \qquad \text{Equation 4-68}$$

m_b , m_a and m_s are mass of the beam, actuator and sensor.

Then,

$$\begin{aligned}&\delta T=\int_0^l m(x)(\frac{\partial\chi}{\partial t})\delta(\frac{\partial\chi}{\partial t})dx\\&as \qquad m(x)=m_b(x)+m_a(x)+m_s(x)\end{aligned} \qquad \text{Equation 4-69}$$

4.2.2.1.2 Potential energy

As the beam has a layer of piezoelectric on its top as an actuator and a layer of piezoelectric as a sensor in bottom layer, the total potential energy for the beam model is derived as Equation 4-70 [82]:

$$U=\frac{1}{2}\int_v\sigma_x^b\varepsilon_x dv_b+\frac{1}{2}\int_{va}\sigma_x^{pa}\varepsilon_x dv_a-\frac{1}{2}\int_{va}D_{za}\in_{za}dv_a+\frac{1}{2}\int_{vs}\sigma_x^{ps}\varepsilon_x dv_s-\frac{1}{2}\int_{vs}D_{zs}\in_{zs}dv_s \qquad \text{Equation 4-70}$$

a) Potential energy of the beam

$$U_b = \frac{1}{2}\int_{v_b} \sigma_x^b \varepsilon_x dv_b = \frac{1}{2}\int_{v_b} E_b \varepsilon_x^2 dv_b$$ Equation 4-71

As the stress strain relationship for the beam is:

$$\sigma_x = E\varepsilon_x$$
$$\varepsilon_x = -z\frac{\partial^2 \chi}{\partial x^2}$$ Equation 4-72

Using Equation 4-72, the potential energy for the beam is as follow:

$$\delta U_b = \int_{va} E_b \varepsilon_x \delta\varepsilon_x dv_b = w_b \int_0^l \int_{-h_b/2}^{+h_b/2} E_b z^2 (\frac{\partial^2 \chi}{\partial x^2})\delta(\frac{\partial^2 \chi}{\partial x^2})$$
$$= \frac{E_b w_b h_b^3}{12}\int_0^l (\frac{\partial^2 \chi}{\partial x^2})\delta(\frac{\partial^2 \chi}{\partial x^2})$$ Equation 4-73

b) Potential energy of the piezoelectric actuator

As there is a layer of piezoelectric on the top surface of the model that works as an actuator, the potential energy of the piezoelectric actuator has an effect on the total potential energy of the model. The total potential energy of piezoelectric actuator is as Equation 4-74:

$$U_a = \frac{1}{2}\int_{va} \sigma_x^a \varepsilon_x dv_a - \frac{1}{2}\int_{va} D_{za} \in_{za} dv_a$$ Equation 4-74

The constitutive relations, for piezoelectric material can be written in the form of [81]:

$$\sigma = E\varepsilon - e \in$$
$$D = e\varepsilon + \xi \in$$ Equation 4-75

As the polarization direction for the piezoelectric material is in the z-axis direction and also the piezoelectric material is transversely isotropic, the constitutive equation of the piezoelectric material is defined as:

$$\sigma_{xp} = E_p \varepsilon_x - e_{31} \in_z$$
$$D_z = e_{31}\varepsilon_x + \xi_{33} \in_z \qquad \text{Equation 4-76}$$

where σ is the stress vector, E is the elasticity coefficient matrix, ε is the strain vector, e_{31} is the piezoelectric constant, $\in_z$ the electric intensity in the z-direction , D is the displacement vector and ξ_{33} is the dielectric constant [81].

Also, the equation for the electric intensity of the piezoelectric actuators and sensors is defined as:

$$\in_{za} = \frac{V_a}{h_a}$$
$$\in_{zs} = \frac{V_s}{h_s} \qquad \text{Equation 4-77}$$

Subscript of a and s show the properties of the piezoelectric actuator and sensor respectively. V indicates the external voltage that is applied to the actuator and sensor.

Using Equation 4-76, the potential energy of the piezoelectric actuator can be written as Equation 4-78:

$$U_a = \frac{1}{2}\int_{va} (E_a\varepsilon_x - e_{31} \in_{za})\varepsilon_x dv_a - \frac{1}{2}\int_{va} (e_{31}\varepsilon_x + \xi_{33} \in_{za}) \in_{za} dv_a$$
$$= \frac{1}{2}\int_{va} (E_a\varepsilon_x^2 - e_{31} \in_{za} \varepsilon_x)dv_a - \frac{1}{2}\int_{va} (e_{31}\varepsilon_x \in_{za} + \xi_{33} \in_{za}^2)dv_a \qquad \text{Equation 4-78}$$

Finally substituting Equation 4-72 into Equation 4-78, δU_a is as:

$$\delta U_a = w_a \int_0^l \int_{h_b/2}^{h_b/2+h_a} E_a z^2 (\frac{\partial^2 \chi}{\partial x^2}) \delta (\frac{\partial^2 \chi}{\partial x^2}) - \frac{1}{2} w_a \int_0^l \int_{-h_b/2}^{h_b/2+h_a} e_{31} \in_{za} \delta(-z \frac{\partial^2 \chi}{\partial x^2})$$
$$-\frac{1}{2} w_a \int_0^l \int_{h_b/2}^{h_b/2+h_a} e_{31} (-z \frac{\partial^2 \chi}{\partial x^2}) \delta \in_{za} - \frac{1}{2} w_a \int_0^l \int_{-h_b/2}^{h_b/2+h_a} e_{31} \in_{za} \delta(-z \frac{\partial^2 \chi}{\partial x^2})$$
$$-\frac{1}{2} w_a \int_0^l \int_{h_b/2}^{h_b/2+h_a} e_{31} (-z \frac{\partial^2 \chi}{\partial x^2}) \delta \in_{za} - w_a \int_0^l \int_{h_b/2}^{h_b/2+h_a} \xi_{33} \in_{za} \delta \in_{za}$$
$$= \frac{w_a E_a}{3} \left[\left(\frac{h_b}{2} + h_a \right)^3 - \left(\frac{h_b}{2} \right)^3 \right] \int_0^l (\frac{\partial^2 \chi}{\partial x^2}) \delta (\frac{\partial^2 \chi}{\partial x^2})$$
$$-\frac{w_a e_{31} \in_{za}}{4} \left[\left(\frac{h_b}{2} + h_a \right)^2 - \left(\frac{h_b}{2} \right)^2 \right] \int_0^l \delta (\frac{\partial^2 \chi}{\partial x^2}) + \frac{w_a e_{31}}{4} \left[\left(\frac{h_b}{2} + h_a \right)^2 - \left(\frac{h_b}{2} \right)^2 \right] \int_0^l (\frac{\partial^2 \chi}{\partial x^2}) \delta \in_{z} \quad \text{Equation 4-79}$$
$$+\frac{w_a e_{31} \in_{za}}{4} \left[\left(\frac{h_b}{2} + h_a \right)^2 - \left(\frac{h_b}{2} \right)^2 \right] \int_0^l \delta (\frac{\partial^2 \chi}{\partial x^2})$$
$$+\frac{w_a e_{31}}{4} \left[\left(\frac{h_b}{2} + h_a \right)^2 - \left(\frac{h_b}{2} \right)^2 \right] \int_0^l (\frac{\partial^2 \chi}{\partial x^2}) \delta \in_{za} + w_a h_a \xi_{33} \in_{za} \int_0^l \delta \in_{za}$$
$$= \frac{w_a E_a}{3} \left[\left(\frac{h_b}{2} + h_a \right)^3 - \left(\frac{h_b}{2} \right)^3 \right] \int_0^l (\frac{\partial^2 \chi}{\partial x^2}) \delta (\frac{\partial^2 \chi}{\partial x^2}) - \frac{w_a e_{31} \in_{za}}{2} \left[\left(\frac{h_b}{2} + h_a \right)^2 - \left(\frac{h_b}{2} \right)^2 \right] \int_0^l \delta (\frac{\partial^2 \chi}{\partial x^2})$$
$$-\frac{w_a e_{31}}{2} \left[\left(\frac{h_b}{2} + h_a \right)^2 - \left(\frac{h_b}{2} \right)^2 \right] \int_0^l (\frac{\partial^2 \chi}{\partial x^2}) \delta \in_{za} + w_a h_a \xi_{33} \in_{za} \int_0^l \delta \in_{za}$$

c) Potential energy of the piezoelectric sensor

The potential energy from the piezoelectric sensor is considered in the total potential energy as it is working as a sensor on the bottom surface of the beam. Using Equation 4-76 the potential energy of the piezoelectric layer that acts as a sensor is derived as:

$$U_s = \frac{1}{2} \int_{vs} \sigma_x^s \varepsilon_x dv_s - \frac{1}{2} \int_{vs} D_{zs} \in_{zs} dv_s$$
$$= \frac{1}{2} \int_{vs} (E_s \varepsilon_x - e_{31} \in_{zs}) \varepsilon_x dv_s - \frac{1}{2} \int_{va} (e_{31} \varepsilon_x + \xi_{33} \in_{zs}) \in_{zs} dv_a \quad \text{Equation 4-80}$$
$$= \frac{1}{2} \int_{vs} (E_a \varepsilon_x^2 - e_{31} \in_{zs} \varepsilon_x) dv_s - \frac{1}{2} \int_{vs} (e_{31} \varepsilon_x \in_{zs} + \xi_{33} \in_{zs}^2) dv_s$$

Substituting Equation 4-72 into Equation 4-78, δU_S that it is used in the Hamilton principle is as:

$$\begin{aligned}
\delta U_s &= w_s \int_0^l \int_{-h_b/2-h_s}^{-h_b/2} E_s z^2 (\frac{\partial^2 \chi}{\partial x^2}) \delta (\frac{\partial^2 \chi}{\partial x^2}) - \frac{1}{2} w_s \int_0^l \int_{-h_b/2-h_s}^{-h_b/2} e_{31} \in_{zs} \delta (-z \frac{\partial^2 \chi}{\partial x^2}) \\
&- \frac{1}{2} w_s \int_0^l \int_{-h_b/2-h_s}^{-h_b/2} e_{31} (-z \frac{\partial^2 \chi}{\partial x^2}) \delta \in_{zs} - \frac{1}{2} w_s \int_0^l \int_{-h_b/2-h_s}^{-h_b/2} e_{31} \in_{zs} \delta (-z \frac{\partial^2 \chi}{\partial x^2}) \\
&- \frac{1}{2} w_s \int_0^l \int_{-h_b/2-h_s}^{-h_b/2} e_{31} (-z \frac{\partial^2 \chi}{\partial x^2}) \delta \in_{zs} - w_a \int_0^l \int_{h_b/2}^{h_b/2+h_a} \xi_{33} \in_{zs} \delta \in_{zs} \\
&= \frac{w_s E_s}{3} \left[\left(\frac{h_b}{2} + h_s \right)^3 - \left(\frac{h_b}{2} \right)^3 \right] \int_0^l (\frac{\partial^2 \chi}{\partial x^2}) \delta (\frac{\partial^2 \chi}{\partial x^2}) \\
&- \frac{w_s e_{31} \in_{zs}}{4} \left[\left(\frac{h_b}{2} \right)^2 - \left(\frac{h_b}{2} + h_s \right)^2 \right] \int_0^l \delta (\frac{\partial^2 \chi}{\partial x^2}) + \frac{w_s e_{31}}{4} \left[\left(\frac{h_b}{2} \right)^2 - \left(\frac{h_b}{2} + h_s \right)^2 \right] \int_0^l (\frac{\partial^2 \chi}{\partial x^2}) \delta \in_{zs} \\
&+ \frac{w_s e_{31} \in_{zs}}{4} \left[\left(\frac{h_b}{2} \right)^2 - \left(\frac{h_b}{2} + h_s \right)^2 \right] \int_0^l \delta (\frac{\partial^2 \chi}{\partial x^2}) \\
&+ \frac{w_s e_{31}}{4} \left[\left(\frac{h_b}{2} \right)^2 - \left(\frac{h_b}{2} + h_s \right)^2 \right] \int_0^l (\frac{\partial^2 \chi}{\partial x^2}) \delta \in_{zs} + w_s h_s \xi_{33} \in_{zs} \int_0^l \delta \in_{zs} \\
&= \frac{w_s E_s}{3} \left[\left(\frac{h_b}{2} + h_a \right)^3 - \left(\frac{h_b}{2} \right)^3 \right] \int_0^l (\frac{\partial^2 \chi}{\partial x^2}) \delta (\frac{\partial^2 \chi}{\partial x^2}) - \frac{w_s e_{31} \in_{zs}}{2} \left[\left(\frac{h_b}{2} \right)^2 - \left(\frac{h_b}{2} + h_s \right)^2 \right] \int_0^l \delta (\frac{\partial^2 \chi}{\partial x^2}) \\
&- \frac{w_s e_{31}}{2} \left[\left(\frac{h_b}{2} \right)^2 - \left(\frac{h_b}{2} + h_s \right)^2 \right] \int_0^l (\frac{\partial^2 \chi}{\partial x^2}) \delta \in_{zs} + w_s h_s \xi_{33} \in_{zs} \int_0^l \delta \in_{zs}
\end{aligned}$$

Equation 4-81

Also the potential energy from rotational spring, δU_{spring}, in the beam model, using Equation 4-23 is considered as a part of the total potential energy.

The total potential energy for the beam model is:

$$\delta U_{total} = \delta U_b + \delta U_a + \delta U_s + \delta U_{spring}$$

Equation 4-82

As it is seen in Hamilton principle, Equation 4-30, the work that is done by the external force on the beam must be considered for deriving the equation of motion. In this proposed model for the human forearm, tremor is applied to the model as a distributed transverse load *f(x,t)*. The work done by this external force is derived from Equation 4-28.

The Hamilton principle, Equation 4-30, is used to find the equation of motion of the beam. Using Equation 4-28, Equation 4-69 and Equation 4-82, the Hamilton principle for the Euler-Bernoulli beam model for forearm is obtained as:

$$\begin{aligned}
&\int_{t1}^{t2}\Bigg\{\left[\int_0^l m(x)(\frac{\partial\chi}{\partial t})\delta(\frac{\partial\chi}{\partial t})dx\right]-\Bigg[(\frac{E_b w_b h_b^3}{12}\int_0^l(\frac{\partial^2\chi}{\partial x^2})\delta(\frac{\partial^2\chi}{\partial x^2})\\
&+(\frac{w_a E_a}{3}\left[\left(\frac{h_b}{2}+h_a\right)^3-\left(\frac{h_b}{2}\right)^3\right]\int_0^l(\frac{\partial^2\chi}{\partial x^2})\delta(\frac{\partial^2\chi}{\partial x^2})-\frac{w_a e_{31}\in_{za}}{2}\left[\left(\frac{h_b}{2}+h_a\right)^2-\left(\frac{h_b}{2}\right)^2\right]\int_0^l\delta(\frac{\partial^2\chi}{\partial x^2})\\
&-\frac{w_a e_{31}}{2}\left[\left(\frac{h_b}{2}+h_a\right)^2-\left(\frac{h_b}{2}\right)^2\right]\int_0^l(\frac{\partial^2\chi}{\partial x^2})\delta\in_{za}+w_a h_a\xi_{33}\in_{za}\int_0^l\delta\in_{za})\\
&+(\frac{w_s E_s}{3}\left[\left(\frac{h_b}{2}+h_a\right)^3-\left(\frac{h_b}{2}\right)^3\right]\int_0^l(\frac{\partial^2\chi}{\partial x^2})\delta(\frac{\partial^2\chi}{\partial x^2})-\frac{w_s e_{31}\in_{zs}}{2}\left[\left(\frac{h_b}{2}\right)^2-\left(\frac{h_b}{2}+h_s\right)^2\right]\int_0^l\delta(\frac{\partial^2\chi}{\partial x^2})\\
&-\frac{w_s e_{31}}{2}\left[\left(\frac{h_b}{2}\right)^2-\left(\frac{h_b}{2}+h_s\right)^2\right]\int_0^l(\frac{\partial^2\chi}{\partial x^2})\delta\in_{zs}+w_s h_s\xi_{33}\in_{zs}\int_0^l\delta\in_{zs})+(k_s\frac{\partial\chi}{\partial x}\delta(\frac{\partial\chi}{\partial x}))\Bigg]\\
&+\left[\int_0^l f(x,t)\delta\chi dx\right]\Bigg\}dt=0
\end{aligned}$$

Equation 4-83

Finally using integration by parts the equation of motion of the Euler-Bernoulli beam model as a human forearm model that is covered with a piezoelectric actuator on top and a piezoelectric sensor on the bottom level is obtained as Equation 4-84, Equation 4-85 and Equation 4-86:

$$\begin{aligned}
&m(x)\frac{\partial^2\chi}{\partial t^2}+\left[\frac{E_b w_b h_b^3}{12}+\frac{2E_b w_b}{3}\left[\left(\frac{h_b}{2}+h_p\right)^3-\left(\frac{h_b}{2}\right)^3\right]\right]\frac{\partial^4\chi}{\partial x^4}\\
&+\frac{e_{31}}{h_a}\left[\left(\frac{h_b}{2}\right)^2-\left(\frac{h_b}{2}+h_p\right)^2\right]\frac{\partial^2 V_a}{\partial x^2}-\frac{e_{31}}{h_s}\left[\left(\frac{h_b}{2}\right)^2-\left(\frac{h_b}{2}+h_p\right)^2\right]\frac{\partial^2 V_s}{\partial x^2}\\
&=f(x,t)
\end{aligned}$$

Equation 4-84

$$\frac{e_{31}w}{3}\left[\left(\frac{h_b}{2}\right)^2-\left(\frac{h_b}{2}+h_p\right)^2\right]\frac{\partial^2\chi}{\partial x^2}-\xi_{33}w_aV_a=0 \qquad \text{Equation 4-85}$$

$$\frac{e_{31}w}{3}\left[\left(\frac{h_b}{2}\right)^2-\left(\frac{h_b}{2}+h_p\right)^2\right]\frac{\partial^2\chi}{\partial x^2}+\xi_{33}w_sV_s=0 \qquad \text{Equation 4-86}$$

as there is no electrical field applied to the piezoelectric sensor and also all the charges only exist in the surfaces of piezoelectric layers the Equation 4-76 is reduced to:

$$D_z=e_{31}\varepsilon_x \qquad \text{Equation 4-87}$$

where ε_x is the terminating strain of the sensor layer and D_z is the electric displacement [70]. The summations of all the charges that are on all points of the piezoelectric sensor layer are developed on the sensor surface. If *Q(t)* is the closed circuit charge that is measured through the electrodes of the piezoelectric sensor [8], then *Q(t)* can be written as:

$$Q(t)=\frac{1}{2}\left[\int_{A_s(z=-h_b/2)}D_z dA_s+\int_{A_s(z=-h_b/2-h_s)}D_z dA_s\right] \qquad \text{Equation 4-88}$$

where A_s is the area of the piezoelectric sensor on both sides of that. Substituting Equation 4-72 and Equation 4-87 into Equation 4-88 the closed circuit charge will be as:

$$Q(t)=\frac{w_sl_s}{2}e_{31}(h_s+h_b)\frac{\partial^2\chi}{\partial x^2} \qquad \text{Equation 4-89}$$

The induced current on the piezoelectric sensor is defined as:

$$i(t)=\frac{dQ(t)}{dt} \qquad \text{Equation 4-90}$$

It is needed to have a relation between closed circuit charge and generated voltage by sensor. Due to piezoelectric material properties, the induced current on the piezoelectric sensor is converted into the electrical voltage as [70]:

$$V_s(t) = G_s i(t) = G_s \frac{dQ(t)}{dt} \quad \text{Equation 4-91}$$

where G_s is the amplifier gain.

A control algorithm is used to actively control the vibration of the beam that is modeled as a human forearm. The vibration on the beam is as a human forearm tremor that is controlled in the closed loop control system. When the beam model starts to vibrate, the piezoelectric sensor that acts as a strain sensor, generates a voltage. This generated voltage is applied to the control system and actuates the piezoelectric actuator as an input voltage. The control algorithm is shown in Figure 4-11.

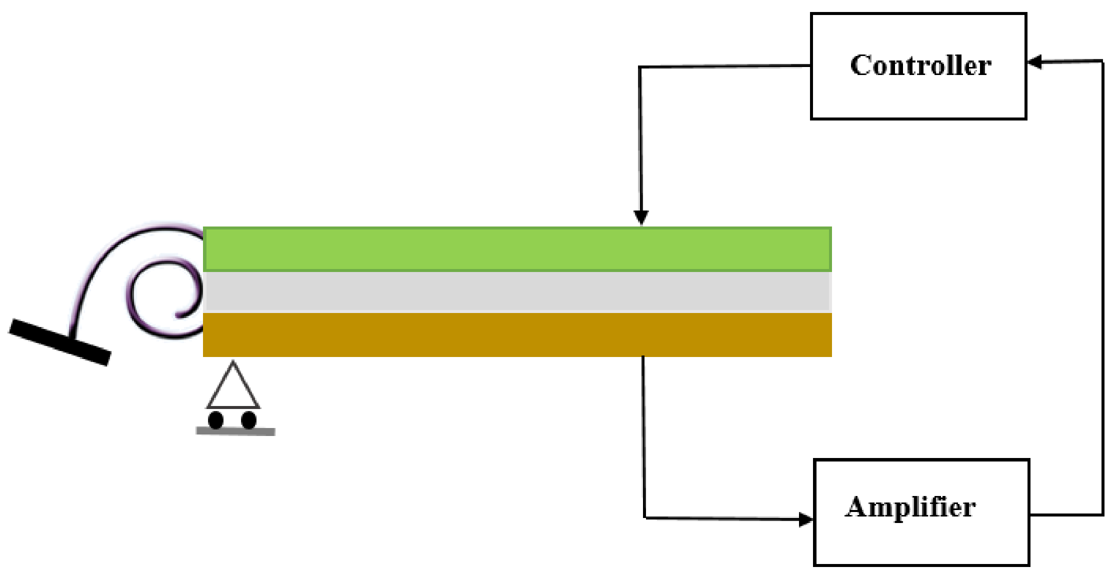

Figure 4-11. Active vibration control algorithm for human forearm model with a piezoelectric sensor and actuator

The actuating voltage can be shown as Equation 4-92:

$$V_a(t) = G_a V_s(t) = G_a G_s \frac{dQ(t)}{dt} = G_T \frac{dQ(t)}{dt} \quad \text{Equation 4-92}$$

where the G_a is the feedback control gain and $G_T = G_a G_s$ is the control gain.

Using Equation 4-89 and Equation 4-92 the actuating voltage is derived as Equation 4-93:

$$V_a(t) = G_T \frac{w_s l_s}{2} e_{31}(h_s + h_b) \frac{\partial^2}{\partial x^2} \frac{\partial \chi}{\partial t}$$ Equation 4-93

Substituting Equation 4-86 and Equation 4-93 into Equation 4-84 the equation of motion of the beam model that is covered with a sensor and an actuator on its surfaces is obtained as:

$$m\frac{\partial^2 \chi}{\partial t^2} + k_1 \frac{\partial^4 \chi}{\partial x^4} + k_2 \frac{\partial^4}{\partial x^4}\frac{\partial \chi}{\partial t} = f(x,t)$$

$$as$$

$$k_1 = (k_3 + \frac{e_{31}^2 k_4^2}{\xi_{33} w_p h_p})$$

$$k_2 = \frac{e_{31} k_4}{h_a}(G_T \frac{w_s l_s}{2} e_{31}(h_s + h_b))$$ Equation 4-94

$$k_3 = \frac{E_b w_b h_b^3}{12} + \frac{2E_p w_b}{3}\left[\left(\frac{h_b}{2} + h_p\right)^3 - \left(\frac{h_b}{2}\right)^3\right]$$

$$k_4 = \frac{w_b}{3}\left[\left(\frac{h_b}{2}\right)^2 - \left(\frac{h_b}{2} + h_p\right)^2\right]$$

The equation of motion of the model is partial differential equation and can be solved with Galerkin approximation.

Transverse deflection, χ , can be expressed as:

$$\chi(x,t) = \sum_{i=1}^{\infty} Z_i(x) q_i(t)$$ Equation 4-95

where q(t) is the time-dependent function and *Z(x)* is the fundamental vibration mode shape [64].

$$Z(x) = E_1 \sin(\beta x) + E_2 \cos(\beta x) + E_3 \sinh(\beta x) + E_4 \cosh(\beta x)$$ Equation 4-96

where E_1 to E_4 are constants and can be obtained from boundary conditions of the beam. As the beam is free at one end and has a pin joint and a rotational spring at the other end, the boundary conditions of the beam are as in Equation 4-50.

The boundary condition of the beam in the form of matrix is as Equation 4-97:

$$\begin{bmatrix} 0 & 1 & 0 & 1 \\ -k_s\beta & -EI\beta^2 & -k_s\beta & EI\beta^2 \\ -EI\beta^3\cos\beta l & EI\beta^3\sin\beta l & EI\beta^3\cosh\beta l & EI\beta^3\sinh\beta l \\ -EI\beta^2\sin\beta l & -EI\beta^2\cos\beta l & EI\beta^2\sinh\beta l & EI\beta^2\cosh\beta l \end{bmatrix}\begin{bmatrix} E_1 \\ E_2 \\ E_3 \\ E_4 \end{bmatrix} = \begin{bmatrix} 0 \\ 0 \\ 0 \\ 0 \end{bmatrix} \quad \text{Equation 4-97}$$

For a nontrivial solution of the constants *E1* to *E4*, the determinant made by coefficients of boundary condition matrix is set equal to zero [64].

Substituting $\chi(x,t)$ from Equation 4-95 into Equation 4-94 , the equation of motion of the beam is:

$$\sum_{i=1}^{\infty} m\frac{\partial^2 q_i}{\partial t^2}Z_i(x) + \sum_{i=1}^{\infty} k_1 q_i(t)\frac{\partial^4 Z_i(x)}{\partial x^4} + \sum_{i=1}^{\infty} k_2 \frac{\partial^4 Z_i(x)}{\partial x^4}\frac{\partial q_i(t)}{\partial t} = f(x,t) \quad \text{Equation 4-98}$$

There is an orthogonality conditions between different mode shapes of the beam as:

$$\int_0^l m(x).Z_i(x).Z_j(x) = \begin{cases} 1 & i = j \\ 0 & i \neq j \end{cases} \quad \text{Equation 4-99}$$

Then multiplying Equation 4-98 by $Z_i(x)$ and integrating from 0 to l , it gives:

$$\begin{aligned} &\sum_{i=1}^{\infty}\int_0^l m\frac{\partial^2 q_i}{\partial t^2}Z_i(x)Z_i(x)dx + \sum_{i=1}^{\infty}\int_0^l k_1 q_i(t)Z_i(x)\frac{\partial^4 Z_i(x)}{\partial x^4}dx \\ &+\sum_{i=1}^{\infty}\int_0^l k_2 Z_i(x)\frac{\partial^4 Z_i(x)}{\partial x^4}\frac{\partial q_i(t)}{\partial t}dx = \int_0^l Z_i(x)f(x,t)dx \end{aligned} \quad \text{Equation 4-100}$$

Finally, using Equation 4-99 the equation of motion of the Euler-Bernoulli beam model which has a piezoelectric actuator on its top surface and a piezoelectric sensor on its bottom surface is derived as Equation 4-101:

$$\frac{\partial^2 q}{\partial t^2} + g_1 \frac{\partial q(t)}{\partial t} + g_2 q(t) = g_3$$

$$g_1 = \int_0^l k_2 Z(x) \frac{\partial^4 Z(x)}{\partial x^4} dx$$

$$g_2 = \int_0^l k_1 Z(x) \frac{\partial^4 Z(x)}{\partial x^4} dx$$

$$g_3 = \int_0^l f(x,t) Z(x) dx$$

Equation 4-101

As the human forearm tremor is a kind of sinusoidal movement, the external force that is applied to the beam model as a tremor is a harmonic force. Also tremor amplitude for PD is about 5 mm and its severity is variable and increases from elbow to wrist joint. In this case the forearm tremor is applied as an external force in the form of Equation 4-102:

$$f(x,t) = F(x).\sin(\omega_1 t)$$
$$F(x) = 5x$$

Equation 4-102

Solving Equation 4-101 the vibration of the Euler-Bernoulli beam model with two layers of piezoelectric as a sensor and an actuator on its bottom and top surfaces is expressed as:

$$q(t) = e^{-\frac{g_1 t}{2}} \left(A_1 \sin \frac{\sqrt{g_1^2 - 4g_2}}{2} t + A_2 \cos \frac{\sqrt{g_1^2 - 4g_2}}{2} t\right) + D_1 \sin \omega_1 t + D_2 \cos \omega_1 t$$

$$D_1 = \left(\frac{-g_2 + \omega_1^2}{g_1 \omega_1}\right) D2$$

$$D_2 = \frac{g_1 \omega_1 \int_0^l Z(x) F(x) dx}{-(g_2 - \omega_1^2)^2 - g_1^2 \omega_1^2}$$

Equation 4-103

Also, the constants A_1 and A_2 can be obtained from the initial condition of the beam. Finally, the vibration of the forearm beam model which helps to analyse the effect of proposed AFC system on tremor suppression in human forearm model is derived as Equation 4-104:

$$
\begin{aligned}
q(t) = e^{-\frac{g_1}{2}} \Bigg(& \frac{4\omega_1(-g_2+\omega_1^2)}{g_1\sqrt{g_1^2-4g_2}} \frac{\int_0^l Z(x)F(x)dx}{-(g_2-\omega_1^2)^2-g_1^2\omega_1^2} \sin\frac{\sqrt{g_1^2-4g_2}}{2}t \\
& - \frac{g_1\omega_1\int_0^l Z(x)F(x)dx}{-(g_2-\omega_1^2)^2-g_1^2\omega_1^2} \cos\frac{\sqrt{g_1^2-4g_2}}{2}t \Bigg) \\
& + (-g_2+\omega_1^2)\frac{\int_0^l Z(x)F(x)dx}{-(g_2-\omega_1^2)^2-g_1^2\omega_1^2}\sin\omega_1 t + \frac{g_1\omega_1\int_0^l Z(x)F(x)dx}{-(g_2-\omega_1^2)^2-g_1^2\omega_1^2}\cos\omega_1 t
\end{aligned}
\qquad \text{Equation 4-104}
$$

4.2.2.2 Results

In this section, the results of active vibration control for tremor suppression on human forearm model is presented. The human forearm model is modelled as a beam that has a layer of piezoelectric sensor on its bottom layer and a piezoelectric actuator layer on its top surface. The properties of beam and piezoelectric material are listed in Table 4-2. The beam properties is chosen in the way to get to the closest real human forearm properties. Analytical expressions for vibration of the beam are derived, and the effects of control gain, the piezoelectric constant, e_{31} and the dielectric constant, ξ_{33} on the vibration of the beam are discussed to see the effect of each property on the vibration of the beam. The external force for the analysis is considered as $f(x,t) = 5.x.\sin(5t)$. The effects of these properties on the vibration of the beam are presented in Figure 4-12 to Figure 4-15. All figures illustrate the vibration of the beam with the physical properties of the beam which are listed in Table 4-2 and are drawn based on Equation 4-104 around the first mode of vibration.

Table 4-2. Physical properties of the beam model covered with a paired piezoelectric sensor and actuator

$l = 300mm$	$E_p = 104GPa$
$w_b = 70mm$	$E_b = 14GPa$
$w_b = 70mm$	$\rho_b = 1810kgm^{-3}$
$w_p = 70mm$	$\rho_p = 6390kgm^{-3}$
$h_b = 30mm$	$\xi_{33} = 1.59 \times 10^{-8} F / m$
$h_p = 30mm$	$e_{31} = -2.92C / m^2$
$d_{31} = 11pCN^{-1}$	$G_T = 1800$

Figure 4-12 shows the vibration of the beam model which has a sensor/actuator pair on its bottom and top surface. The beam model is in the closed loop active vibration control system and the control gain is 1800, (G_T=1800). As can be seen in the Figure 4-12, the vibration of the beam is decreasing in the time and gets close to zero after 40s. The result shows that this active vibration control system with one piezoelectric sensor and one piezoelectric actuator is an effective system in tremor suppression in the human forearm model.

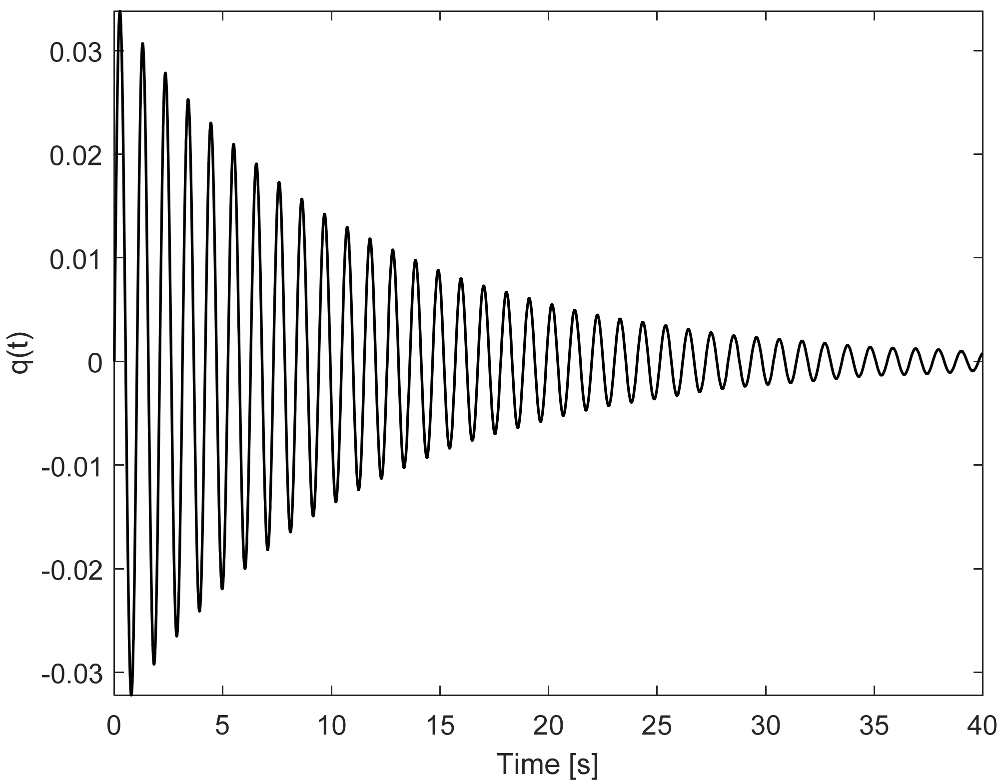

Figure 4-12. The vibration of the beam model in AVC system for the gain of 1800

The effect of control gain G_T on the beam's response is shown in the Figure 4-13 for four different control gains of 0, 600, 1200 and1800. As the figure shows, when the control gain is increased the vibration of the beam is decreased.

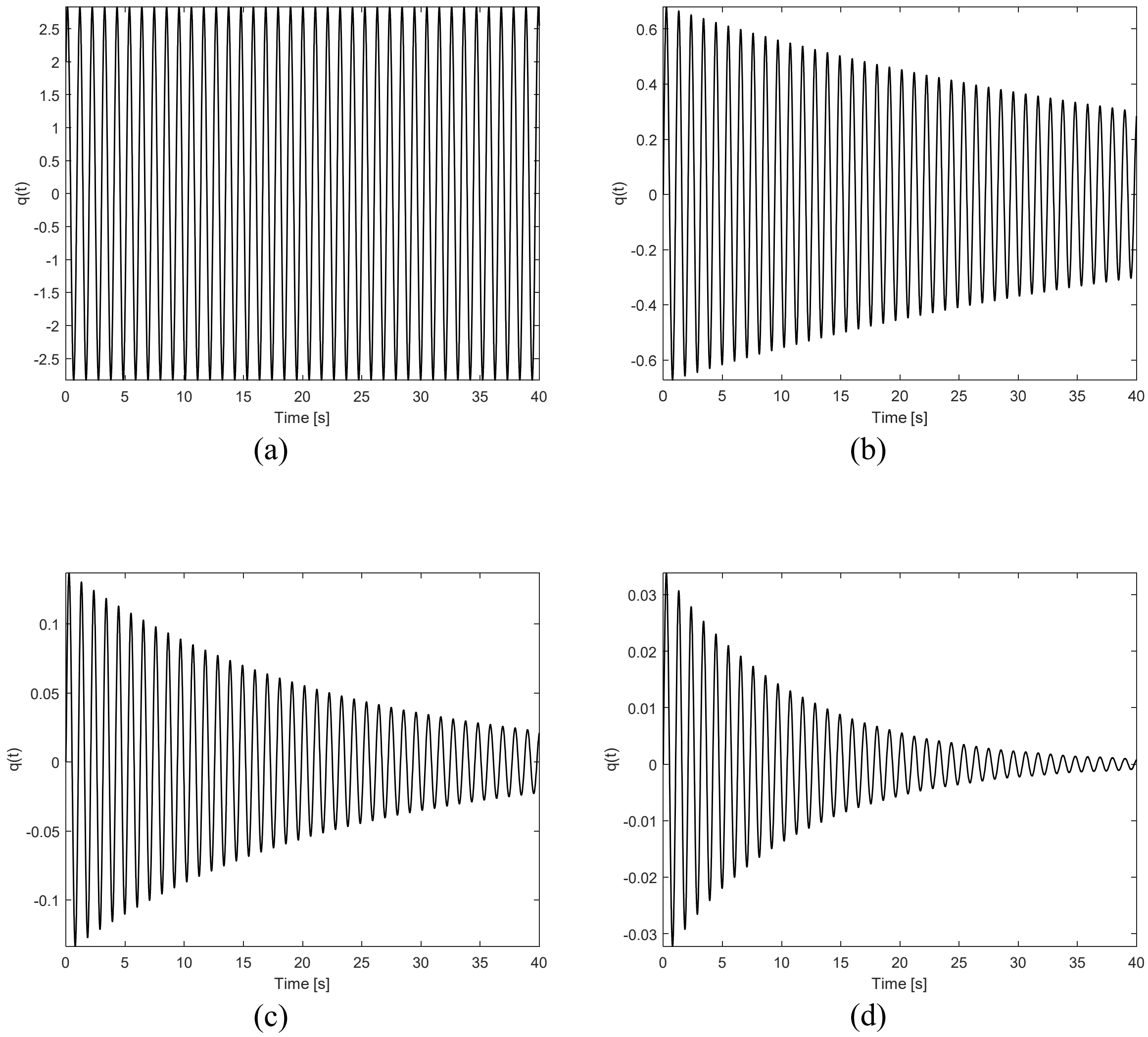

Figure 4-13. The vibration of the beam model in AVC system for the gain of (a) GT=0, (b) GT=600, (c) GT=1200, (d) GT=1800

The effect of piezoelectric constant, e_{31}, on the vibration of the beam is shown in the Figure 4-14. Result shows that when the absolute value of the piezoelectric constant is increased, the vibration of the beam will be decreased.

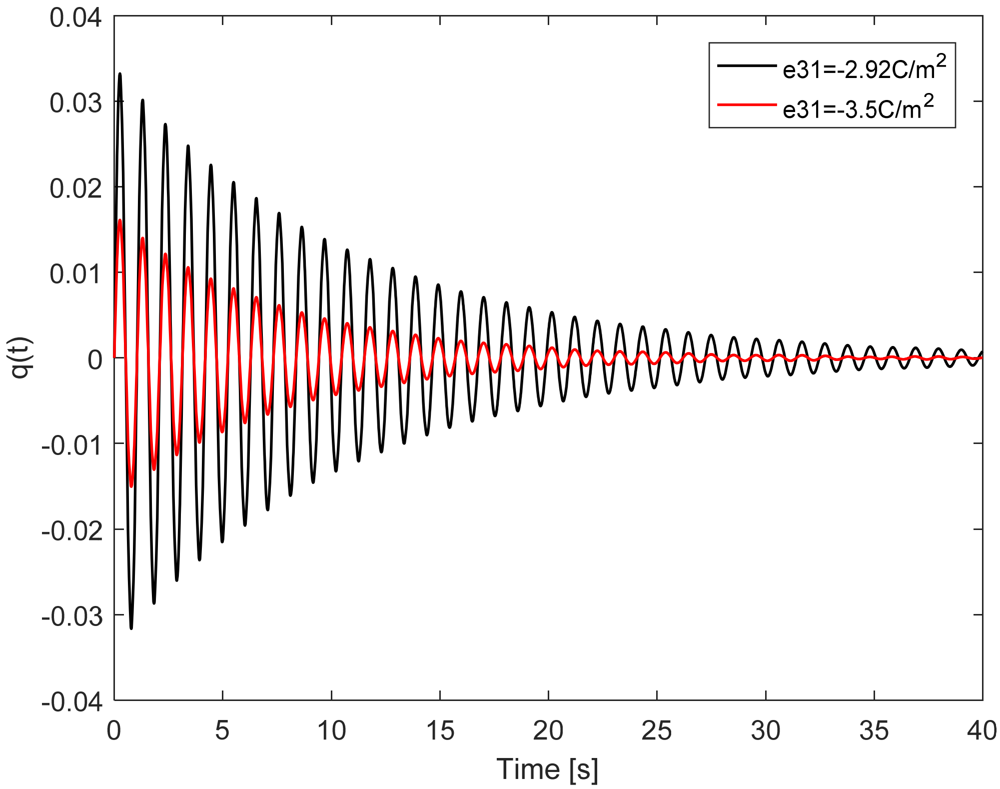

Figure 4-14. The vibration of the beam model with a paired piezoelectric sensor and actuator for different piezoelectric constant

Figure 4-15 shows the effect of the dielectric constant, ξ_{33}, on the vibration of the beam. As the figure illustrates when the dielectric constant is changed, the vibration of the beam will be changed by a small value. The result shows that the dielectric constant doesn't have a significant effect on the beam vibration.

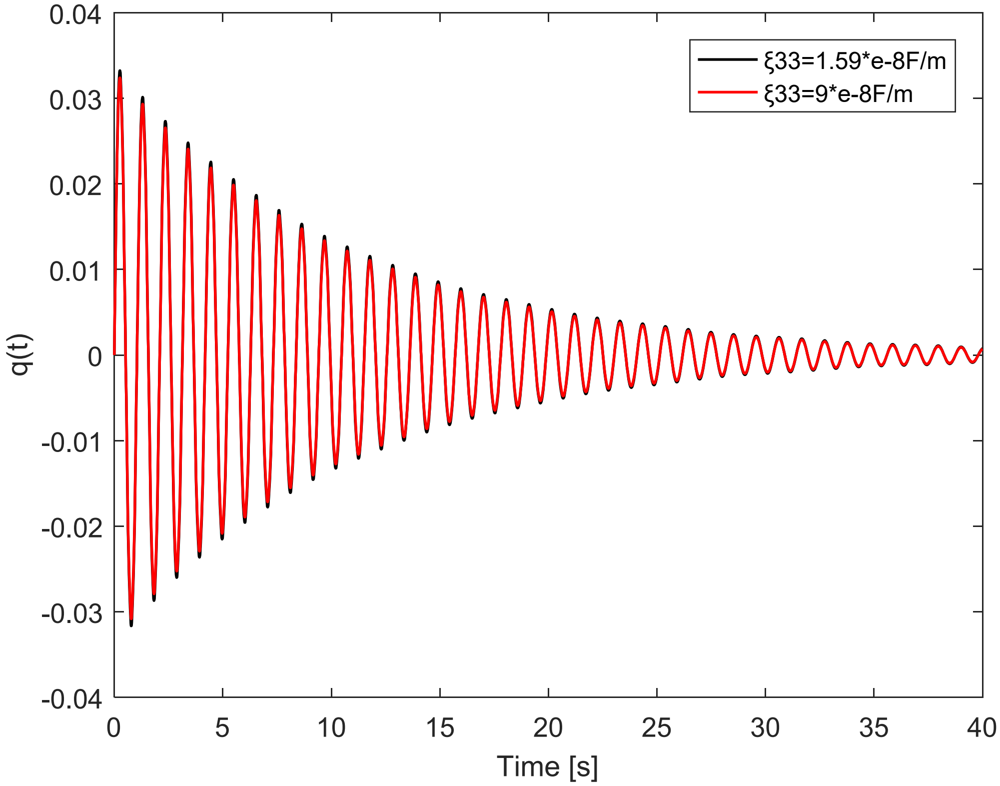

Figure 4-15. The vibration of the beam model with a paired piezoelectric sensor and actuator for different piezoelectric dielectric constant

4.3 Conclusion

In the first section of this chapter, 4.2.1, vibration control of a human forearm model was investigated. Human forearm model was developed as a Timoshenko beam which had a piezoelectric actuator on its top surface. The equations of motion of the proposed beam model which considered the effect of shear deformation and rotary inertia, have been derived. The effect of piezoelectric properties and the coupling of electrical and mechanical fields in the stress–strain relation of the system have been considered. The natural frequency and mode shape of the beam have been analytically obtained. The effect of some parameters, such as modulus of elasticity and density of the piezoelectric actuator and also the piezoelectric coefficient on the forced vibration of this beam have been studied. Results show that, among the different parameters, the modulus of elasticity and density of the piezoelectric layer have greater impact on the response of the beam model to vibration control. Also, presence of an actuator layer has caused smoothing phenomenon in mode shape of the beam. Finally, as the results show, it is concluded that the uses of piezoelectricity as described in this work present a new effective tool for vibration control.

In the second part of this chapter, 4.2.2, an active vibration control (AVC) for investigating the human forearm tremor was proposed. The main aim of this proposed AVC is tremor suppression from the human forearm. Human forearm was modelled as an Euler-Bernoulli beam covered with a layer of piezoelectric sensor on its bottom surface and a piezoelectric actuator on its top surface. Vibration of the beam model was derived, and the effects of control gain, the piezoelectric constant, e_{31} and the dielectric constant, ξ_{33} on the vibration of the beam was studied. The results showed that the proposed AVC is a significant control system for tremor suppression as increasing the control gain reduced the vibration in the model.

The results of this chapter are noteworthy as the active vibration control in the different structures such as the beams has great of significance in the real-world application. The proposed control system using a piezoelectric actuator can be used for tremor control. Also, the Proposed AVC with paired piezoelectric sensor and actuator can be used in an assistive device for tremor suppression.

Chapter 5: Tremor Classification for Human Hand in Parkinson's Disease

5.1 Introduction

Tremor as a neurological disorder has some characteristics which help researchers to find the best treatment to supress it from the human body. The frequency and amplitude of tremor are different from one patient to another. Some patients experience a severe kind of tremor in their hand but others have less problem as their tremor is weak. The main aim of this chapter is tremor classification for a group of Parkinson's patients.

One of the most accepted way for tremor recording is using electromyography that is discussed in 2.4.4. Tremor data was recorded as EMG signals, from 14 patients who were affected by Parkinson's disease and had tremor in their upper limb especially in the forearm and hand. Different signal-processing stages are applied to the raw signal to get accurate and useful information. Some pre-processing steps on the EMG data are done which can be divided into four main stages; filtering and data segmentation, feature extraction, feature reduction and classification. Then extreme learning machine (ELM) has been used to classify the data to three different classifications; severe, moderate and weak. The results indicate that the proposed system including PCA, ELM and the majority vote is able to recognize the tremor severity by using only four EMG channels. Also, the results of this chapter related to tremor amplitude and frequency were used in chapter 3 and 4 to define the proper harmonic external force as tremor on the model.

5.2 Data Acquisition Method and Processing

5.2.1 Subject's information

To conduct the laboratory tests, 14 patients from both genders, aged from 45 to 85 years, were examined. There were 12 male and 2 female participants in the experiment. All participants were provided with all the information about data collection method and aim of research and they signed consent forms prior to participating in the study. All the information and consent forms that were provide to the patients were approved by the university research ethics committee. The ethical approval is given in Appendix C. The laboratory tests were conducted in the Parkinson's disease Research Clinic at the Brain and Mind Centre, University of Sydney and the collected data was analysed at the University of Technology Sydney.

Electromyography (EMG) was utilized to collect the data from the patients' forearm and hand. Electroencephalography (EEG) is also used to collect the data from the patients' head and analyse their brain activity. Table 5-1 shows the information about participants.

Table 5-1. Participant's information involved in the experiment

Subject number	Gender	Age	Height (cm)	Weight (kg)	Tremor condition
1	Male	84	165	58	Weak
2	Male	65	175	100	Weak
3	Male	77	177	82	Weak
4	Male	57	97	181	Moderate
5	Female	76	162	55	Severe
6	Male	66	192	80	Moderate
7	Male	60	182	90	weak
8	Male	76	164	67	Weak
9	Male	45	185	95	Weak
10	Male	77	183	100	Weak
11	Male	85	175	74	Moderate
12	Male	69	170	75	Weak
13	Female	65	159	68	Weak
14	Male	70	180	96	Severe

5.2.2 Data acquisition protocol

The subjects were asked to do six different actions with their hand which cover most of the movement which participants implement in their daily activities. All six actions are shown in Figure 5-1 .

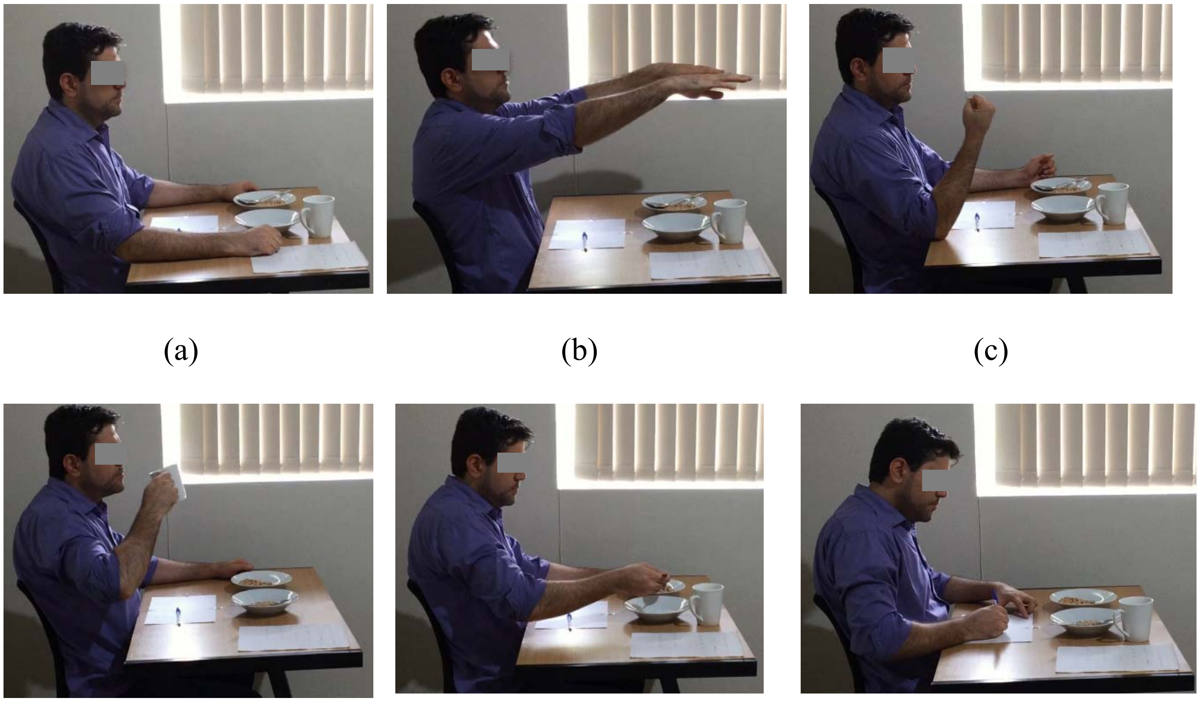

(a) (b) (c)

(d) (e) (f)

Figure 5-1. All six actions that were done by participant during data recording

- **First task**: Resting tremor of the hand is assessed in each subject as this tremor is typically observed in Parkinson's disease. In the resting position the affected body part is completely supported against gravity and it is not activated, Figure 5-1(a). Subjects were asked to place their forearm and hand comfortably on the desk for 10 seconds. They did this task two times and there was a 5-seconds interval between the two actions.
- **Second task**: Postural hand tremor requires subjects to stretch and maintain their forearm in the special posture, Figure 5-1(b). The subject was required to extend the hand with the fingers parallel and close to each other. In this action, the muscles were activated voluntarily. The hand was extended such that there was a 0° angular deviation from horizontal at the radial-ulnar joint. Each trial took 10 seconds and there was a 5-seconds rest between each trial, with 2 trials in total.

- **Third task**: The subject was asked to flex and extend the forearm for 3 different times and there was a 5-second interval between these trials, Figure 5-1(C).
- **Forth task:** The subject was asked to pick up a cup from the desk and drink and finally return the cup to the desk. This action was done three times with 5-second interval, Figure 5-1(d).
- **Fifth task:** The subject transferred chickpeas from one plate to another one with a spoon for three times with 5 seconds interval, Figure 5-1(e).
- **Sixth task:** There was a printed spiral on the paper and participant was asked to draw a line on the spiral for 10 seconds. This task was done for three times with 5 seconds interval, Figure 5-1(f). Figure 5-2 shows the spiral used in this experiment.

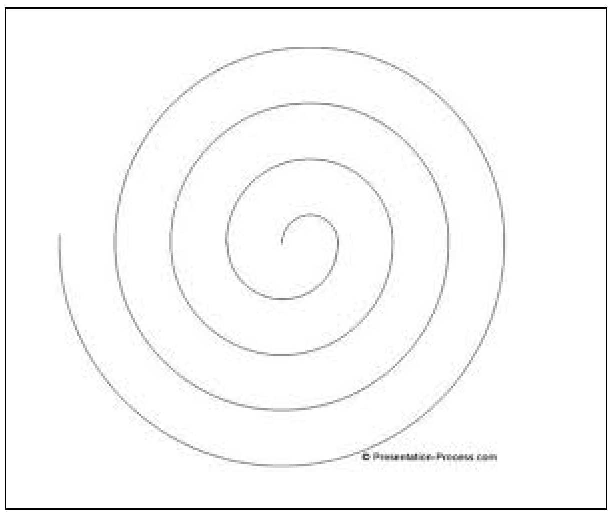

Figure 5-2. Spiral used for drawing task in the experiment

5.2.3 Data acquisition device

The SynAmps RT are used for EMG and EEG recording during the experiment which is a high-speed digital acquisition system and has a broadband amplifier. The SynAmps as a DC amplifier records different type of multichannel neurophysiological signals, such as EMG, EEG, Electrocardiography (ECG) and Electrooculography (EOG). There is an analogue component in the SynAmps RT to amplify low level signals and also there is a digital component to help to digitize, log external events, and transfer data to a host computer. The developed design of SynAmps is practical to record signals from multiple electrode in high speed. Also, it is able to acquire data at much higher rates with greater precision from more channels rather than data which is recorded from a single computer carrying out the same task. The CURRY 8 was used as a software package for SynAmps RT which is the most sophisticated program and comprehensive package for data recording and analysing. Also CURRY 8 has an interface with MATLAB in different aspects which help to export the data into MATLAB and import the results back into CURRY 8. Four EMG channels attached across the four muscles of the forearm and tremor data as an EMG signal, were recorded and processed by SynAmps RT and CURRY 8 system from Cumpumedics Neuroscan Inc.

Also, an inertial measurement unit (IMU) was attached to the subject's wrist to record acceleration of the tremor to find the frequency of the subject's tremor. IMU is an electronic device that works as a combination of accelerometers, magnetometers and gyroscopes to measure and record some movement characteristics such as, body's acceleration, force, and also the magnetic field neighbouring the body.

Shimmer's wearable IMU was used for data acquisition which is a small wireless sensor platform for wearable applications. As this IMU has a large storage and low-power standards and also it has integrated kinematic sensors, it is suitable for long-term data acquisition and motion capture. ConsensysPRO was used as a Shimmer's software which allows for quick configuration of Shimmer for data recording, display and storage. Figure 5-3 and Figure 5-4 shows the Shimmer's IMU which was used in the experiment and attachment position for IMU on the subject wrist simultaneously.

Figure 5-3. IMU used for data recording in the experiment

Figure 5-4. The position of IMU attachment on the subject's wrist

As EMG records muscle activity the first step is choosing the most appropriate muscles that provide clear and correct information from tremor in forearm and hand. There are different muscles in the forearm which contributed to do different movements. Four superficial muscles in the forearm were chosen to record data from them. These four muscles are flexor carpi ulnaris, extensor carpi ulnaris, extensor carpi radialis longus and pronator teres. The position of these muscles is shown in Figure 5-5. Also, sensor positions on the subject forearm are shown in Figure 5-6.

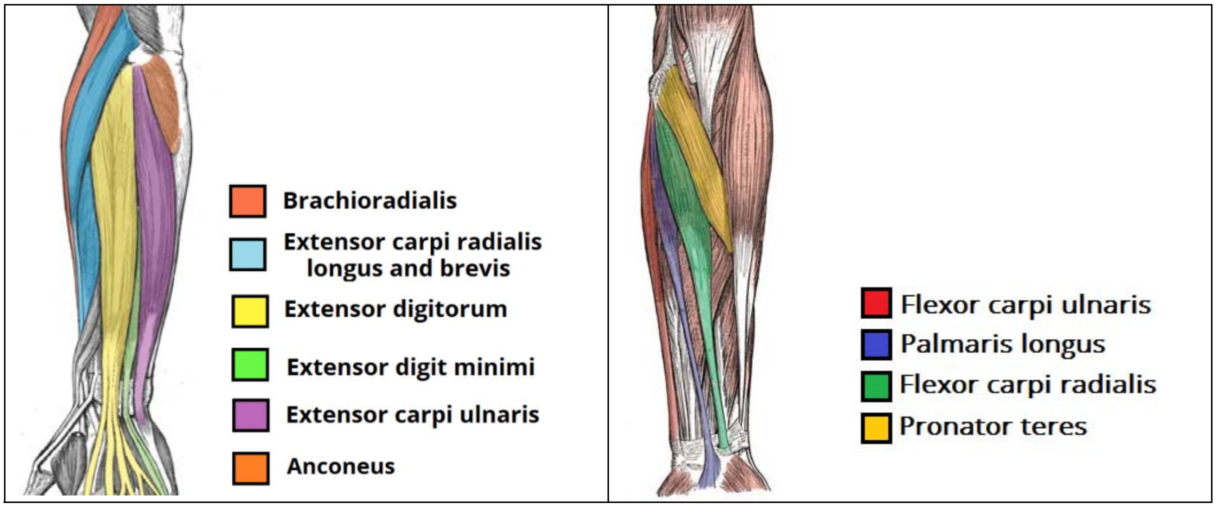

Figure 5-5. Position of muscles in the forearm

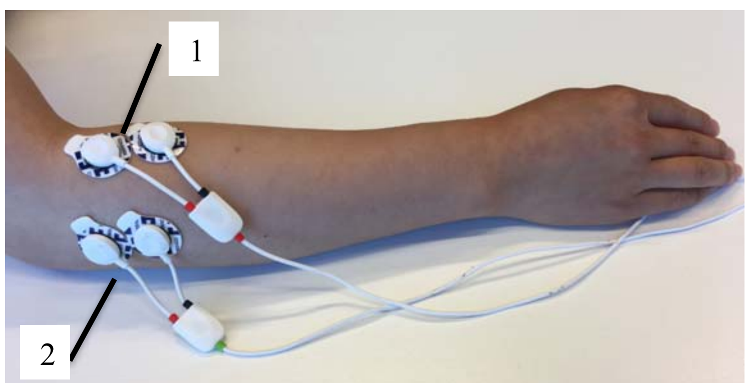

(a)

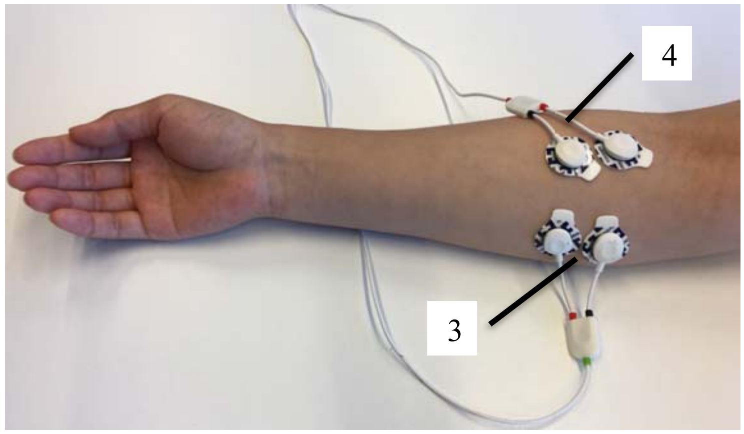

(b)

Figure 5-6. Position of sensor attachment on the forearm; (a) 1-extensor carpi radialis longus, 2- extensor carpi ulnaris and (b) 3- flexor carpi ulnaris, 4- pronator teres

For data collecting the subject was seated in a straight-backed chair and four EMG sensors were placed on the belly of these four muscles and on the participant's forearm and a reference electrode was placed on the capitulum elbow during data recording.

The position of sensor placement was shaved and cleaned with alcohol wipe and an adhesive electrode was attached on each of the sensors to firmly attach them to the patient's skin. The forearm and hand of the subjects were not constrained to the table in any way during the data collection. Also, for EEG recording, the subject wore an EEG cap on his / her head. This cap contains some sensors which collect electrical signals from the brain. Figure 5-7 shows the experiment set up for data recording.

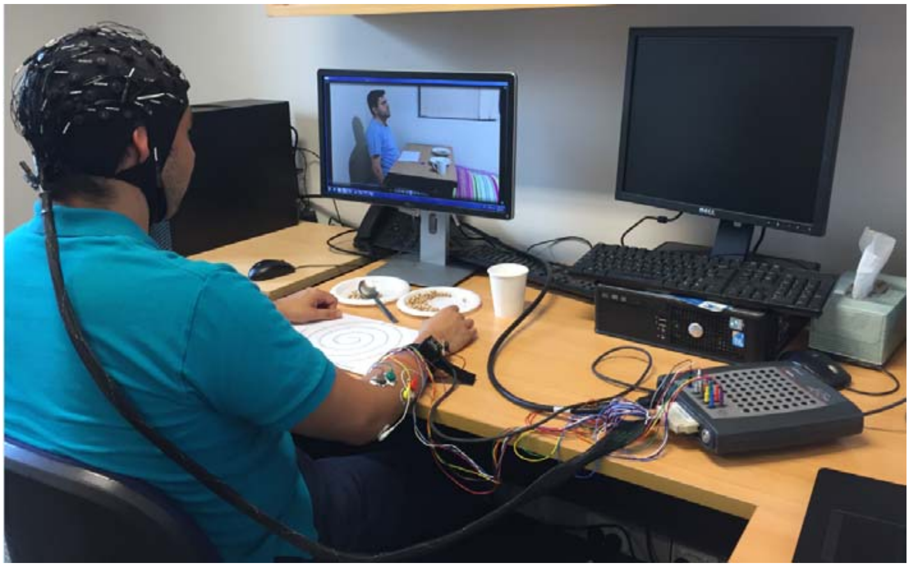

Figure 5-7. Experiment setup for tremor recording

5.3 EMG DATA PROCESSING

The raw EMG signal provides valuable information about muscle activity; however, it is in a useless form when it is recorded. This EMG signal information is useful only if it can be quantified. When compared with the other bio-signals, the EMG is a noisy signal as it gains the noise during travel through different types of muscle tissue. Therefore, classifying and analyzing the EMG signals is not easy. Different signal-processing stages are required to apply to the raw signal to get accurate and useful information. The main pre-processing step on the EMG data can be divided into four main stages; filtering and data segmentation, feature extraction, feature reduction and classification. Figure 5-8 shows the stages implemented in the proposed pattern recognition system.

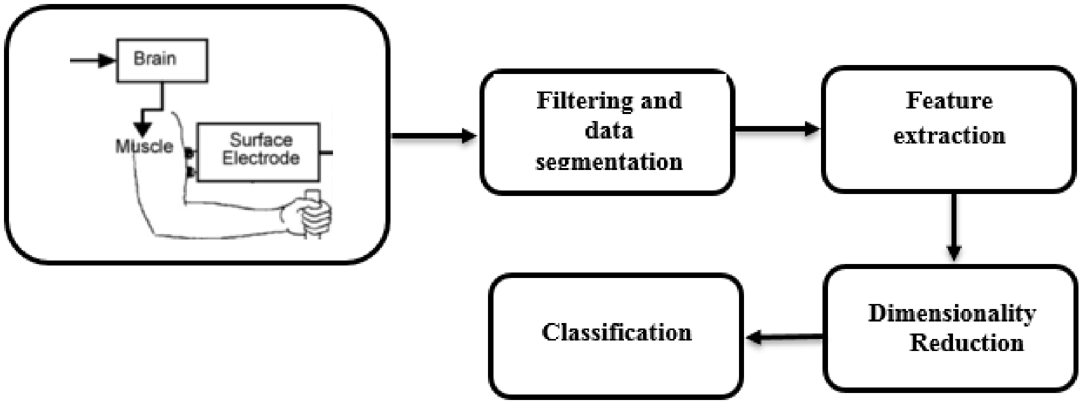

Figure 5-8. Proposed pattern recognition system

The main features of tremor signal are amplitude and frequency, which are used to recognize the kind of human tremor and help to assess its severity. Tremor frequency is mostly dependent on the pathophysiological mechanism. Amplitude of tremor shows short as well as long term variability, which is also modified by the effectiveness of treatment.

Seeking to address this deficit in research, this chapter expounds up on a machine-learning approach to objectively measure and accurately evaluate tremor severity in PD. The aim of this work is to connect the automatic diagnosis and current clinical digenesis in order to attain a more objective and sophisticated diagnosis and to provide clinical convenience as tremor is classified into three different categories; severe, moderate and weak.

5.3.1 Filtering

The goal of filtering is to eliminate the unwanted noises. In this study EMG signals were recorded at a sampling rate of 1000 Hz. Then the signals were band-pass-filtered between 10 and 500 Hz. Although the power line noise 50 Hz or 60 Hz can be removed using a notch filter but as this filter could remove the information of the EMG signal, it is not recommended to use it. Therefore, instead of a notch filter, differential amplification was used. More information about filtering was given in section 2.10.2.1.

5.3.2 Data segmentation

After data filtering, data segmentation is the next step for EMG classification process. There are two ways of data segmentation; disjoint windowing and overlapped windowing. The disjoint windowing associates with the window length but the overlapped windowing is related with the window length and window increment. The period between two consecutive windows is called window increment. Generally, when the window increment is equal to the window length, the disjoint windowing is the same as overlapped windowing. Also, the window increment should not be greater than the total time of the recognition system and should not exceed the window length [100, 103]. The window length determination should remark the optimal delay time of an electromyography control system as below [137]:

$$D_T = \frac{1}{2}Twl + \frac{n}{2}T_{inc} + \tau \qquad \text{Equation 5-1}$$

where D_T denotes the delay time for electromyography system, Twl is the length of the window, n shows the number of votes in the post-processing stage, T_{inc} is the increment of the window and τ represents the processing time of the pattern-recognition system. More information about data segmentation was given in section 2.10.2.2.

In this chapter the overlapped windowing has been used for data segmentation. Different windows length has been tested to get the better accuracy with fixed window increment of 30 ms, and it was found that 300 ms gives the better accuracy. Figure 5-9 shows the analysis of the selected windows of 300 ms in length and spaced 30 ms apart. The 300 ms is the maximum allowable windows length as for real-time application an adjacent segment length with the processing time of generating classified control commands should be equal or less than 300 ms.

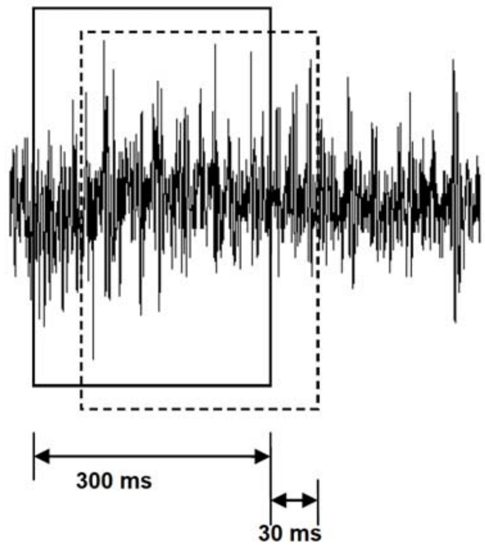

Figure 5-9. Sliding analysis window

5.3.3 Feature extraction

A feature may not be relevant individually, but it becomes relevant when it joins other features. In this study, to obtain features which are related to the characteristics of the tremor, 6 optimum feature sets are defined which contain 19 individual features which include; Slope Sign Changes (SSC) containing 2 features, Waveform Length (WL) containing 2 features, Zero Crossings (ZC) containing 2 features, sample Skewness (SS) containing 2 features, Autoregressive model parameters (AR) containing 8 features and Hjorth Time Domain parameters (HTD) containing 3 features. Using this combination of features, the recognition system achieves accuracy of 89.73% for picking a cup activity as it will be discussed in Figure 5-14. More information about feature extraction was given in section 2.10.2.3. The equation for these features is given in Table 5-2:

Table 5-2. Extracted features from tremor characteristics

Zero crossing (ZC): This feature uses the number of times that the amplitude value of EMG signal crosses the zero [105].	$\mathrm{ZC} = \sum_{n=1}^{N-1} \left[\mathrm{sgn}(x_n \times x_{n+1}) \cap \lvert x_n - x_{n+1} \rvert \geq \text{threshold} \right]$ $\mathrm{sgn}(x) = \begin{cases} 1 & x \geq \text{hreshold} \\ 0 & \text{otherwise} \end{cases}$
Slope Sign Change (SSC): This feature counts the number of times that the sign of slope changes [105].	$\mathrm{SSC} = \sum_{n=2}^{N-1} f\left[(x_n - x_{n-1}) \times (x_n - x_{n+1}) \right]$ $f(x) = \begin{cases} 1 & x \geq \text{threshold} \\ 0 & \text{otherwise} \end{cases}$
Waveform length (WL): This feature uses the cumulative length of the waveform over the time segment [105].	$\mathrm{WL} = \sum_{n=1}^{N-1} x \lvert_{n+1} - x_n \rvert$
Hjorth time domain parameters (HTD): This time domain feature introduced by Hjorth. The parameters for this feature are activity, mobility, and complexity [100] .	$\text{Activity}: m_0 = \mathrm{var}(x(t))$ $\text{Mobility}: m_1 = \sqrt{\dfrac{m_0(\frac{dx(t)}{dt})}{m_0(x(t))}}$ $\text{Complexity}: m_2 = \dfrac{m_1(\frac{dx(t)}{dt})}{m_1(x(t))}$
Autoregressive (AR): This feature describe each sample as a linear combination of previous samples plus a white noise error term [105].	$x_i = \sum_{p=1}^{P} a_p x_{i-p} + w_i$

5.3.4 Dimensionality reduction

The next step for data processing is reducing dimension of extracted features. All the features extracted from different EMG signals are joined together to make a large feature set. The dimension of the feature set requires to be reduced as the dimension of formed feature set is huge. The dimension of feature must be reduced in the way to keep the information of original features. To reduce the feature dimension there are different methods such as linear discriminant analysis (LDA) [138], principle component analysis (PCA), spectral regression discriminant analysis (SRDA) [109], orthogonal fuzzy neighbourhood discriminant analysis (OFNDA) [139]. More details about feature reduction was given in 2.10.2.4. PCA was used in this study to reduce the dimension of the feature set. PCA formulation and explanation was given in 2.10.2.4.2.

5.3.5 Classification

In the last step of EMG data processing, the best classifier must be chosen to get to the most accurate results. In this study extreme learning machine (ELM) has been used to classify the data. ELM is well recognized as a single-hidden-layer feed-forward network (SLFNs) with extremely fast learning speed and high generalization performance. ELM was proposed by [117, 140]. Details about classification was given in 2.10.2.5

5.4 POST-PROCESSING

The myoelectric patterns sometimes can be misclassified, i.e. the correct intention can fail to be identified using the pattern recognition algorithm. This misclassification will affect the real time controllability. During the real time operation to reduce the impact of these misclassifications, these systems should use post-processing algorithms. Usually the post-processing algorithms are applied when the predictions have been made by the classifier and using the information to improve the control.

Three main post-processing algorithms were found; Majority Vote, Bayesian Fusion and Decision-Based Velocity Ramp. These algorithms were developed for electromyography control system. For these three types, the algorithms take two different approaches. Majority Vote and Bayesian Fusion try to identify misclassified and prevent them from being outputted, while the Velocity Ramp makes sure that new controls are outputted, however, with low speed [141].

In this study Majority Vote algorithm has been used to refine the classification output. It employs the results from the n present state and m previous states and makes a new classification result based on the class that comes out most frequently. In this research, n = 0 and m = 4 were used.

In post processing it produces new results of classification data depending on the class which appears more frequently from the results of the current state and the previous states as show in Figure 5-10. This combination of dimensionality reduction, feature extraction and the majority vote, produces a fast and accurate classification system.

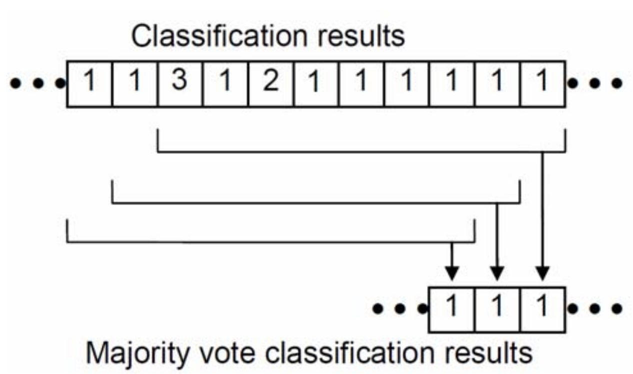

Figure 5-10. Majority vote post-processing

5.5 RESULTS

To investigate the performances for tremor severity by using PCA, ELM and the majority vote, some experiments have been done on a 2.8 GHz intel core i5 based computer with 8GB RAM. Figure 5-11 shows the performance test for pattern recognition for three classes of tremor severity; weak tremor (item1), moderate tremor (item2) and severe tremor (item3) for the activity of picking up a cup. In this test the system can recognize between these three types of tremor with the classification accuracy of 89.73%.

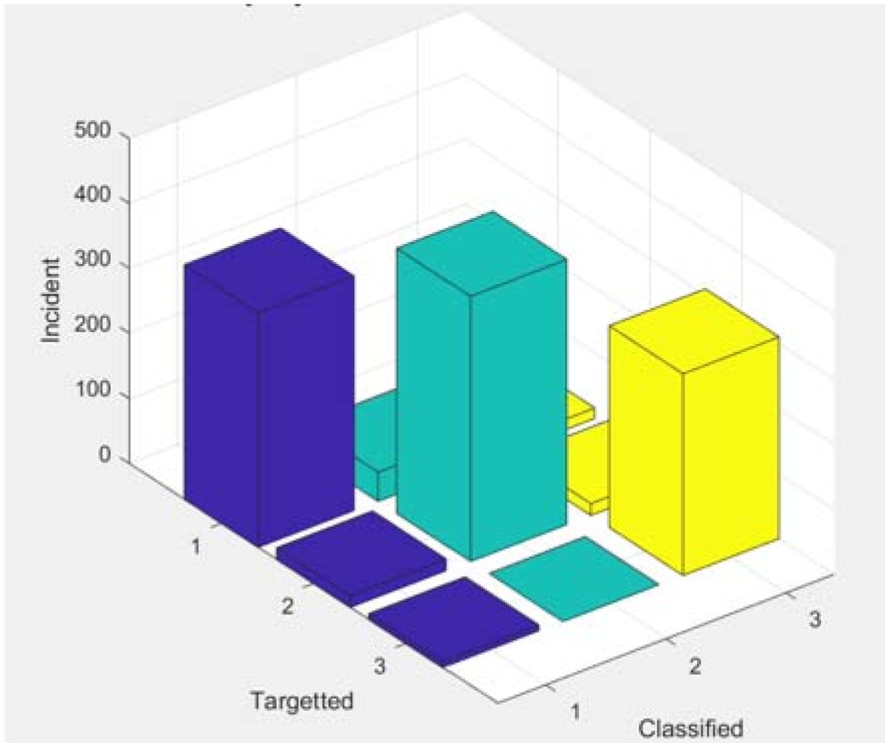

Figure 5-11. The majority vote for three subjects with different tremor severity; 1-Weak, 2-Moderate and 3- Severe

To find the best window length for three subjects with different tremor severity (weak, Medium and Severe) by varying the window length from 100 ms to 450 ms with fixed window increment of 30 ms using four EMG channels. The experiment results are presented in Figure 5-11. This figure shows that the average accuracy increases as the window length increases. Therefore, the experiment showing maximum window length achieves the best accuracy. However, for real time application, the window's length should not exceed 300 ms. As it was agreed, delay less than 300ms is acceptable for myoelectrical control [4].

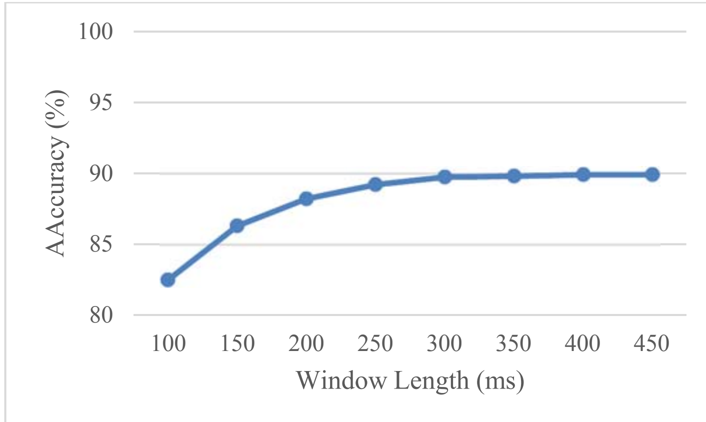

Figure 5-12. Average classification accuracy across 8 different window lengths

Another subject with weak tremor has been added to the test for picking up a cup action. Figure 5-13 shows the recognition of the system and how the system can recognize it.

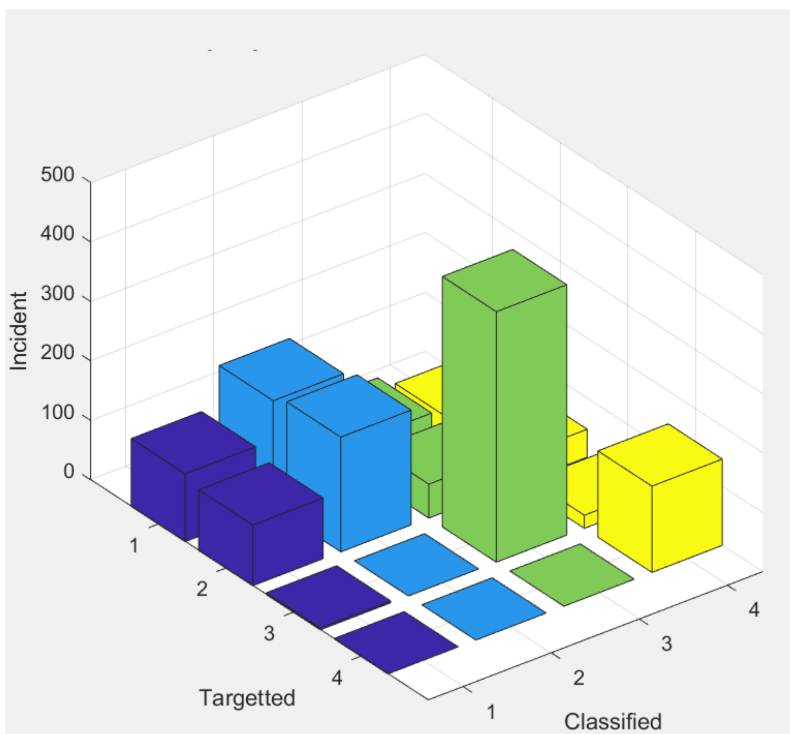

Figure 5-13. The majority vote for four subjects with different tremor severity. 1-Weak, 2-Weak, 3- Moderate and 4- Severe

However, there were high variations in recognizing the postural position and drawing for 14 subjects, as shown in Figure 5-14. The most accuracy has been obtained when the subject tries to pick the cup up from desk. In this figure, Rest, Pos., Flex./ext., cup, spoon and drawing denote the forearm resting, postural, flexion- extension, pick up a cup, transfer chickpeas with spoon and drawing respectively.

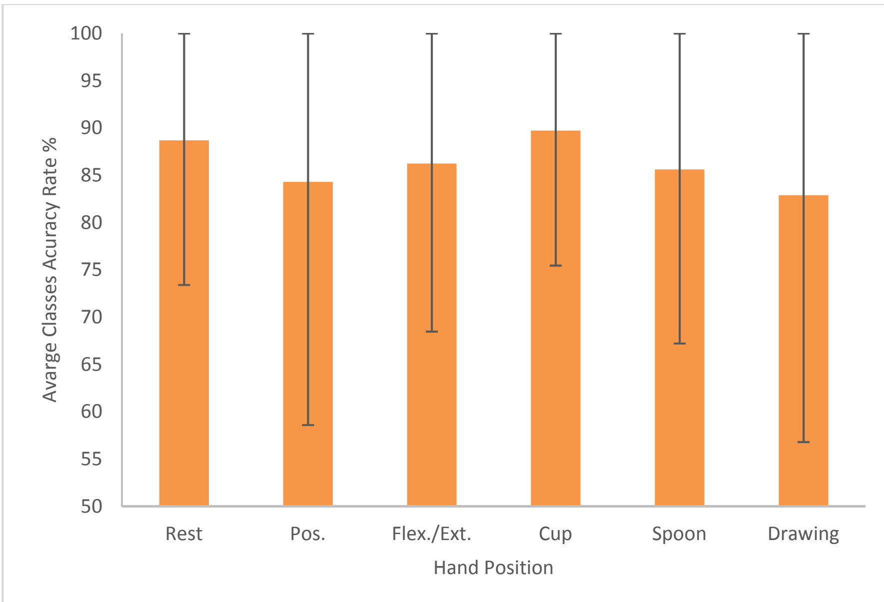

Figure 5-14. Average accuracy of the activities across 14 subjects

Table 5-3 shows the confusion matrix of the classification results. In this table it can be noticed that the most misclassified is drawing to postural position by accuracy of 2.35%. Two classes, picking up a cup and rest position are perfectly classified. However, the rest position is slightly misclassified to other classes.

Table 5-3. The confusion matrix of the classification result

		Classified					
		Rest	Pos.	Flex. / ext.	Pickup cup	Spoon	Drawing
Intended	**Rest**	88.7	0.00	2.3	0.89	0.76	0.32
	Pos.	1.24	84.3	1.44	0.83	1.01	2.35
	Flex./ext.	0.18	0.54	86.24	1.92	2.11	2.10
	Pickup Cup	1.48	1.33	0.54	89.73	0.087	0.90
	Spoon	0.95	2.24	0.39	0.57	85.61	0.52
	Drawing	2.26	0.00	0.21	0.82	0.47	82.9

5.6 Conclusion

The proposed system which consists of the PCA, ELM and the majority vote was able to recognize the tremor severity with the classification accuracy of 89.73% for picking up a cup activity by using only four EMG channels. ELM is a novel learning algorithm much faster than the traditional gradient-based learning algorithms for single-hidden layer feedforward neural networks (SLFNs). This chapter presented a method for assessing hand tremor which was recognized by using EMGs signal processing. This approach allows the researchers to determine tremor severity. It is based on off-line analysis. The proposed method provides better accuracy of determining tremor severity compared to the reported studies in which they used Fourier transformation method. This method is can be validated to be tested on another database including a wide range of patients with tremors.

CHAPTER 6: CONCLUSIONS AND RECOMMENDATIONS FOR FUTURE WORKS

6.1 CONCLUSIONS

Tremor suppression from human hand and forearm in PD was investigated in this study. The main aim of this research was developing the control system to attenuate the tremor in people affected by PD as they have many difficulties in their daily life. AFC or AVC is an effective way for tremor control and reduction. An AFC was proposed to investigate the effect of control system on tremor reduction. A Piezoelectric actuator and a PD controller were embedded in the AFC system to analyse tremor suppression in three different models included a 4-DOF biomedical model of the hand, a 1-DOF musculoskeletal model of the elbow joint and a 3-DOF musculoskeletal model of the wrist joint. The proposed AFC system was simulated in MATLAB to investigate the effect of AFC control system on tremor reduction.

The results illustrated that the tremor amplitude for a 4-DOF biomedical model of the hand that was composed of mass-spring-damper system without control system was between -3mm to -4 mm. This amplitude was decreased to -1.5×10^{-9} m to $+1.5\times10^{-9}$ m after using AFC system for tremor control.

Also, the effect of AFC was investigated on a 1-DOF musculoskeletal model of the elbow joint. Forearm was modelled as a pendulum and effect of the moment that a muscle generates through active electrical stimulation was considered. The muscle model was developed from the classic Hill-type muscle model. In this model, the muscle response to a stimulation signal was composed of two parts: activation dynamics and contraction dynamics. The results showed the elbow joint tremor was between -6 degrees to +6 degrees without control system but after using AFC system on the model, the tremor decreased significantly and was between -6×10^{-3} degrees to $+6\times10^{-3}$ degrees, which was much smaller than joint angle without AFC system.

3-DOF musculoskeletal model of the wrist joint with four main muscles that contribute to wrist movement was considered. The muscle moment that was generated through active electrical stimulation in FE, RUD and PS directions was considered in equation of motion of the wrist joint. Hill-type muscle model was used to study activation dynamics and contraction dynamics of the model. Results were derived for all 3 direction of movement. The tremor of the wrist joint in flexion-extension before and after using AFC method showed that wrist tremor before using AFC method was about -5 degrees to +5 degrees. After using AFC, wrist joint tremor in FE was decreased to about -1×10^{-2} degrees to 1×10^{-2} degrees. Also, wrist tremor in RUD without control system was about about -5 degrees to +7 degrees which was attenuated after applying AFC system to about -6×10^{-3} degrees to 7×10^{-3} degrees. Furthermore, results proved that AFC system is effective for wrist tremor suppression in SP as the tremor without AFC in SP was about -2 degrees to +3 degrees and it was reduced to about -1.5×10^{-2} degrees to 1.2×10^{-2} degrees in AFC system.

As was discussed, the proposed AFC system was an effective tool for tremor suppression as it had significant effect on all three models. Comparing the result, tremor in wrist joint was decreased significantly after using AFC.

Also, active vibration control using piezoelectric material as a smart material was investigated in the beam model of the forearm. At first the effect of a piezoelectric actuator was studied on vibration control. The forearm was modelled as a beam and a layer of piezoelectric material was embedded on its top surface. Tremor was applied on the beam as an external harmonic force and the applied voltage to the piezoelectric actuator was harmonic too. The result identified that the piezoelectric material was one of the best choices for tremor control. Using the piezoelectric actuator caused the vibration of the beam to be decreased and also from beam mode shape, deflection of the beam with the piezoelectric actuator was smoother. Results showed that the difference between the minimum and maximum point of beam mode shape in the presence of a piezoelectric layer was less than deflection for the beam without a piezoelectric actuator.

The effect of piezoelectric properties on the beam vibration was studied. The effect of piezoelectric strain constant, d_{31}, on the vibration of the beam showed that when the d_{31}

increased, the vibration amplitude of the beam is increased. Also, when the applied voltage to piezoelectric actuator increased the vibration of the beam was increased too. The effect of piezoelectric density, ρ_p on the vibration of the beam was identified when the piezoelectric density increased and the maximum amplitude of the beam vibration increased. Similarly, the effect of elasticity modulus of piezoelectric actuator, *Ep*, on the vibration of the beam was studied. The result illustrated that increasing *Ep* caused the beam vibration to be reduced.

Using both piezoelectric sensor and actuator in the closed loop control system showed that this AVC system is an effective method for tremor suppression actively. Human forearm was modelled as a beam which had two layers of piezoelectric on its top and bottom surface as an actuator and sensor respectively. An external harmonic force was applied to the beam model as human forearm tremor is a kind of sinusoidal movement. Results showed that with the control gain of 1800, (G_T=1800) the vibration of the beam is decreasing in the time and gets close to zero after 40s. The effect of control gain G_T on the beam's response is also studied. From results, increasing G_T had a direct effect on the vibration decreasing. Furthermore, the effect of some piezoelectric properties was investigated on the forearm model vibration. The absolute value of the piezoelectric constant, e_{31} is increased and results showed that the vibration of the beam decreased. The dielectric constant, ξ_{33}, is another piezoelectric characteristic which did not have a significant effect on the beam vibration. From the result when the dielectric constant was changed, the vibration of the beam changed by a small value.

As a conclusion, using proposed AFC or AVC on the different human forearm or hand models had a very considerable effect on tremor suppression. Results of tremor suppression using AFC system can be used for designing assistive device to help Parkinson's patients in their daily activity for tremor control.

Finding tremor characteristics such as tremor amplitude and frequency, help to developing the best treatment for its attenuation. Tremor severity is altered for different patients and tremor classification for PD subjects provides valuable information for the researchers.

Getting to this aim, human hand tremor was recorded from 14 patients who were affected by Parkinson's disease using electromyography (EMG). The patients were asked to do some special activities with their hand and forearm during data recording. Different signal-processing techniques were applied to the raw EMG signal to get precise and suitable information from recorded signals. Extreme learning machine (ELM) was used to classify data to three different classifications; severe, moderate and weak. The proposed system which consists of the PCA, ELM and the majority vote was successful in recognising the tremor severity with the classification accuracy of 89.73% for picking up a cup activity. However, the rest position is slightly misclassified to another classes. Classification results can be used to help researchers to identify the level of tremor severity in Parkinson's patients. When the kind of tremor and its characteristics were identified, the next step is finding the best way for tremor reduction.

6.2 Recommendations for Future Works

Though some successful and promising results have been accomplished in this work, there still exists a long distance between the found results and the real-world applications for implementing the tremor control systems in a human body. The problems faced during this research need to be surmounted and many innovative solutions should be developed in the future.

The following issues are recommended for future research:

- Developing a new active control system which includes another kinds of actuators (such as electromagnetic, electric, etc.) and controllers (such as PID, ID, PI, etc.) to get to the best AFC system for tremor suppression.
- Developing a new model of human hand and forearm which has closer properties to the real hand and forearm characteristics.

- Considering the effect of muscle dynamics on the motion of the forearm beam model.
- Using other kind of smart materials instead of piezoelectric material in the forearm beam model to see the effect of them on tremor suppression.
- Using soft materials instead of piezoelectric material as a sensor and actuator in forearm beam model.
- Using different number of piezoelectric sensors and actuators in the model which could be located in different parts of the beam model to analyse the effect of piezoelectricity on tremor reduction.
- Developing an assistive device such as a wearable glove, which will apply the AFC system for people who are affected with PD to help them in their daily activities. Using a different number of piezoelectric sensors and actuators on the glove, helps to get to the best design for tremor suppression.
- Developing an assistive wearable glove for tremor reduction in PD which is made from soft material as soft materials provide more flexibility for patients.
- Using AFC method for tremor cancellation in a surgical instrument to supress physiological tremor of a surgeon hand.
- Considering more subjects with different levels of tremor severity for data recording.
- Developing an algorithm using new methods like Bayesian Fusion methods for tremor classification

APPENDIX A

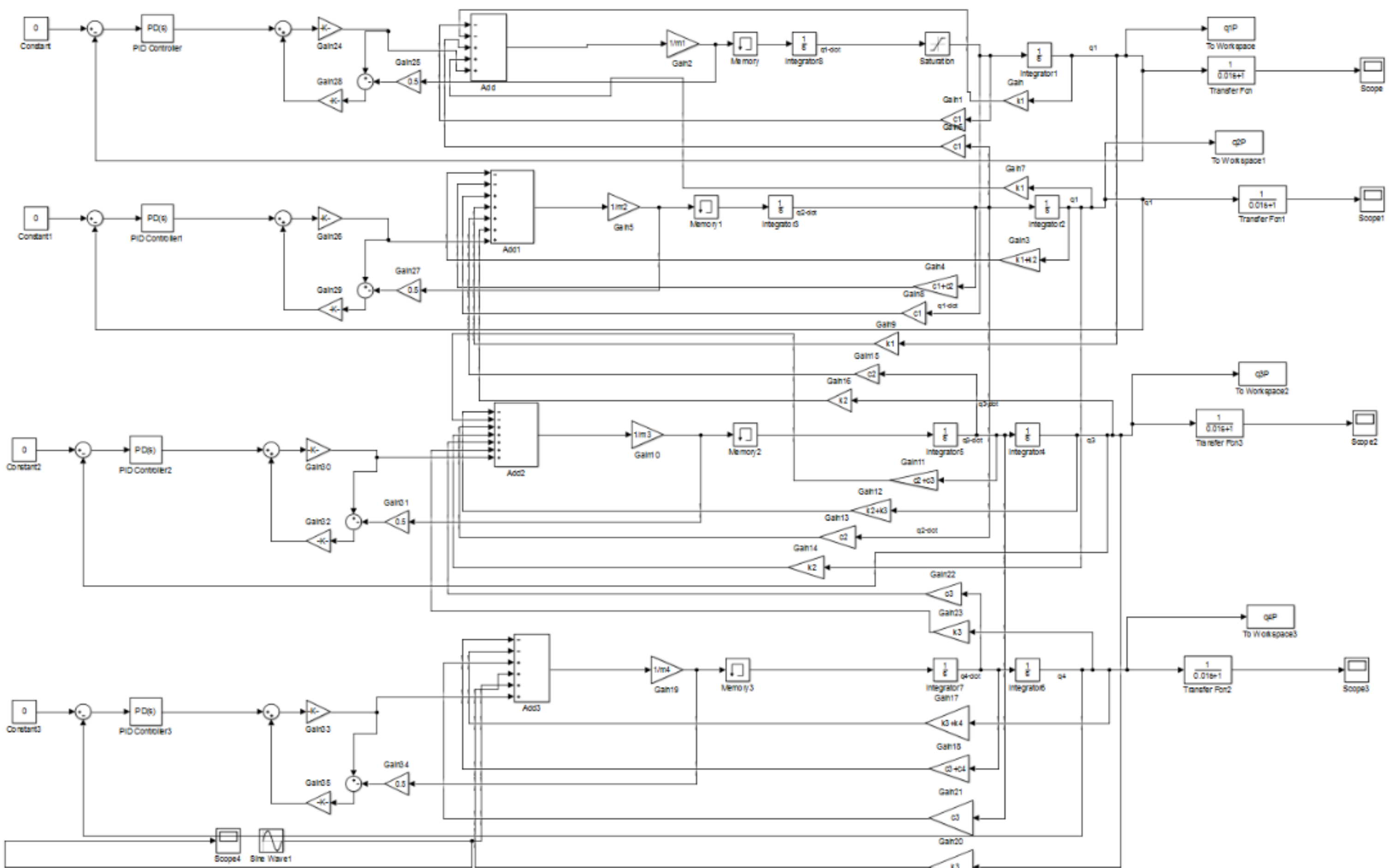

APPENDIX B

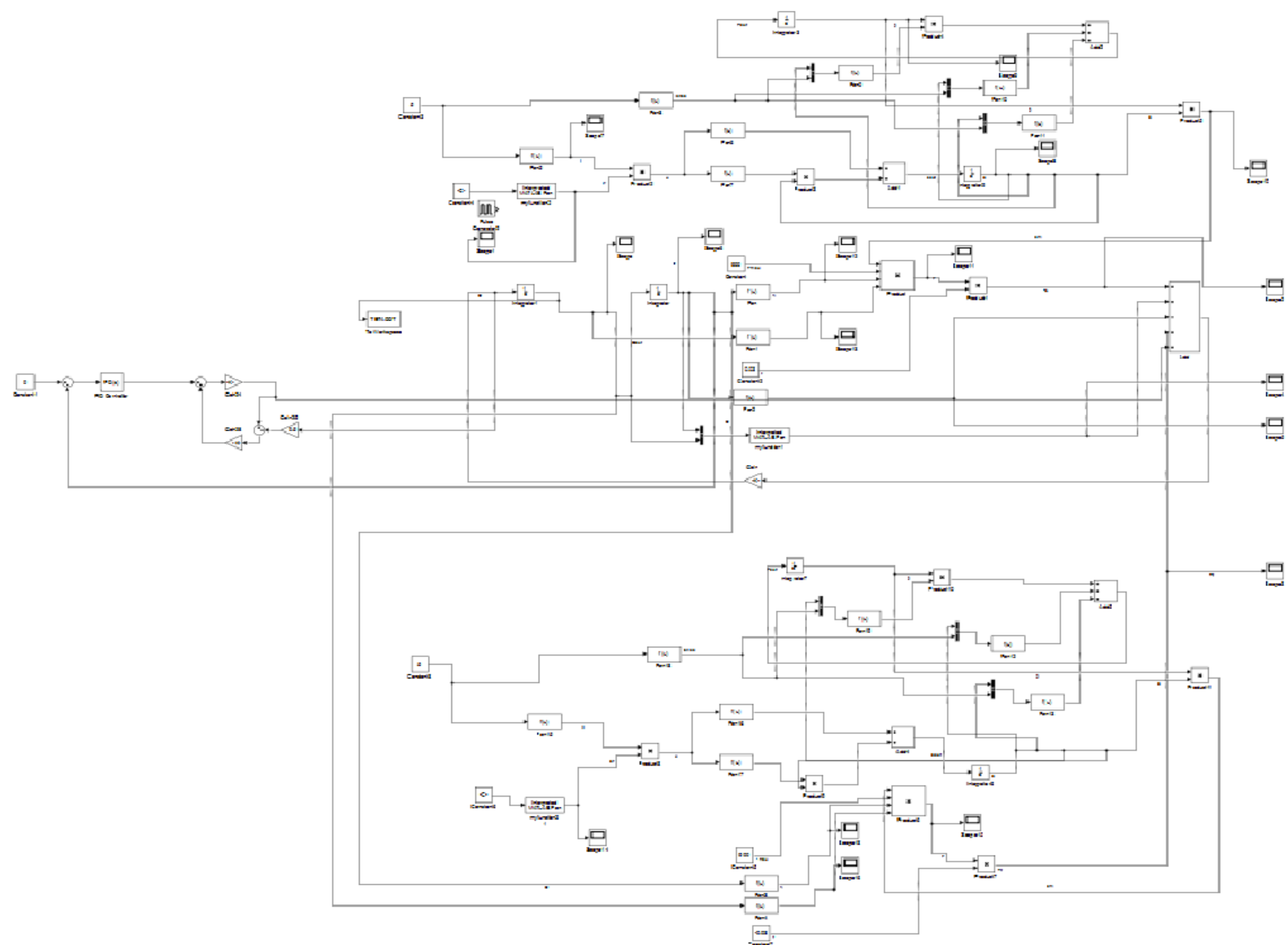

Appendix C: Ethical Approval

THE UNIVERSITY OF SYDNEY

Research Integrity & Ethics Administration
Human Research Ethics Committee

Thursday, 27 April 2017

Assoc Prof Simon Lewis
Central Clinical School: Medicine; Sydney Medical School
Email: simon.lewis@sydney.edu.au

Dear Simon

The University of Sydney Human Research Ethics Committee (HREC) has considered your application.

After consideration of your response to the comments raised your project has been approved.

Approval is granted for a period of four years from **27 April 2017** to **27 April 2021**

Project title: **Tremor Suppression for Human Hand with Soft Robot**

Project no.: **2017/186**

First Annual Report due: **27 April 2018**

Authorised Personnel: **Lewis Simon; Hall Julie; Al-Jumaily A; Hosseini Seyedehmarzieh;**

Documents Approved:

Date Uploaded	Version number	Document Name
19/04/2017	Version 4	Consent form
19/04/2017	Version 4	PIS v04
26/02/2017	Version 3	Withdrawal form
26/02/2017	Version 1	Methodology

Condition/s of Approval

- Research must be conducted according to the approved proposal.
- An annual progress report must be submitted to the Ethics Office on or before the anniversary of approval and on completion of the project.
- You must report as soon as practicable anything that might warrant review of ethical approval of the project including:
  - Serious or unexpected adverse events (which should be reported within 72 hours).
  - Unforeseen events that might affect continued ethical acceptability of the project.
- Any changes to the proposal must be approved prior to their implementation (except where an amendment is undertaken to eliminate *immediate* risk to participants).
- Personnel working on this project must be sufficiently qualified by education, training and experience for their role, or adequately supervised. Changes to personnel must be reported and approved.

Research Integrity & Ethics Administration
Level 2, Margaret Telfer Building (K07)
The University of Sydney
NSW 2006 Australia

T +61 2 9036 9161
E human.ethics@sydney.edu.au
W sydney.edu.au/ethics

ABN 15 211 513 464
CRICOS 00026A

THE UNIVERSITY OF SYDNEY

- Personnel must disclose any actual or potential conflicts of interest, including any financial or other interest or affiliation, as relevant to this project.
- Data and primary materials must be retained and stored in accordance with the relevant legislation and University guidelines.
- Ethics approval is dependent upon ongoing compliance of the research with the *National Statement on Ethical Conduct in Human Research*, the *Australian Code for the Responsible Conduct of Research*, applicable legal requirements, and with University policies, procedures and governance requirements.
- The Ethics Office may conduct audits on approved projects.
- The Chief Investigator has ultimate responsibility for the conduct of the research and is responsible for ensuring all others involved will conduct the research in accordance with the above.

This letter constitutes ethical approval only.

Please contact the Ethics Office should you require further information or clarification.

Sincerely

Dr Jim Rooney
Deputy Chair
Human Research Ethics Committee

The University of Sydney HRECs are constituted and operate in accordance with the National Health and Medical Research Council's (NHMRC) National Statement on Ethical Conduct in Human Research (2007) and the NHMRC's Australian Code for the Responsible Conduct of Research (2007).

Page 2 of 2

REFERENCES

[1] C. N. Riviere, R. S. Rader, and N. V. Thakor, "Adaptive cancelling of physiological tremor for improved precision in microsurgery," *Biomedical Engineering, IEEE Transactions on,* vol. 45, pp. 839-846, 1998.

[2] W. T. Ang, P. Pradeep, and C. Riviere, "Active tremor compensation in microsurgery," in *Engineering in Medicine and Biology Society, 2004. IEMBS'04. 26th Annual International Conference of the IEEE*, 2004, pp. 2738-2741.

[3] A. Cheraghizanjani, A. As'arry, Z. Yusop, M. M. Zain, and M. Hussein, "Measurement and Behaviour Classification of Tremor Patients," *International Journal of Biology and Biomedical Engineering,* pp. 155-162, 2011.

[4] A. As'arry, M. M. Zain, M. Mailah, M. Hussein, and Z. Yusop, "Active tremor control in 4-DOFs biodynamic hand model," *International Journal of Mathematical Models and Methods in Applied Sciences,* vol. 5, pp. 1068-1076, 2011.

[5] M. Hussein, A. As' arry, M. M. Zain, M. Mailah, and M. Abdullah, "Experimental study of human hand-arm model response," in *Mechatronics and its Applications, 2009. ISMA'09. 6th International Symposium on*, 2009, pp. 1-6.

[6] M. Z. M. Zain, A. As' arry, S. Kazi, M. Mailah, M. Hussein, and M. Abdullah, "Development of experimental-rig for human postural tremor behaviour," *International Journal of Human Factors Modelling and Simulation,* vol. 1, pp. 339-351, 2010.

[7] G. K. Wenning, S. Kiechl, K. Seppi, J. Müller, B. Högl, M. Saletu*, et al.*, "Prevalence of movement disorders in men and women aged 50–89 years (Bruneck Study cohort): a population-based study," *The lancet neurology,* vol. 4, pp. 815-820, 2005.

[8] E. Rocon, J. Belda-Lois, J. Sanchez-Lacuesta, and J. Pons, "Pathological tremor management: Modelling, compensatory technology and evaluation," *Technology and Disability,* vol. 16, pp. 3-18, 2004.

[9] E. D. Louis, "Essential tremors: a family of neurodegenerative disorders?," *Archives of neurology,* vol. 66, pp. 1202-1208, 2009.

[10] S. D. Bawankar and N. M. Nitiket, "Tremor Suppression by Using Various Techniques," vol. 9, ed: Discovery, 2014, pp. 51-54.

[11] J. Gao, "Analysis of amplitude and frequency variations of essential and Parkinsonian tremors," *Medical and Biological Engineering and Computing,* vol. 42, pp. 345-349, 2004.

[12] J. J. Ackmann, A. Sances Jr, S. J. Larson, and J. B. Baker, "Quantitative evaluation of long-term Parkinson tremor," *Biomedical Engineering, IEEE Transactions on,* pp. 49-56, 1977.

[13] K. E. Norman, R. Edwards, and A. Beuter, "The measurement of tremor using a velocity transducer: comparison to simultaneous recordings using transducers of displacement, acceleration and muscle activity," *Journal of neuroscience methods,* vol. 92, pp. 41-54, 1999.

[14] A. Beuter, E. Barbo, R. Rigal, and P. J. Blanchet, "Characterization of subclinical tremor in Parkinson's disease," *Movement disorders,* vol. 20, pp. 945-950, 2005.

[15] V. Hömberg, H. Hefter, K. Reiners, and H. Freund, "Differential effects of changes in mechanical limb properties on physiological and pathological tremor," *Journal of Neurology, Neurosurgery & Psychiatry,* vol. 50, pp. 568-579, 1987.

[16] H. Journee, "Demodulation of amplitude modulated noise: a mathematical evaluation of a demodulator for pathological tremor EMG's," *Biomedical Engineering, IEEE Transactions on,* pp. 304-308, 1983.

[17] H. W. Newman and W. J. Friedlander, "A simple device for recording tremors," *Stanford medical bulletin,* vol. 8, p. 191, 1950.

[18] O. Lippold, "Oscillation in the stretch reflex arc and the origin of the rhythmical, 8–12 c/s component of physiological tremor," *The Journal of Physiology,* vol. 206, pp. 359-382, 1970.

[19] L. J. Findley, M. A. Gresty, and M. G. Halmagyi, "A novel method of recording arm movements: a survey of common abnormalities," *Archives of neurology,* vol. 38, pp. 38-42, 1981.

[20] G. Kamen and D. Gabriel, *Essentials of electromyography*: Human Kinetics, 2010.

[21] A. Al-Jumaily and R. A. Olivares, "Electromyogram (EMG) driven system based virtual reality for prosthetic and rehabilitation devices," in *Proceedings of the 11th International Conference on Information Integration and Web-based Applications & Services*, 2009, pp. 582-586.

[22] M. Bacher, E. Scholz, and H. Diener, "24 hour continuous tremor quantification based on EMG recording," *Electroencephalography and clinical neurophysiology,* vol. 72, pp. 176-183, 1989.

[23] S. Breit, S. Spieker, J. Schulz, and T. Gasser, "Long-term EMG recordings differentiate between parkinsonian and essential tremor," *Journal of neurology,* vol. 255, pp. 103-111, 2008.

[24] S. KAZI, M. MAILAH, and Z. M. ZAIN, "Suppression of Hand Postural Tremor Via Active Force Control Method," *Manufacturing Engineering, Automatic Control and Robotics,* 2014.

[25] E. Rocon, M. Manto, J. Pons, S. Camut, and J. M. Belda, "Mechanical suppression of essential tremor," *The Cerebellum,* vol. 6, pp. 73-78, 2007.

[26] M. Bilodeau, D. A. Keen, P. J. Sweeney, R. W. Shields, and R. M. Enoka, "Strength training can improve steadiness in persons with essential tremor," *Muscle & nerve,* vol. 23, pp. 771-778, 2000.

[27] L. H. Craig, A. Svircev, M. Haber, and J. L. Juncos, "Controlled pilot study of the effects of neuromuscular therapy in patients with Parkinson's disease," *Movement disorders,* vol. 21, pp. 2127-2133, 2006.

[28] M. Lakie, E. Walsh, L. Arblaster, F. Villagra, and R. Roberts, "Limb temperature and human tremors," *Journal of Neurology, Neurosurgery & Psychiatry,* vol. 57, pp. 35-42, 1994.

[29] C. Cooper, V. G. H. Evidente, J. G. Hentz, C. H. Adler, J. N. Caviness, and K. Gwinn-Hardy, "The effect of temperature on hand function in patients with tremor," *Journal of Hand Therapy,* vol. 13, pp. 276-288, 2000.

[30] A. Prochazka, J. Elek, and M. Javidan, "Attenuation of pathological tremors by functional electrical stimulation I: Method," *Annals of Biomedical Engineering,* vol. 20, pp. 205-224, 1992.

[31] D. M. Gillard, T. Cameron, A. Prochazka, and M. J. Gauthier, "Tremor suppression using functional electrical stimulation: a comparison between digital and analog controllers," *Rehabilitation Engineering, IEEE Transactions on,* vol. 7, pp. 385-388, 1999.

[32] S. Pledgie, K. E. Barner, S. K. Agrawal, and T. Rahman, "Tremor suppression through impedance control," *Rehabilitation Engineering, IEEE Transactions on,* vol. 8, pp. 53-59, 2000.

[33] P. Feys, W. F. Helsen, S. Verschueren, S. P. Swinnen, I. Klok, A. Lavrysen*, et al.*, "Online movement control in multiple sclerosis patients with tremor: effects of tendon vibration," *Movement disorders,* vol. 21, pp. 1148-1153, 2006.

[34] C. T. Haas, S. Turbanski, K. Kessler, and D. Schmidtbleicher, "The effects of random whole-body-vibration on motor symptoms in Parkinson's disease," *NeuroRehabilitation-An Interdisciplinary Journal,* vol. 21, pp. 29-36, 2006.

[35] R. L. Hewer, R. COOPER, and M. H. MORGAN, "An investigation into the value of treating intention tremor by weighting the affected limb," *Brain,* vol. 95, pp. 579-590, 1972.

[36] R. P. Meshack and K. E. Norman, "A randomized controlled trial of the effects of weights on amplitude and frequency of postural hand tremor in people with Parkinson's disease," *Clinical rehabilitation,* vol. 16, pp. 481-492, 2002.

[37] "A possible melanoma discrimination index based on hyperspectral data: a pilot study," *Skin Research and Technology,* p. n/a, 2011.

[38] S. R. Filipović, J. C. Rothwell, and K. Bhatia, "Low-frequency repetitive transcranial magnetic stimulation and off-phase motor symptoms in Parkinson's disease," *Journal of the neurological sciences,* vol. 291, pp. 1-4, 2010.

[39] W. D. Hall, "Hand-held gyroscopic device," ed: Google Patents, 1991.

[40] J. Kotovsky and M. J. Rosen, "A wearable tremor-suppression orthosis," *Journal of rehabilitation research and development,* vol. 35, pp. 373-387, 1998.

[41] S. Hashemi, M. Golnaraghi, and A. Patla, "Tuned vibration absorber for suppression of rest tremor in Parkinson's disease," *Medical and Biological Engineering and Computing,* vol. 42, pp. 61-70, 2004.

[42] J. Hewit and J. Burdess, "Fast dynamic decoupled control for robotics, using active force control," *Mechanism and Machine Theory,* vol. 16, pp. 535-542, 1981.

[43] J. R. Hewit and K. Bouazza-Marouf, "Practical control enhancement via mechatronics design," *Industrial Electronics, IEEE Transactions on,* vol. 43, pp. 16-22, 1996.

[44] M. Mailah, "Intelligent active force control of a rigid robot arm using neural network and iterative learning algorithms," University of Dundee, 1998.

[45] M. Mailah and G. Priyandoko, "Active force control with input shaping technique for a suspension system," *Jurnal Mekanikal,* pp. 91-104, 2008.
[46] M. Mailah, E. Pitowarno, and H. Jamaluddin, "Robust motion control for mobile manipulator using resolved acceleration and proportional-integral active force control," *arXiv preprint cs/0601057,* 2006.
[47] G. Priyandoko and M. Mailah, "Simulation of suspension system with adaptive fuzzy active force control," *To all Intelligent Active Force Control Research Group,* p. 30, 2007.
[48] R. Bogue, "Exoskeletons and robotic prosthetics: a review of recent developments," *Industrial Robot: An International Journal,* vol. 36, pp. 421-427, 2009.
[49] R. Bogue, "Robotic exoskeletons: a review of recent progress," *Industrial Robot: An International Journal,* vol. 42, pp. 5-10, 2015.
[50] D. Huen, J. Liu, and B. Lo, "Assistive Wearable Robotics: Healthcare's New Clothes," *Newsletter,* vol. 2015, 2015.
[51] E. Rocon, A. Ruiz, J. Pons, J. M. Belda-Lois, and J. Sánchez-Lacuesta, "Rehabilitation robotics: a wearable exo-skeleton for tremor assessment and suppression," in *Robotics and Automation, 2005. ICRA 2005. Proceedings of the 2005 IEEE International Conference on*, 2005, pp. 2271-2276.
[52] M. Manto, E. Rocon, J. Pons, J. M. Belda, and S. Camut, "Evaluation of a wearable orthosis and an associated algorithm for tremor suppression," *Physiological measurement,* vol. 28, p. 415, 2007.
[53] H. In, B. B. Kang, M. Sin, and K.-J. Cho, "Exo-Glove: A Wearable Robot for the Hand with a Soft Tendon Routing System," *Robotics & Automation Magazine, IEEE,* vol. 22, pp. 97-105, 2015.
[54] A. Shooshtari, S. M. Hoseini, S. N. Mahmoodi, and H. Kalhori, "Analytical solution for nonlinear free vibrations of viscoelastic microcantilevers covered with a piezoelectric layer," *Smart Materials and Structures,* vol. 21, p. 075015, 2012.
[55] J. Li, Y. Xue, F. Li, and Y. Narita, "Active vibration control of functionally graded piezoelectric material plate," *Composite Structures,* vol. 207, pp. 509-518, 2019.
[56] H. Saito, S. Murakami, J. Hayashi, K. Oshima, and H. Tanaka, "Piezoelectric material, piezoelectric element, and electronic apparatus," ed: Google Patents, 2019.
[57] N. Jalili, *Piezoelectric-based vibration control: from macro to micro/nano scale systems*: Springer Science & Business Media, 2009.
[58] C. Ziegler, "Cantilever-based biosensors," *Analytical and bioanalytical chemistry,* vol. 379, pp. 946-959, 2004.
[59] C. N. Riviere, W. T. Ang, and P. K. Khosla, "Toward active tremor canceling in handheld microsurgical instruments," *IEEE Transactions on Robotics and Automation,* vol. 19, pp. 793-800, 2003.
[60] S. Hosseini, A. Al-Jumaily, and S. A. Abboud, "Active force control system for hand tremor suppression by different actuators," in *Electronic Devices, Systems and Applications (ICEDSA), 2016 5th International Conference on*, 2016, pp. 1-4.

[61] S. Hosseini and A. Al-Jumaily, "Active force control system for tremor suppression in elbow joint," in *Robotics and Intelligent Sensors (IRIS), 2016 IEEE International Symposium on*, 2016, pp. 140-145.

[62] S. Hosseini, A. Al-Jumaily, and H. Kalhori, "Tremor suppression in wrist joint using active force control method," in *9th Australasian Congress on Applied Mechanics (ACAM9)*, 2017, p. 349.

[63] A. Preumont, *Vibration control of active structures: an introduction* vol. 246: Springer, 2018.

[64] S. S. Rao, *Vibration of continuous systems*: John Wiley & Sons, 2007.

[65] Q. Wang and S. Quek, "Flexural vibration analysis of sandwich beam coupled with piezoelectric actuator," *Smart Materials and Structures,* vol. 9, p. 103, 2000.

[66] M. F. Daqaq, K. A. Alhazza, and H. N. Arafat, "Non-linear vibrations of cantilever beams with feedback delays," *International Journal of Non-Linear Mechanics,* vol. 43, pp. 962-978, 2008.

[67] S. M. Hosseini, A. Shooshtari, H. Kalhori, and S. N. Mahmoodi, "Nonlinear-forced vibrations of piezoelectrically actuated viscoelastic cantilevers," *Nonlinear Dynamics,* vol. 78, pp. 571-583, 2014.

[68] S. M. Hosseini, H. Kalhori, A. Shooshtari, and S. N. Mahmoodi, "Analytical solution for nonlinear forced response of a viscoelastic piezoelectric cantilever beam resting on a nonlinear elastic foundation to an external harmonic excitation," *Composites Part B: Engineering,* vol. 67, pp. 464-471, 2014.

[69] S. Mareishi, H. Kalhori, M. Rafiee, and S. M. Hosseini, "Nonlinear forced vibration response of smart two-phase nano-composite beams to external harmonic excitations," *Curved and Layered Structures,* vol. 2, 2015.

[70] L.-W. Chen, C.-Y. Lin, and C.-C. Wang, "Dynamic stability analysis and control of a composite beam with piezoelectric layers," *Composite Structures,* vol. 56, pp. 97-109, 2002.

[71] R. Gurram, "A study of vibration response characteristics of the human hand-arm system," Concordia University, 1993.

[72] S. M. Hosseini, S. Mareishi, H. Kalhori, and M. Rafiee, "Large amplitude free and forced oscillations of functionally graded beams," *Mechanics of Advanced Materials and Structures,* vol. 21, pp. 255-262, 2014.

[73] M. Korayem and R. Ghaderi, "Vibration response of a piezoelectrically actuated microcantilever subjected to tip–sample interaction," *Scientia Iranica,* vol. 20, pp. 195-206, 2013.

[74] Z. Zhao, S. Wen, F. Li, and C. Zhang, "Free vibration analysis of multi-span Timoshenko beams using the assumed mode method," *Archive of Applied Mechanics,* pp. 1-16, 2018.

[75] S. Rao and R. Gupta, "Finite element vibration analysis of rotating Timoshenko beams," *Journal of Sound and Vibration,* vol. 242, pp. 103-124, 2001.

[76] T. Chuaqui and C. Roque, "Analysis of functionally graded piezoelectric Timoshenko smart beams using a multiquadric radial basis function method," *Composite Structures,* vol. 176, pp. 640-653, 2017.

[77] A. T. Samaei, M. Bakhtiari, and G.-F. Wang, "Timoshenko beam model for buckling of piezoelectric nanowires with surface effects," *Nanoscale research letters,* vol. 7, p. 201, 2012.

[78] A. Kargani, Y. Kiani, and M. Eslami, "Exact solution for nonlinear stability of piezoelectric FGM Timoshenko beams under thermo-electrical loads," *Journal of Thermal Stresses,* vol. 36, pp. 1056-1076, 2013.

[79] G. Zhu, R. Yang, S. Wang, and Z. L. Wang, "Flexible high-output nanogenerator based on lateral ZnO nanowire array," *Nano letters,* vol. 10, pp. 3151-3155, 2010.

[80] S. Sugavanam, V. Varadan, and V. Varadan, "Modeling and control of a lightly damped T-beam using piezoceramic actuators and sensors," *Smart materials and structures,* vol. 7, p. 899, 1998.

[81] F.-M. Li and X.-X. Lyu, "Active vibration control of lattice sandwich beams using the piezoelectric actuator/sensor pairs," *Composites Part B: Engineering,* vol. 67, pp. 571-578, 2014.

[82] F. Li, C. Zhang, and C. Liu, "Active tuning of vibration and wave propagation in elastic beams with periodically placed piezoelectric actuator/sensor pairs," *Journal of Sound and Vibration,* vol. 393, pp. 14-29, 2017.

[83] N. Shen, "Analysis of beams containing piezoelectric sensors and actuators," *Smart Materials and Structures,* vol. 3, p. 439, 1994.

[84] O. J. Aldraihem, R. C. Wetherhold, and T. Singh, "Distributed control of laminated beams: Timoshenko theory vs. Euler-Bernoulli theory," *Journal of intelligent material systems and structures,* vol. 8, pp. 149-157, 1997.

[85] H. Djojodihardjo, M. Jafari, S. Wiriadidjaja, and K. A. Ahmad, "Active vibration suppression of an elastic piezoelectric sensor and actuator fitted cantilevered beam configurations as a generic smart composite structure," *Composite Structures,* vol. 132, pp. 848-863, 2015.

[86] S.-C. Choi, J.-S. Park, and J.-H. Kim, "Active damping of rotating composite thin-walled beams using MFC actuators and PVDF sensors," *Composite structures,* vol. 76, pp. 362-374, 2006.

[87] X. Wang, M. Morandini, and P. Masarati, "Velocity feedback damping of piezo-actuated wings," *Composite Structures,* vol. 174, pp. 221-232, 2017.

[88] A. M. Woods, M. Nowostawski, E. A. Franz, and M. Purvis, "Parkinson's disease and essential tremor classification on mobile device," *Pervasive and Mobile Computing,* vol. 13, pp. 1-12, 2014.

[89] C. Camara, P. Isasi, K. Warwick, V. Ruiz, T. Aziz, J. Stein*, et al.*, "Resting tremor classification and detection in Parkinson's disease patients," *Biomedical Signal Processing and Control,* vol. 16, pp. 88-97, 2015.

[90] S. Pan, S. Iplikci, K. Warwick, and T. Z. Aziz, "Parkinson's Disease tremor classification–A comparison between Support Vector Machines and neural networks," *Expert Systems with Applications,* vol. 39, pp. 10764-10771, 2012.

[91] P. Palmes, W. T. Ang, F. Widjaja, L. C. Tan, and W. L. Au, "Pattern mining of multichannel sEMG for tremor classification," *IEEE transactions on biomedical engineering,* vol. 57, pp. 2795-2805, 2010.

[92] S. Rissanen, M. Kankaanpää, M. P. Tarvainen, J. Nuutinen, I. M. Tarkka, O. Airaksinen*, et al.*, "Analysis of surface EMG signal morphology in Parkinson's disease," *Physiological measurement,* vol. 28, p. 1507, 2007.

[93] H. Jeon, W. Lee, H. Park, H. J. Lee, S. K. Kim, H. B. Kim*, et al.*, "High-accuracy automatic classification of Parkinsonian tremor severity using machine learning method," *Physiological measurement,* vol. 38, p. 1980, 2017.

[94] L. Ai, J. Wang, and R. Yao, "Classification of parkinsonian and essential tremor using empirical mode decomposition and support vector machine," *Digital Signal Processing,* vol. 21, pp. 543-550, 2011.

[95] D. Surangsrirat, C. Thanawattano, R. Pongthornseri, S. Dumnin, C. Anan, and R. Bhidayasiri, "Support vector machine classification of Parkinson's disease and essential tremor subjects based on temporal fluctuation," in *Engineering in Medicine and Biology Society (EMBC), 2016 IEEE 38th Annual International Conference of the*, 2016, pp. 6389-6392.

[96] Q. W. Oung, H. Muthusamy, S. N. Basah, H. Lee, and V. Vijean, "Empirical Wavelet Transform Based Features for Classification of Parkinson's Disease Severity," *Journal of medical systems,* vol. 42, p. 29, 2018.

[97] R. Merletti, P. A. Parker, and P. J. Parker, *Electromyography: physiology, engineering, and non-invasive applications* vol. 11: John Wiley & Sons, 2004.

[98] R. Garnett, M. O'donovan, J. Stephens, and A. Taylor, "Motor unit organization of human medial gastrocnemius," *The Journal of physiology,* vol. 287, pp. 33-43, 1979.

[99] M. Goldberger, "Spared-root deafferentation of a cat's hindlimb: hierarchical regulation of pathways mediating recovery of motor behavior," *Experimental brain research,* vol. 73, pp. 329-342, 1988.

[100] K. Anam, "Bio-driven control system for the rehabilitation hand device: a new approach," 2016.

[101] R. H. Chowdhury, M. B. Reaz, M. A. B. M. Ali, A. A. Bakar, K. Chellappan, and T. G. Chang, "Surface electromyography signal processing and classification techniques," *Sensors,* vol. 13, pp. 12431-12466, 2013.

[102] R. Gopura, D. Bandara, J. Gunasekara, and T. Jayawardane, "Recent trends in EMG-Based control methods for assistive robots," in *Electrodiagnosis in new frontiers of clinical research*, ed: InTech, 2013.

[103] M. A. Oskoei and H. Hu, "Myoelectric control systems—A survey," *Biomedical Signal Processing and Control,* vol. 2, pp. 275-294, 2007.

[104] K. Anam and A. Al-Jumaily, "Evaluation of extreme learning machine for classification of individual and combined finger movements using electromyography on amputees and non-amputees," *Neural Networks,* vol. 85, pp. 51-68, 2017.

[105] A. Phinyomark, P. Phukpattaranont, and C. Limsakul, "Feature reduction and selection for EMG signal classification," *Expert Systems with Applications,* vol. 39, pp. 7420-7431, 2012.

[106] M. Zardoshti-Kermani, B. C. Wheeler, K. Badie, and R. M. Hashemi, "EMG feature evaluation for movement control of upper extremity prostheses," *IEEE Transactions on Rehabilitation Engineering,* vol. 3, pp. 324-333, 1995.

[107] R. N. Khushaba, A. Al-Jumaily, and A. Al-Ani, "Novel feature extraction method based on fuzzy entropy and wavelet packet transform for myoelectric control," in *2007 International Symposium on Communications and Information Technologies*, 2007, pp. 352-357.

[108] K. Englehart, B. Hudgin, and P. A. Parker, "A wavelet-based continuous classification scheme for multifunction myoelectric control," *IEEE Transactions on Biomedical Engineering,* vol. 48, pp. 302-311, 2001.

[109] D. Cai, X. He, and J. Han, "SRDA: An efficient algorithm for large-scale discriminant analysis," *IEEE transactions on knowledge and data engineering,* vol. 20, pp. 1-12, 2008.

[110] A. M. Martínez and A. C. Kak, "Pca versus lda," *IEEE Transactions on Pattern Analysis & Machine Intelligence,* pp. 228-233, 2001.

[111] E. Scheme and K. Englehart, "Electromyogram pattern recognition for control of powered upper-limb prostheses: state of the art and challenges for clinical use," *Journal of Rehabilitation Research & Development,* vol. 48, 2011.

[112] L. J. Hargrove, E. J. Scheme, K. B. Englehart, and B. S. Hudgins, "Multiple binary classifications via linear discriminant analysis for improved controllability of a powered prosthesis," *IEEE Transactions on Neural Systems and Rehabilitation Engineering,* vol. 18, pp. 49-57, 2010.

[113] G. Tsenov, A. Zeghbib, F. Palis, N. Shoylev, and V. Mladenov, "Neural networks for online classification of hand and finger movements using surface EMG signals," in *Neural Network Applications in Electrical Engineering, 2006. NEUREL 2006. 8th Seminar on*, 2006, pp. 167-171.

[114] A. D. Chan and K. B. Englehart, "Continuous myoelectric control for powered prostheses using hidden Markov models," *IEEE Transactions on Biomedical Engineering,* vol. 52, pp. 121-124, 2005.

[115] A. Hiraiwa, K. Shimohara, and Y. Tokunaga, "EMG pattern analysis and classification by neural network," in *Systems, Man and Cybernetics, 1989. Conference Proceedings., IEEE International Conference on*, 1989, pp. 1113-1115.

[116] C. Cipriani, C. Antfolk, M. Controzzi, G. Lundborg, B. Rosén, M. C. Carrozza*, et al.*, "Online myoelectric control of a dexterous hand prosthesis by transradial amputees," *IEEE Transactions on Neural Systems and Rehabilitation Engineering,* vol. 19, pp. 260-270, 2011.

[117] G.-B. Huang, H. Zhou, X. Ding, and R. Zhang, "Extreme learning machine for regression and multiclass classification," *IEEE Transactions on Systems, Man, and Cybernetics, Part B (Cybernetics),* vol. 42, pp. 513-529, 2012.

[118] K. Anam and A. Al-Jumaily, "Optimized Kernel Extreme Learning Machine for Myoelectric Pattern Recognition," *International Journal of Electrical and Computer Engineering (IJECE),* vol. 8, pp. 483-496, 2018.

[119] X. Yu, "Simulation study of tremor suppression and experiment of energy harvesting with piezoelectric materials," UNIVERSITY OF NORTH TEXAS, 2012.

[120] R. Alkhatib and M. Golnaraghi, "Active structural vibration control: a review," *Shock and Vibration Digest,* vol. 35, p. 367, 2003.

[121] J. Burdess and J. Hewit, "An active method for the control of mechanical systems in the presence of unmeasurable forcing," *Mechanism and machine theory,* vol. 21, pp. 393-400, 1986.

[122] P. K. Sharma and S. Bhaduri, "Active Vibration Control Structures Using Piezoelectric Materials: A Review," 2015.

[123] S. Yun, K. Lee, H. Kim, and H. So, "Development of the pneumatic valve with bimorph type PZT actuator," *Materials chemistry and physics,* vol. 97, pp. 1-4, 2006.

[124] A. Noshadi, M. Mailah, and A. Zolfagharian, "Active force control of 3-RRR planar parallel manipulator," in *Mechanical and Electrical Technology (ICMET), 2010 2nd International Conference on*, 2010, pp. 77-81.

[125] S. Rakheja, J. Wu, R. Dong, A. Schopper, and P.-É. Boileau, "A comparison of biodynamic models of the human hand–arm system for applications to hand-held power tools," *Journal of Sound and Vibration,* vol. 249, pp. 55-82, 2002.

[126] D. D. Reynolds and R. Falkenberg, "A study of hand vibration on chipping and grinding operators, Part II: Four-degree-of-freedom lumped parameter model of the vibration response of the human hand," *Journal of Sound and Vibration,* vol. 95, pp. 499-514, 1984.

[127] D. Zhang and W. T. Ang, "Tremor suppression of elbow joint via functional electrical stimulation: A simulation study," in *Automation Science and Engineering, 2006. CASE'06. IEEE International Conference on*, 2006, pp. 182-187.

[128] N. Lan, "Stability analysis for postural control in a two-joint limb system," *Neural Systems and Rehabilitation Engineering, IEEE Transactions on,* vol. 10, pp. 249-259, 2002.

[129] D. Zhang, P. Poignet, F. Widjaja, and W. T. Ang, "Neural oscillator based control for pathological tremor suppression via functional electrical stimulation," *Control Engineering Practice,* vol. 19, pp. 74-88, 2011.

[130] P. Yao, D. Zhang, and M. Hayashibe, "Simulation of tremor on 3-dimentional musculoskeletal model of wrist joint and experimental verification?," in *Engineering in Medicine and Biology Society (EMBC), 2012 Annual International Conference of the IEEE*, 2012, pp. 4823-4826.

[131] R.-F. Fung, Y.-T. Liu, and C.-C. Wang, "Dynamic model of an electromagnetic actuator for vibration control of a cantilever beam with a tip mass," *Journal of Sound and Vibration,* vol. 288, pp. 957-980, 2005.

[132] M. Ferrarin, F. Palazzo, R. Riener, and J. Quintern, "Model-based control of FES-induced single joint movements," *Neural Systems and Rehabilitation Engineering, IEEE Transactions on,* vol. 9, pp. 245-257, 2001.

[133] T. Edrich, R. Riener, and J. Quintern, "Analysis of passive elastic joint moment in paraplegics," *Biomedical Engineering, IEEE Transactions on,* vol. 47, pp. 1058-1065, 2000.

[134] M. A. Lemay and P. E. Crago, "A dynamic model for simulating movements of the elbow, forearm, and wrist," *Journal of biomechanics,* vol. 29, pp. 1319-1330, 1996.

[135] S. M. Hosseini and A. Al-Jumaily, "Analytical solution for forced vibration of piezoelectrically actuated Timoshenko beam," *Journal of Intelligent Material Systems and Structures,* vol. 30, pp. 1276-1284, 2019.

[136] Y. Tao, *Impacts of various boundary conditions on beam vibrations*: West Virginia University, 2015.

[137] T. Farrell and R. F. Weir, "Analysis window induced controller delay for multifunctional prostheses," 2008.

[138] K. Fukunaga, *Introduction to statistical pattern recognition*: Elsevier, 2013.

[139] R. N. Khushaba, A. Al-Ani, and A. Al-Jumaily, "Orthogonal fuzzy neighborhood discriminant analysis for multifunction myoelectric hand control," *IEEE Transactions on Biomedical Engineering,* vol. 57, p. 1410, 2010.

[140] K. Anam, R. N. Khushaba, and A. Al-Jumaily, "Two-channel surface electromyography for individual and combined finger movements," in *2013 35th Annual International Conference of the IEEE Engineering in Medicine and Biology Society (EMBC)*, 2013, pp. 4961-4964.

[141] K. Englehart and B. Hudgins, "A robust, real-time control scheme for multifunction myoelectric control," *IEEE transactions on biomedical engineering,* vol. 50, pp. 848-854, 2003.